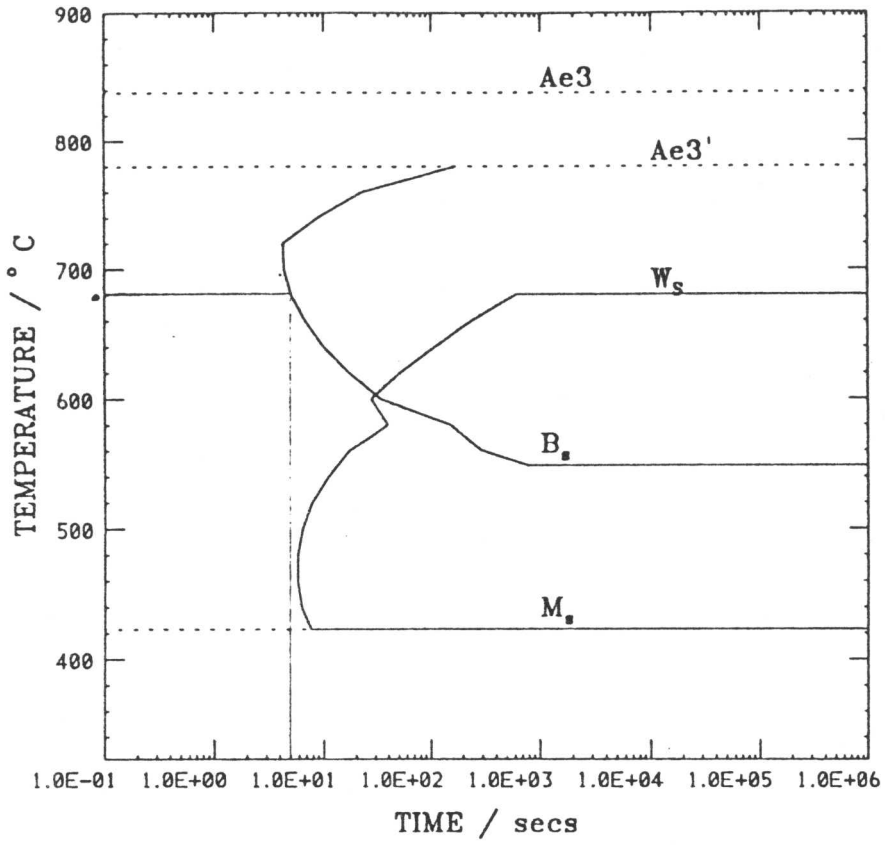

Figure 5.2: Calculated Time–Temperature–Transformation curve for $2\frac{1}{4}$Cr1Mo steel.

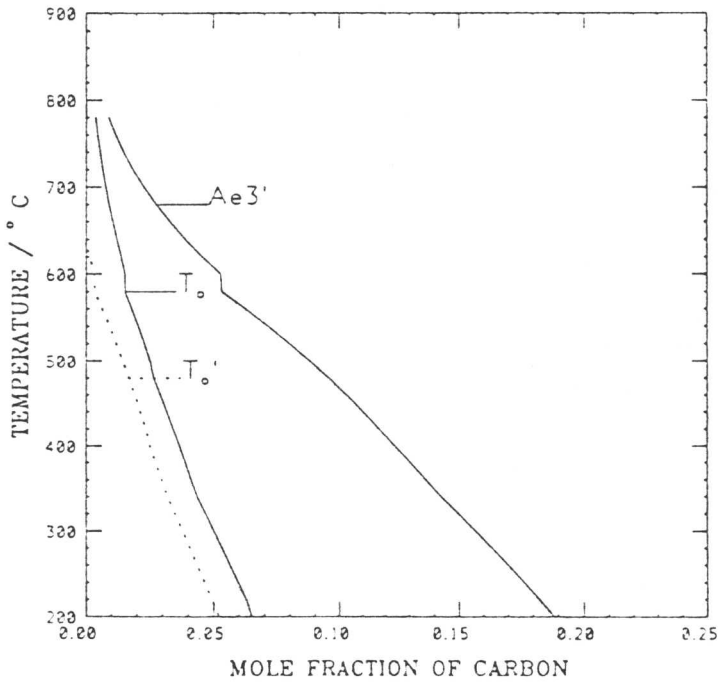

Figure 5.3: Calculated section of the phase diagram for $2\frac{1}{4}$Cr1Mo steel.

function was to limit any decarburisation which might occur during heat treatment. They were then austenitised at 1050°C for 15 minutes in a furnace before transfer to an adjacent fluidised bed at 480°C for 30 minutes. Optical and scanning electron micrographs illustrating the predominantly bainitic microstructure with small islands of martensite are presented in Figure 5.4a) and b). It is well known that the bainite reaction does not go to completion when cementite formation does not accompany the growth of bainite. It is then possible to calculate the expected volume fraction of bainite at 480°C using the equation

$$V_b = \frac{x_{T_0} - \overline{x}}{x_{T_0} - x_\alpha}, \tag{5.3}$$

where x_{T_0} is the mole fraction of carbon remaining in austenite when the reaction stops, $\overline{x}$ is the average carbon concentration in the alloy and x_α is the carbon concentration in bainitic ferrite (assumed to be zero). The phase diagram in Figure 5.3 predicts a value for x_{T_0} of $\simeq$0.026 at 480°C and $\overline{x}$ is 0.0069, giving a volume fraction of $\simeq$0.7 at 480°C. This is in good agreement with the observed volume fractions in Figure 5.4. As the transformation temperature is lowered the volume fraction of bainite will increase.

The initial microstructure was also characterised in the TEM using thin foil specimens. The micrograph in Figure 5.5 illustrates the bainitic and martensitic areas, the martensite being heavily dislocated. There is also a small amount of retained austenite present at the edges of the bainite sheaves; the electron diffraction pattern in Figure 5.6 shows reflections attributable to the retained austenite.

A carbon extraction replica taken from the as–transformed fully bainitic specimen is presented in Figure 5.7. It is interesting to note that there are no cementite particles in the bainitic regions immediately after isothermal transformation. This implies that it is upper bainite which forms at 480°C because lower bainite would contain carbides as a consequence of the transformation mechanism. The bainite reaction has been discussed extensively in Chapter 2. The formation of upper bainite results in the rejection of carbon into the austenite surrounding the bainite plates. Some of this enriched austenite is retained on quenching after isothermal transformation. Immediately tempering begins, the austenite starts to decompose to a mixture of ferrite and cementite. This cementite will initially have a composition consistent with formation by a paraequilibrium mechanism owing to the large differences in the diffusion rates of carbon and substitutional solute elements.

Whether it is upper or lower bainite which can be found in the microstructure following isothermal transformation above M_s has been investigated widely for plain Fe–C steels. Oka and Okamoto (1986) proved that steels with more than 0.8 wt.% of carbon do not contain any upper

bainite, observing only lower bainite at all transformation temperatures above M_s. In addition, Ohmori and Honeycombe (1971) found only upper bainite in plain carbon steels containing less than 0.4 wt.% carbon. Few similar studies have been made for alloy steels. The steel used in this work has a carbon concentration of 0.15 wt.%. It is of great interest, therefore, to investigate whether or not lower bainite can be formed by isothermal transformation near M_s. To this end, the value of M_s was first determined by austenitising a specimen in a thermomechanical simulator at 1050°C for 15 mins, followed by quenching to room temperature using nitrogen gas. Graphs in which the relative length change is plotted against temperature and time are presented in Figure 5.8a) and b) respectively. The M_s temperature was found to be 420°C. This is in good agreement with the value of 390°C predicted by the model described in section 5.3.1.

Two similar isothermal transformations experiments to those used to create the starting bainitic microstructure used in the majority of this work were then carried out, again in the thermomechanical simulator. In both cases specimens were austenitised at 1050°C for 15 mins and then one specimen was isothermally transformed at 450°C, and the other at 400°C, each for 30 mins. It is important to note that although 400°C is slightly below M_s, a considerable volume fraction of bainite is to be expected on isothermal transformation so near M_s. Graphs showing plots of temperature against time and relative length change against time for the transformation at 450°C are presented in Figures 5.8c) and d), and at 400°C in Figures 5.8e) and f). The specimen isothermally transformed at 400°C was then examined in the TEM to determine if there was any lower bainite present in the microstructure.

A low magnification transmission electron micrograph is presented in Figure 5.9. Careful examination of the picture reveals that there are large areas of both lower and upper bainite. A higher magnification image of the upper bainitic region presented in Figure 5.10 clearly shows plates of upper bainite separated by films of retained austenite. Low and high magnification images of the lower bainitic region are presented in Figure 5.11 and Figure 5.12 respectively. The most striking feature of these images is that the cementite precipitates are in one orientation only with respect to the lower bainitic ferrite. There is also evidence of some films of retained austenite in the lower bainitic regions, but it is not as extensive as in the upper bainitic regions. The microstructure contained approximately 45% lower bainite, 45% upper bainite and also 10% martensite. A martensite lath is illustrated in Figure 5.13. The cementite within the lath is found in three different orientations, in contrast to that in the lower bainite. It should be noted that this martensite has formed during isothermal transformation just below M_s and has tempered on continued holding at 400°C. This is still consistent with the fact that there are no

carbides found in the specimens transformed at 480°C which contained a mixture of martensite and bainite. In that case the martensite formed on quenching and therefore no tempering occurred allowing cementite precipitation, and the bainite was all upper bainite and therefore did not contain any carbides.

The differences in scale of both the laths and the carbide precipitation in the lower bainite and the martensite are clearly illustrated in Figure 5.14. The martensite lath is much coarser than the bainite, whereas cementite precipitation is on a much finer scale in the martensite due to the increased carbon concentration and occurs in more than one orientation. Chapter 2 discussed the rejection of carbon from plates of upper bainite during growth. As a consequence of this, the austenite matrix will become richer in carbon. In the later stages of transformation the bainite growing from the enriched austenite may then decompose to lower bainite. This explains why the mixture of upper and lower bainite is observed in this case.

5.3.4 Starting mixed allotriomorphic ferrite and bainitic microstructure

The necessary heat treatment cycle to produce a mixed microstructure is austenitisation at 1050°C for 15 minutes, followed by holding at 700°C for 1 hour, then further transformation at 480°C for 30 minutes, then finally quenching to room temperature. It proved extremely difficult to control the amount of decarburisation in the specimens using a furnace at 1050°C and two fluidised beds at 700 and 480°C respectively. The heat treatments were therefore performed on the smaller 8 ×12 mm cylindrical specimens in a thermomechanical simulator. This enabled the exact heating cycle and cooling rates to be accurately programmed. The experiments were essentially performed in vacuum, however, nitrogen gas was introduced into the chamber to quench the specimen between the transformation temperatures. The vacuum pumps were then switched back on to pump out the gas once the specimen had reached the next required transformation temperature. Three test experiments were performed in which the only difference was the speed with which the vacuum pumps were activated after the introduction of the N_2 gas to quench the specimen from 1050°C to 700°C. The heat treatment cycle and graphs showing the relative length change versus time for three of the test specimens are presented in Figure 5.15a)–d).

It can be seen from Figure 5.15b) that specimen 1 shows the maximum relative length change of $\simeq$0.01, with specimens 2 and 3 showing relative length changes of $\simeq$0.008 and $\simeq$0.007 respectively. The relative length change corresponds to the amount of growth of allotriomorphic ferrite and therefore specimen 1 should contain the highest volume fraction of ferrite, with specimens 2 and 3 having progressively lower volume fractions. Optical micrographs of specimens 1, 2 and 3 are presented in Figure 5.16, Figure 5.17 and Figure 5.18 respectively. It can seen that

a)

b)

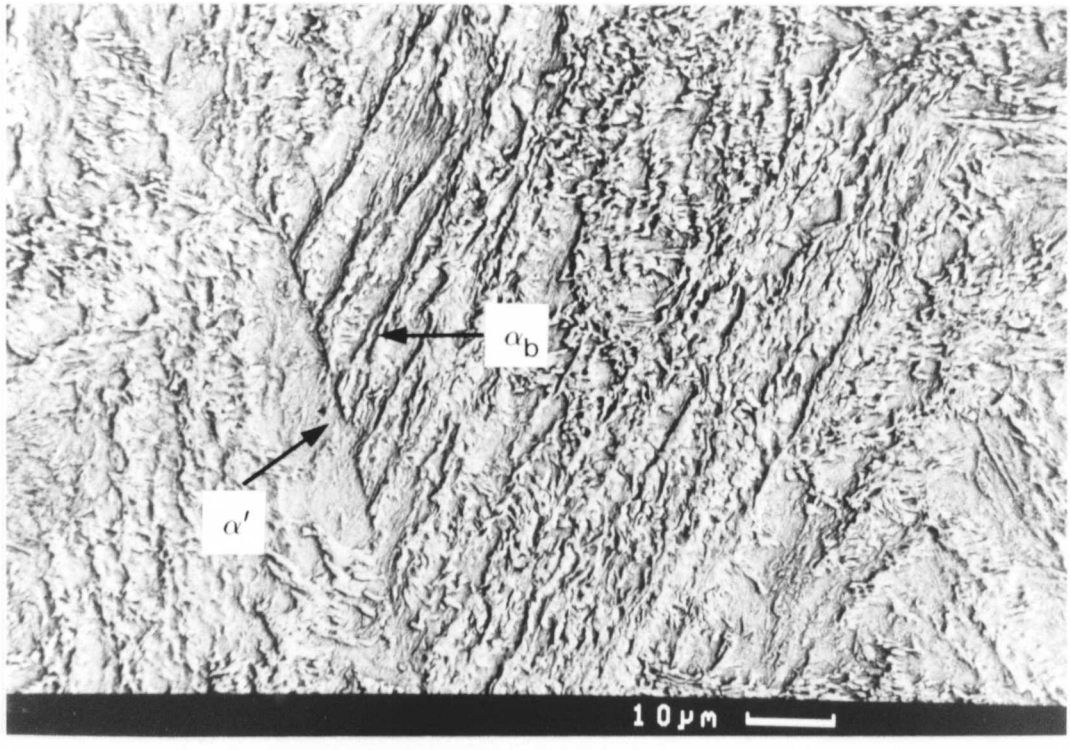

Figure 5.4: a) Optical and b) scanning electron micrographs of the starting bainitic microstructure – Austenitised 1050°C 15 minutes, 480°C 30 minutes and then water quenched.

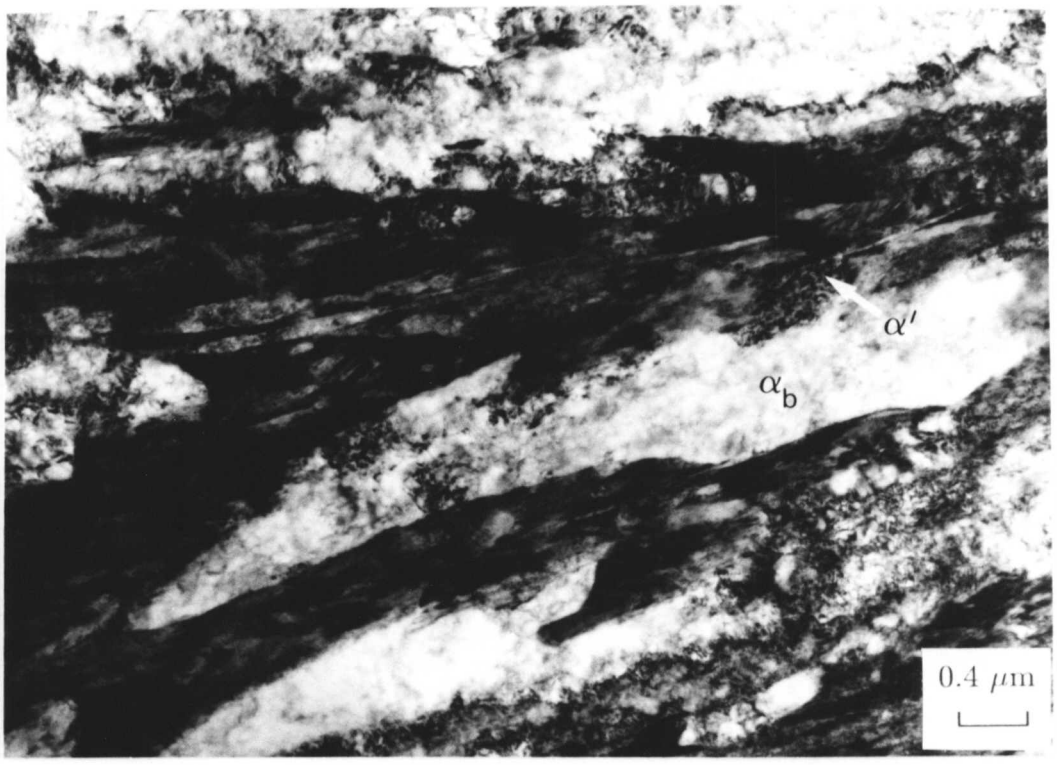

Figure 5.5: Transmission electron micrograph showing a mixture of bainite and martensite, the martensite being heavily dislocated. There is also a small amount of retained austenite – Austenitised 1050°C 15 minutes, 480°C 30 minutes and then water quenched.

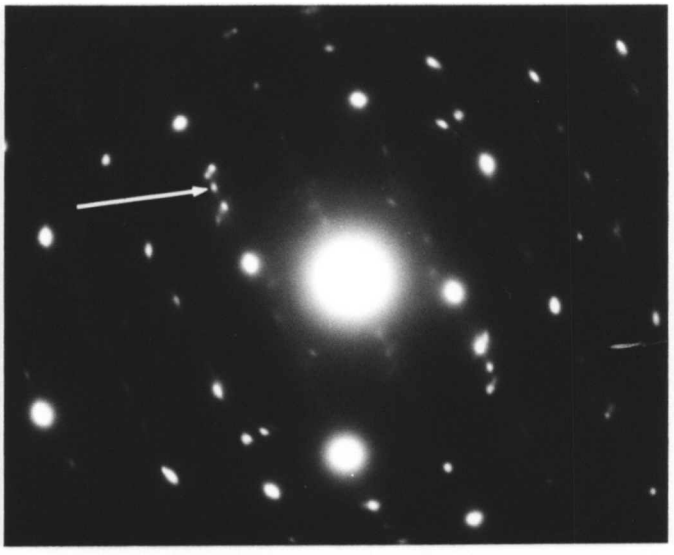

Figure 5.6: Selected area electron diffraction pattern showing reflections due to retained austenite within the microstructure.

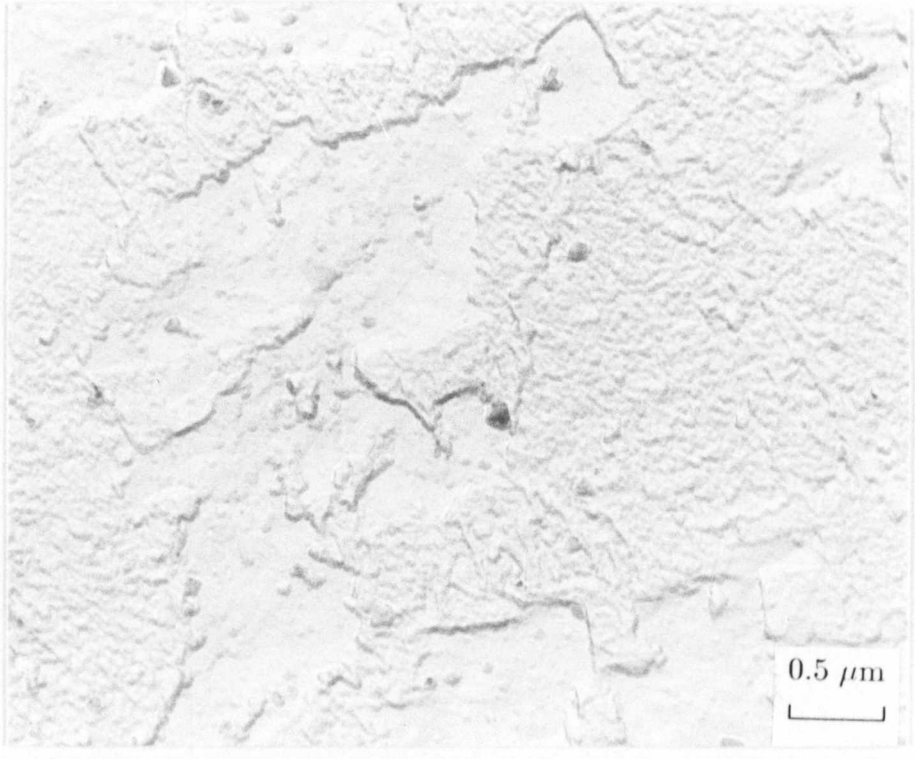

Figure 5.7: Carbon extraction replica taken from the as–transformed fully bainitic microstructure illustrating that there are no carbides present.

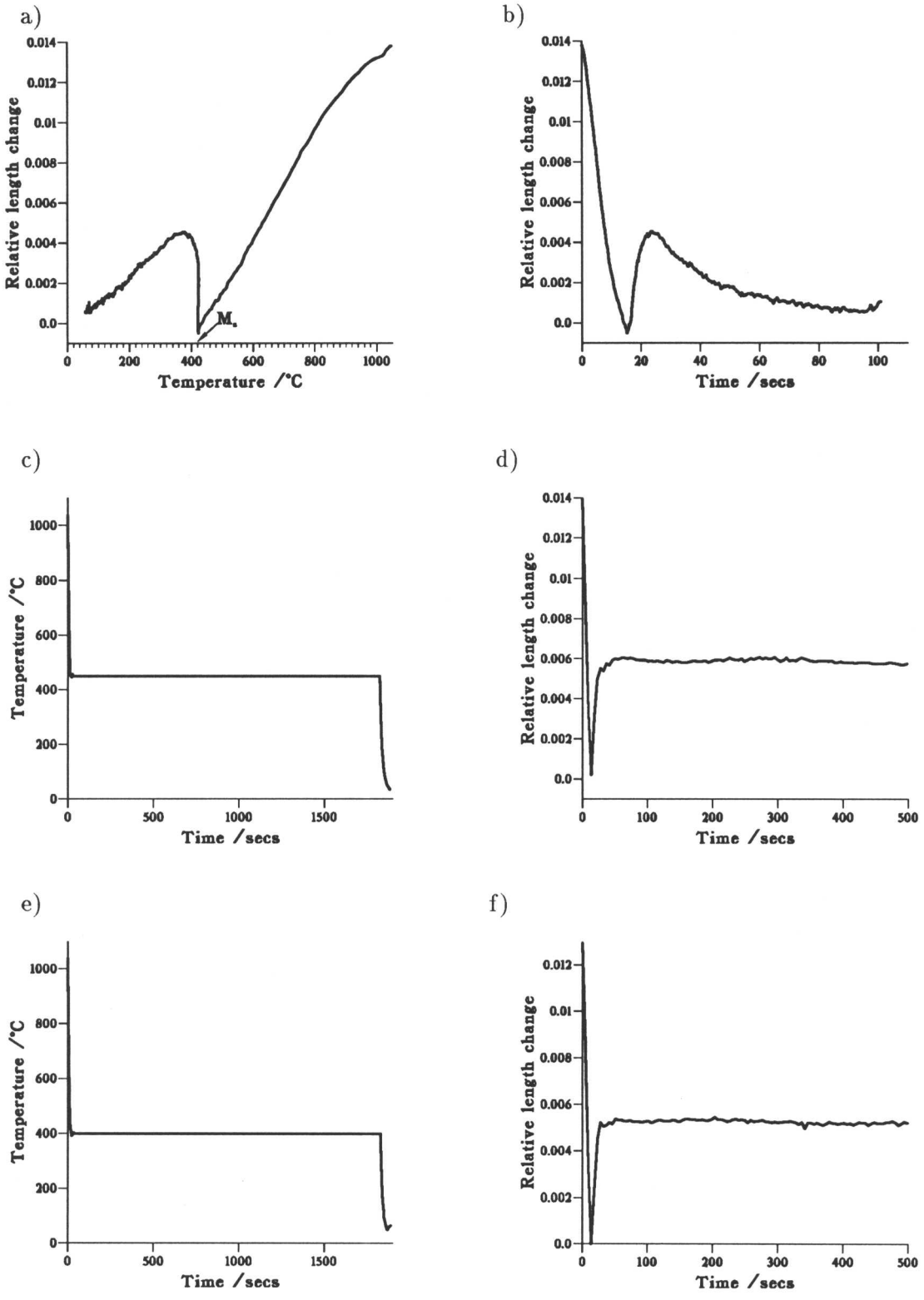

Figure 5.8: Relative length change against temperature a) and time b) for gas quenching a specimen from austenite to determine the M_s temperature. Temperature against time and relative length change against time for isothermal transformation at 450°C c) and d), and at 400°C e) and f).

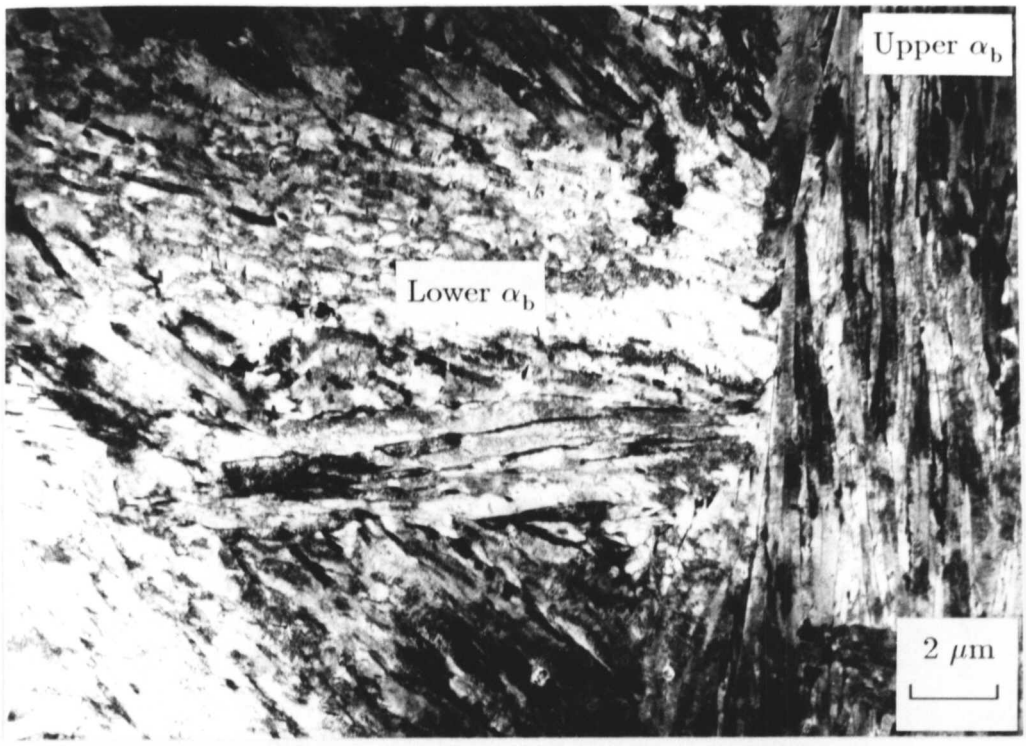

Figure 5.9: Low magnification image illustrating lower and upper bainitic regions in a specimen austenitised at 1050°C for 15 mins followed by isothermal transformation at 400°C for 30 mins.

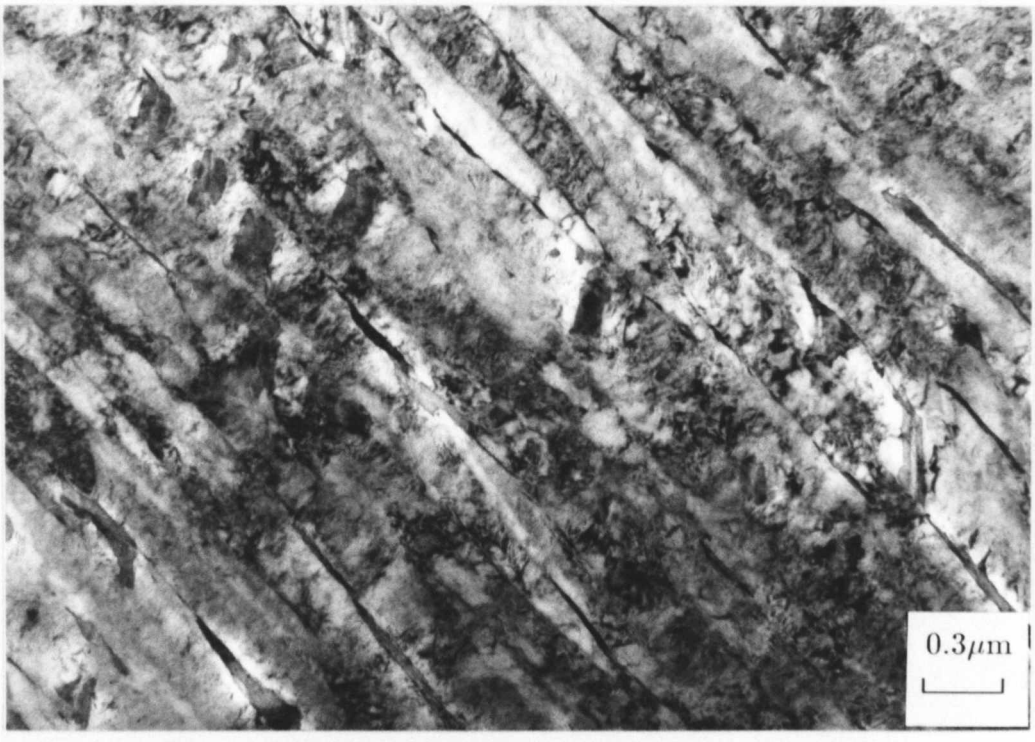

Figure 5.10: Transmission electron micrograph illustrating plates of upper bainite with films of retained austenite in between.

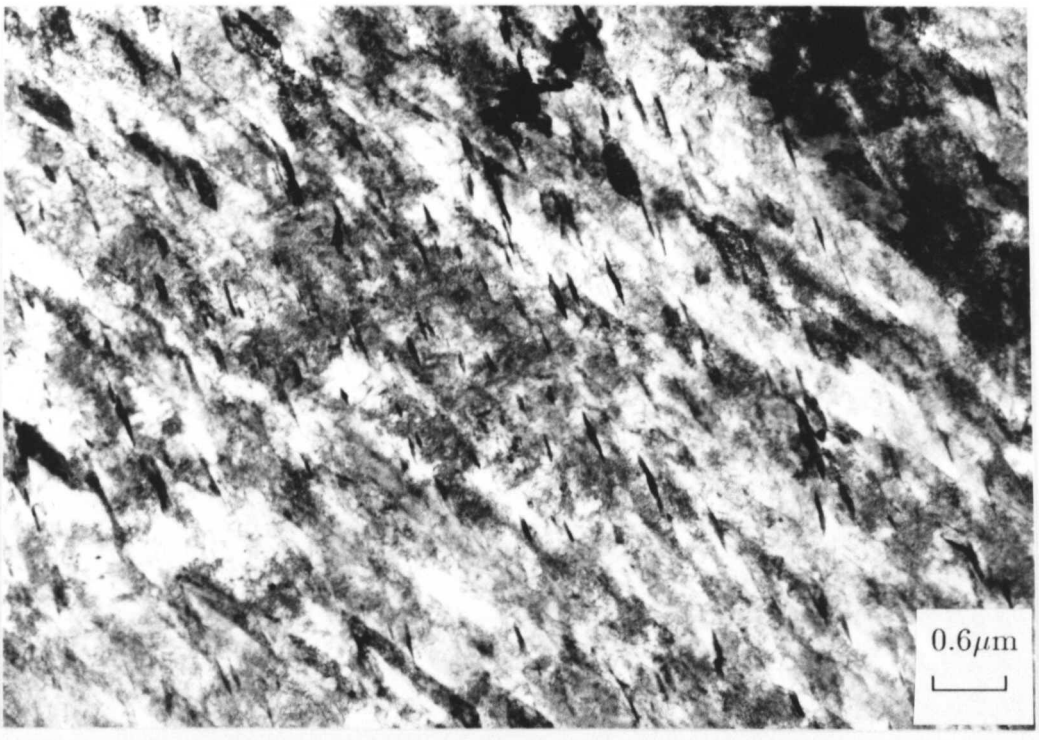

Figure 5.11: Low magnification image illustrating a lower bainitic region in the specimen isothermally transformed at 400°C for 30 mins. Cementite particles are observed in only one orientation with respect to the bainitic ferrite.

Figure 5.12: High magnification image of a lower bainite plate in this case showing cementite precipitation parallel to the axis of the plate.

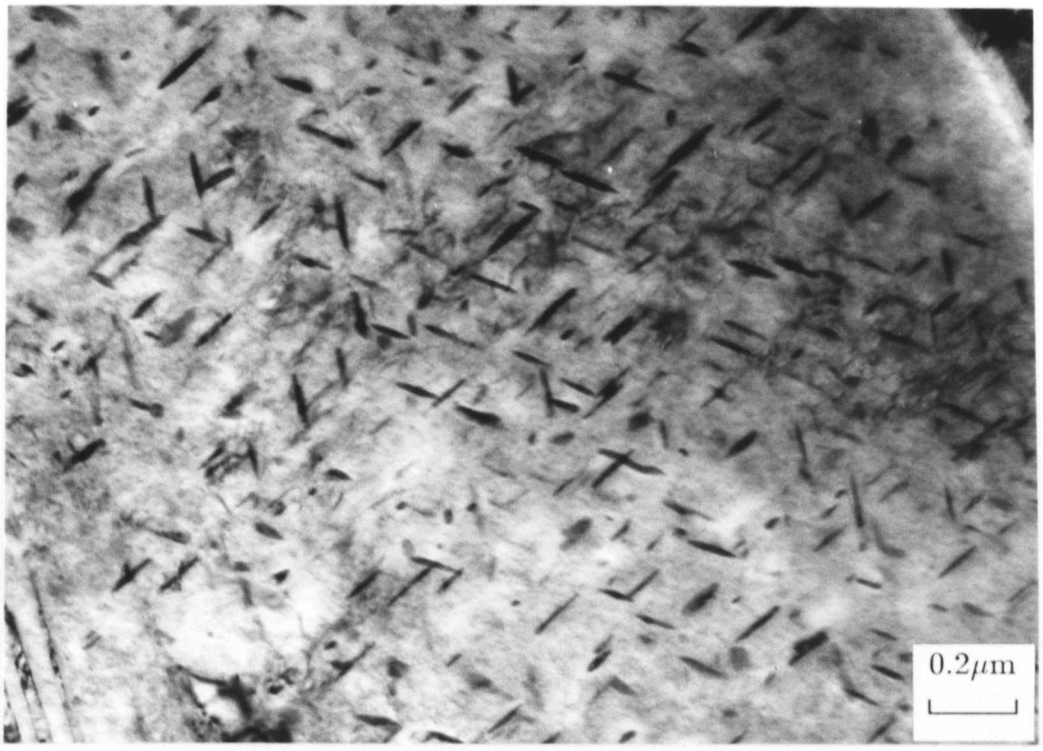

Figure 5.13: High magnification image illustrating a tempered martensite lath in a specimen austenitised at 1050°C for 15 mins followed by isothermal transformation at 400°C for 30 mins. Note that the cementite precipitates in more than one orientation to the martensite lath.

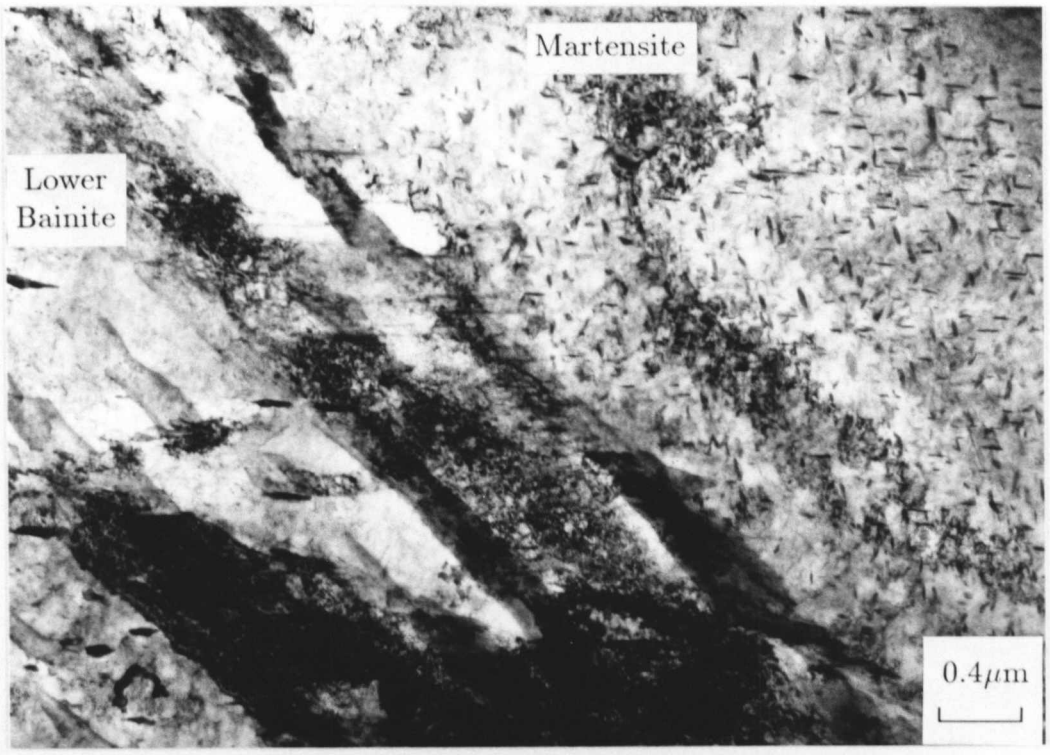

Figure 5.14: A clear illustration of the differences between a coarse martensite lath and smaller plates of lower bainite, particularly with respect to the cementite precipitation.

the observed volume fractions of allotriomorphic ferrite are approximately 0.5, 0.25 and 0.15 respectively. The difference between the three specimens is only the time before the removal of the quenching gas at 700°C. These results are not understood because there was no evidence that any decarburisation had taken place. The desired volume fraction was $\simeq$50% and therefore subsequent specimens for production of the starting microstructures for the tempering heat treatments were heat treated under the same conditions as specimen 1. A TEM micrograph showing two adjacent grains of allotriomorphic ferrite within the bainitic/martensitic matrix is presented in Figure 5.19.

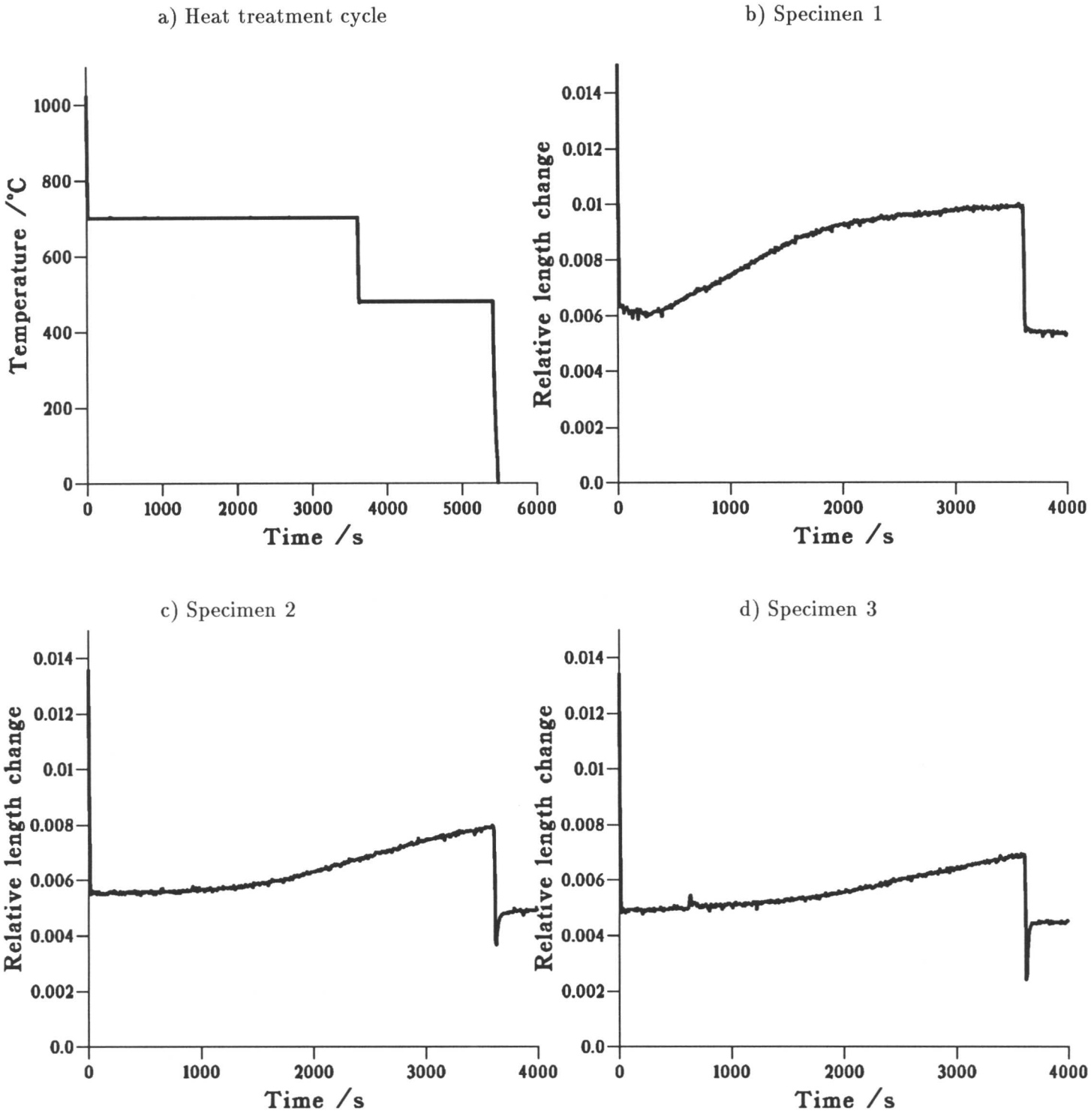

Figure 5.15: a) Heat treatment cycle and b)-d) graphs showing relative length change against time for specimens 1, 2 and 3 heat treated in the thermomechanical simulator to produce mixed microstructures of allotriomorphic ferrite and bainite.

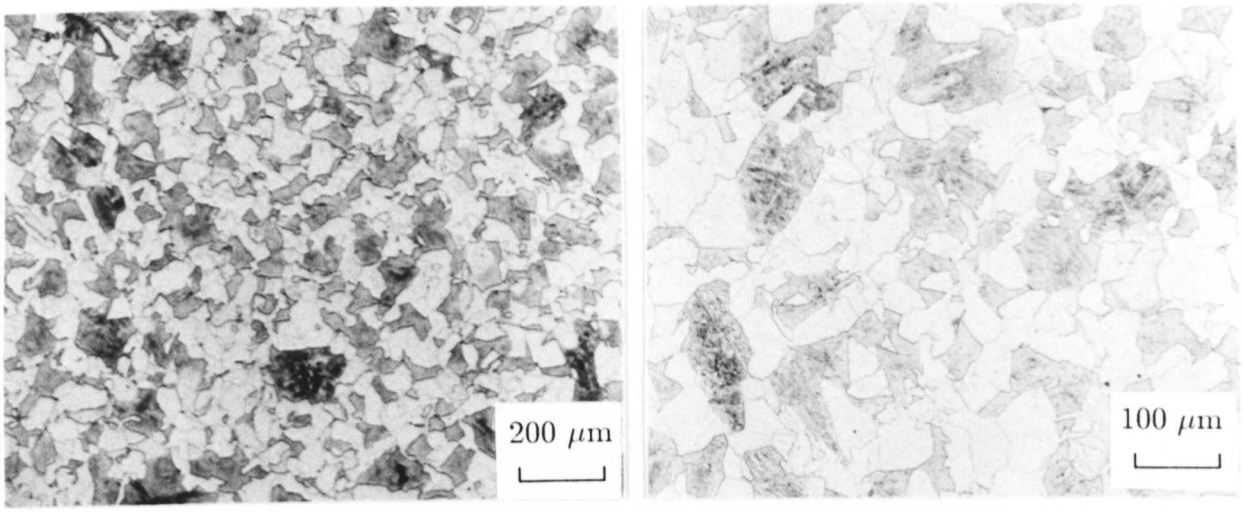

Figure 5.16: Optical micrographs of specimen 1 – Heat treated in the thermomechanical simulator – Austenitised 1050°C 15 minutes, 700°C 1 hour and 480°C 30 minutes. Gas cooled.

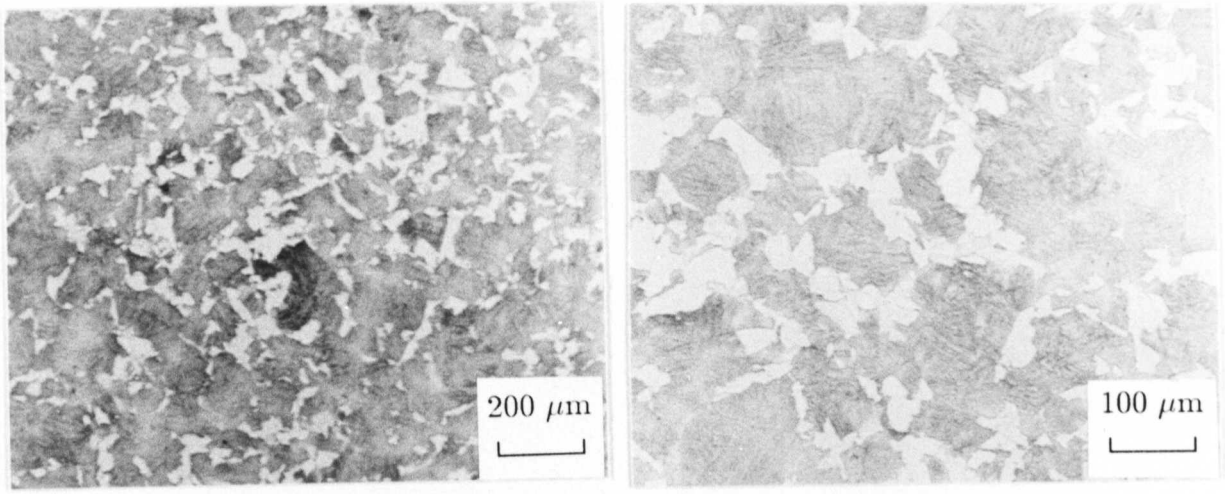

Figure 5.17: Optical micrographs of specimen 2 – Heat treated in the thermomechanical simulator – Austenitised 1050°C 15 minutes, 700°C 1 hour and 480°C 30 minutes. Gas cooled.

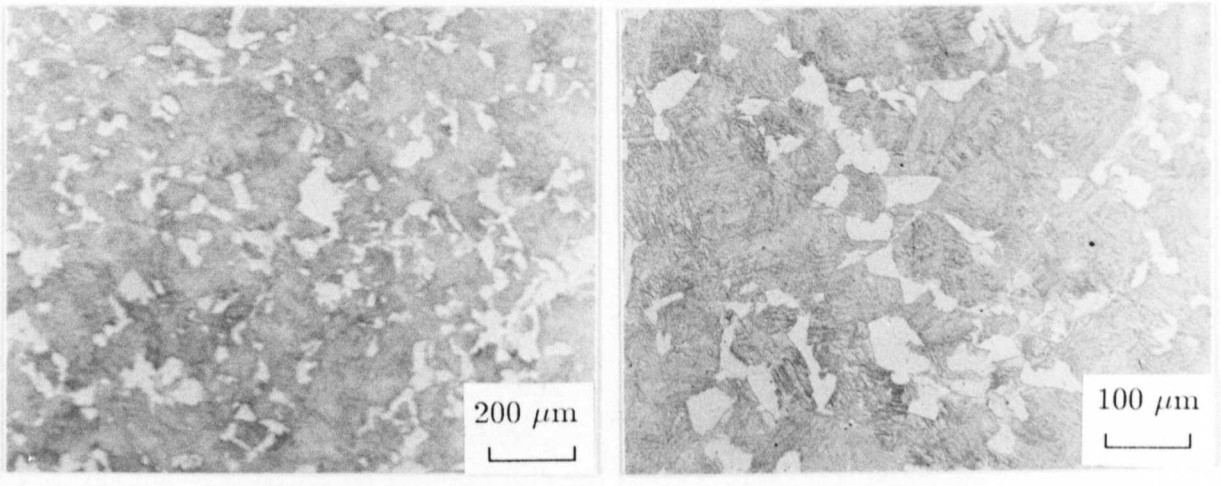

Figure 5.18: Optical micrographs of specimen 3 – Heat treated in the thermomechanical simulator – Austenitised 1050°C 15 minutes, 700°C 1 hour and 480°C 30 minutes. Gas cooled.

5.4 Tempering heat treatments

Prior to entering service $2\frac{1}{4}$Cr1Mo steel is usually given a stress–relief heat treatment at 700°C for varying times depending on the specimen size. In these experiments the stress–relief heat treatment was not given. The main purpose of the experimental work was to investigate changes in cementite composition, both with time and with the onset of alloy carbide precipitation, with a view to improving predictive models for $\frac{1}{2}$Cr$\frac{1}{2}$Mo$\frac{1}{4}$V and 1Cr$\frac{1}{2}$Mo steels rather than predicting the remanent life of $2\frac{1}{4}$Cr1Mo steel *per se*.

5.4.1 Calculation of the enrichment rate of cementite in $2\frac{1}{4}$Cr1Mo steel

Power stations operate at temperatures close to 565°C, and therefore it was decided to temper the majority of the specimens at this temperature. Specimens were also tempered at 620°C and 510°C, being 55°C above and below this temperature, in order to investigate the temperature dependence of enrichment rates. Suitable tempering times at these temperatures were chosen with the aid of the computer model described in chapter 3. MTDATA calculations were carried out to determine the equilibrium chromium content in cementite and ferrite at these three temperatures. Cementite and ferrite were the only phases allowed to exist in the MTDATA calculations, and therefore the predicted rates of cementite enrichment do not take into consideration the effect of alloy carbide precipitation. This point will be discussed later on in this chapter.

The calculated equilibrium chromium levels in cementite and ferrite at the temperatures of the tempering heat treatments are presented in Table 5.2. The predicted volume fraction of cementite was 0.022; this was almost independent of temperature in the range of interest. Finite difference calculations were then carried out using these calculated equilibrium values to set the interface concentrations. The calculations assumed an average particle size of 60 nm, determined by preliminary TEM investigations. The results of the calculations are presented in Figure 5.20.

Table 5.2: Equilibrium chromium levels in cementite and ferrite calculated using MTDATA at temperatures 510, 565 and 620°C.

Temperature /°C	Cementite		Ferrite	
	At.%	Wt.%	At.%	Wt.%
510	51.51	61.99	0.95	0.88
565	45.22	53.99	1.13	1.05
620	38.91	46.11	1.32	1.23

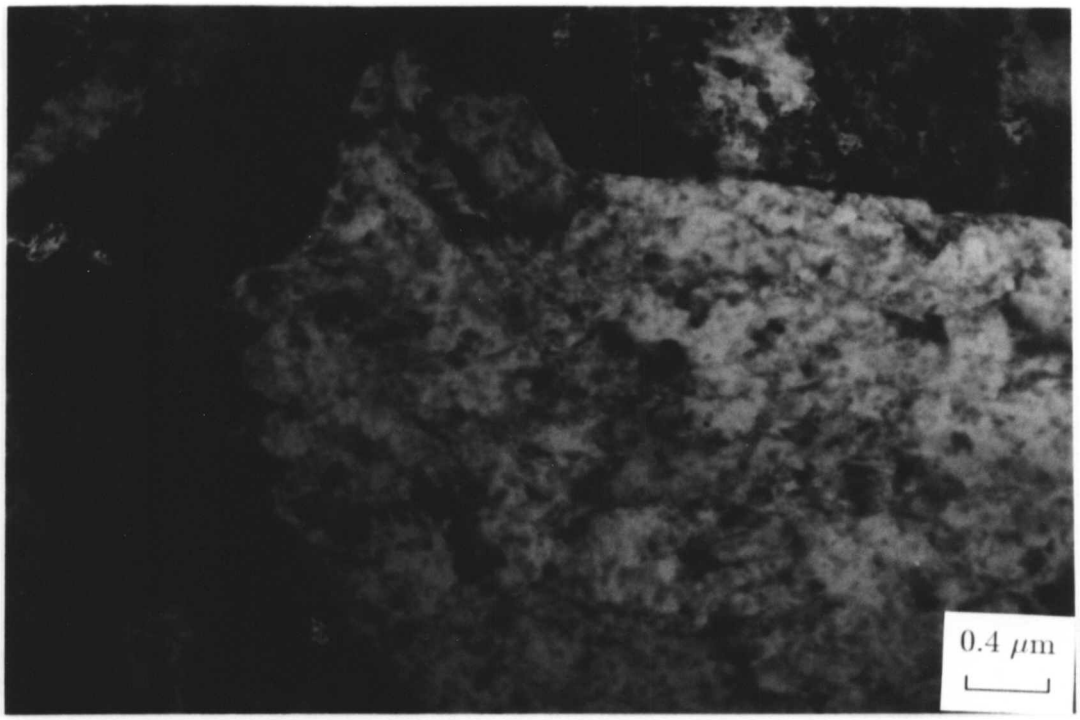

Figure 5.19: A transmission electron micrograph showing two adjacent grains of allotriomorphic ferrite within the bainitic/ martensitic matrix – Austenitised 1050°C 15 minutes, 700°C 1 hour and 480°C 30 minutes.

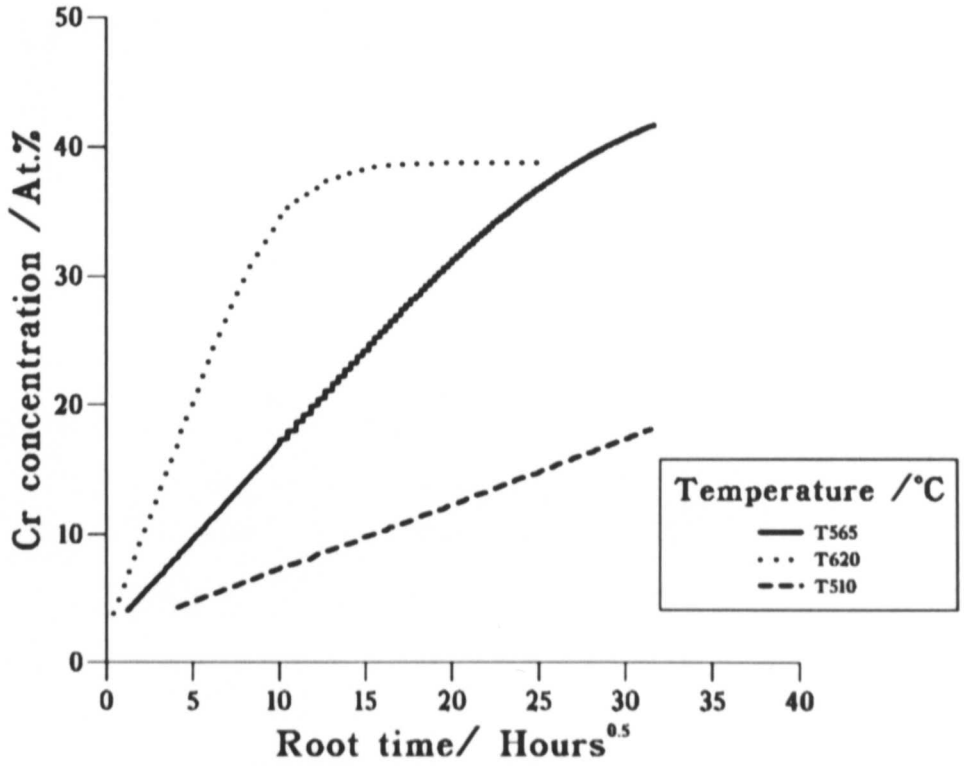

Figure 5.20: Calculated rate of cementite enrichment at 510, 565 and 620°C using finite difference model.

5.4.2 Tempering times for bainitic microstructures

The tempering times at temperatures 510, 565 and 620°C decided upon using the results of the calculations described above are presented in Table 5.3.

Table 5.3: Tempering heat treatment temperatures and times for the bainitic specimens

Temperature /°C	Time /Hours
510	1, 128, 256
565	$\frac{1}{6}$, 1, 4, 7, 32, 64, 128, 178, 239, 512, 1048, 2072
620	1, 10, 25

5.4.3 Tempering times for mixed microstructures

The mixed microstructures were tempered at 565°C only because the purpose of this investigation was to determine any changes in the rate of enrichment compared with the fully bainitic microstructures and therefore to study the effect of temperature was not the main purpose of the investigation. These specimens were tempered for a few times, given in Table 5.4, covering the range during which cementite was known to exist in the fully bainitic specimens.

Table 5.4: Tempering heat treatment temperatures and times for the mixed microstructure specimens

Temperature /°C	Time /Hours
565	1, 46.5, 80, 128, 180

5.5 Results and discussion from bainitic microstructures

5.5.1 Hardness measurements

Macrohardness measurements on all the bainitic specimens are presented in Figure 5.21. The starting hardness was 373 HV, which then decreased gradually as tempering proceeded. For the series of specimens tempered at 565°C there was a peak in hardness observed corresponding to the precipitation of M_2C after 32 hours, and a slight peak possibly corresponding to the precipitation of M_7C_3 after 128 hours. The specimens tempered at 510°C and 620°C showed slower and faster drops in hardness respectively compared with those tempered at 565°C. This is to be expected as microstructural changes will be accelerated as the temperature is increased.

5.5.2 Microstructural evolution during tempering at 565°C

Changes in the microstructure observed optically with tempering at 565°C were slight. This is demonstrated in Figure 5.22 which shows an optical micrograph for the specimen tempered

for 2072 hours. The bainitic and martensitic regions are, however, more distinguishable than in the microstructure prior to tempering.

The evolution of carbides within the different regions of the microstructure was extensively studied on carbon extraction replicas. Detailed microanalyses from the carbide particles are discussed in section 5.5.3. A TEM image from a carbon extraction replica of the specimen tempered at 565°C for 10 minutes is presented in Figure 5.23, and from a thin foil in Figure 5.24. Both illustrate the early stages of carbide precipitation. The micrograph from the thin foil illustrates a plate of martensite which has begun to precipitate cementite in three distinct orientations on tempering. The replica image illustrates cementite plates precipitating parallel to the direction of the bainitic sheaves; this is probably from the carbon rich retained austenite in between the upper bainite.

Figure 5.25 shows that further cementite precipitation has occurred after tempering for 64 hours. It would seem that not all the cementite precipitates immediately after isothermal transformation, but that there is further precipitation as tempering proceeds; any cementite precipitating after tempering for some time may not have an initial composition given exactly by a paraequilibrium mode of formation.

Figure 5.26, Figure 5.27 and Figure 5.28 illustrate the microstructure after tempering for 128 hours. Figure 5.26 is a very low magnification TEM image showing carbide particles delineating lath boundaries in the bainitic and martensitic regions. The bars across the image are the copper grid on which the replica is supported. Figure 5.27 illustrates cementite precipitation which occurs in the martensitic regions in the Widmanstätten pattern usually associated with the tempering of alloy martensites. Figures 5.28a) and b) are low and high magnification images respectively showing that cementite precipitation occurs in the bainitic regions mainly on the boundaries of the sheaves, whereas there is extensive precipitation of needle–shaped M_2C within the sheaves coexisting with only a few cementite particles. The fine M_2C needles also precipitate in a regular Widmanstätten array.

The difference in the precipitation behaviour within the bainitic and martensitic regions becomes more marked after tempering for 178 hours. The cementite in the martensitic regions continues to enrich with respect to all the substitutional solute elements. The low and high magnification images in Figure 5.29a) and b) illustrate this dense cementite precipitation in regular Widmanstätten arrays. There are very few needles of M_2C carbide within the vicinity of this cementite. Convergent beam and selected area electron diffraction patterns are presented in Figure 5.29c) and d), confirming that the carbide with this composition is cementite. The typical composition of the cementite in these regions measured by EDX (not allowing for the

carbon concentration) is

25 wt.% Cr, 5 wt.% Mn, 7 wt.% Mo, and 63 wt.% Fe.

Precipitation in the bainitic regions is illustrated in Figure 5.30. There is extensive precipitation of M_2C within the sheaves. The cementite in between the sheaves appears to have dissolved to some extent compared with Figure 5.28a) showing cementite in a similar position after tempering for 128 hours. The M_2C actually contains a considerable amount of dissolved chromium, a typical composition being

25 wt.% Cr, 0.5 wt.% Mn, 70.5 wt.% Mo, and 4 wt.% Fe.

It was found that the cementite adjacent to the regions of M_2C precipitation had a different composition from that in the martensitic regions. The average composition was

16 wt.% Cr, 6 wt.% Mn, 0.5 wt.% Mo, and 77.5 wt.% Fe,

from which it can be seen that the Mo content is reduced to almost nothing, and the Cr content has also been reduced by a significant amount. Two such cementite particles are marked with arrows in Figure 5.30b). It would appear that the precipitation of the more thermodynamically stable M_2C has drawn both Mo and Cr from the less stable cementite, which has started to dissolve. It was confirmed by selected area electron diffraction (Figure 5.30c) that the carbide with a lower Mo content than that found in the martensitic regions was indeed still cementite. There were also a few larger Cr–rich particles found at the edges of some of the regions containing M_2C. These were identified as M_7C_3, and can be seen in the lower right of Figure 5.30a).

A thin foil was also examined made from the specimen tempered for 178 hours at 565°C. Figure 5.31 illustrates the upper bainitic sheaves dominant in the microstructure. A few cementite particles and a larger M_7C_3 particle can be seen on the lath boundaries; there is also extensive M_2C precipitation within the laths. Figure 5.32 illustrates a similar upper bainitic region; a large MnS inclusion can be seen within the microstructure, and there is extensive cementite precipitation on the plate boundaries and M_2C within the sheaves. Figure 5.33 is a nice illustration of the differences between the different regions of the microstructure. There is dense cementite precipitation in the martensitic region and much finer M_2C precipitation in the bainitic region. A selected area electron diffraction pattern is illustrated in Figure 5.34. The larger spots are from ferrite, and the smaller spots in between from the cementite within the martensitic region. The pattern exhibits the well known Bagaryatski (1950, cited by Bhadeshia, 1992) orientation relationship for cementite in tempered martensite:–

$$\{001\}_\theta \parallel \{211\}_{\alpha'}$$

$$< 100 >_{\theta} \| < 0\bar{1}1 >_{\alpha'} .$$

After 238.5 hours the microstructure consists predominantly of M_7C_3 and M_2C. The cementite in the bainitic regions has been completely replaced by M_2C with some larger M_7C_3 particles on the boundaries between sheaves. Some cementite with the higher chromium remains in the martensite, although there is also precipitation of M_7C_3 on the edges of these regions. This is illustrated in Figure 5.35a). A selected area electron diffraction pattern from an M_7C_3 particle is presented in Figure 5.35b); characteristic streaks from the presence of stacking faults in the structure (discussed in Chapter 2) are clearly visible. The specimens tempered for 512 and 1048 hours (Figure 5.36 and Figure 5.37 respectively) showed further precipitation of M_7C_3 at the expense of the martensitic cementite. All the cementite had dissolved in the specimen tempered for 1048 hours. There was a slight enrichment of the M_7C_3 with respect to the chromium concentration with increasing tempering time; this is discussed in section 5.5.4. After 2072 hours the M_7C_3 precipitates have coarsened slightly (Figure 5.38). The carbide M_6C has also begun to precipitate at the expense of some of the M_2C needles which have dissolved. This is illustrated in Figure 5.39a) which shows aligned M_2C carbides together with some smaller, squarer particles which have been identified by selected area electron diffraction as M_6C (Figure 5.39b). A selected area diffraction pattern from the M_2C needles is also presented in Figure 5.39c). The needles of M_2C were too fine to take selected area electron diffraction patterns, except from a cluster, prior to this tempering time.

It has been shown above that the carbide type is very sensitive to position within a given microstructure. After a short period of tempering M_2C dominates within the bainitic plates, whereas mixtures of M_2C, M_7C_3 and M_3C are to be found at the bainite plate boundaries and predominantly M_3C in the martensitic regions. This is probably because far less carbon is available within the upper bainitic plates, whereas the plate boundaries are the sites for cementite precipitation during the growth of upper bainite. More carbon is available (in the form of cementite, or dissolved in carbon–enriched retained austenite) in the vicinity of the plate boundaries which can stimulate the formation of a variety of alloy carbides.

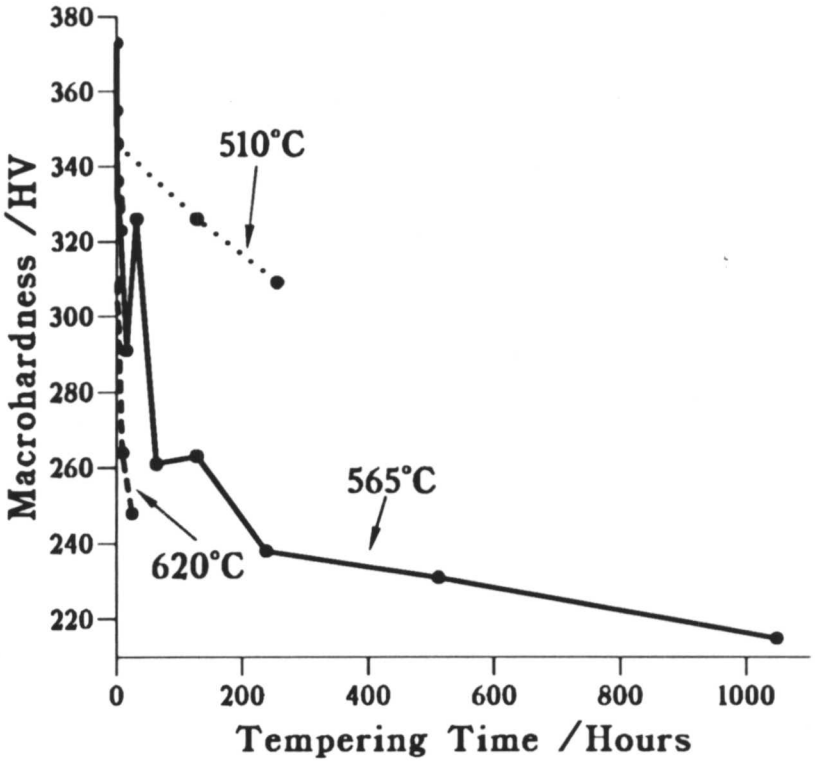

Figure 5.21: Macrohardness measurements as a function of time for specimens tempered at 510, 565 and 620°C.

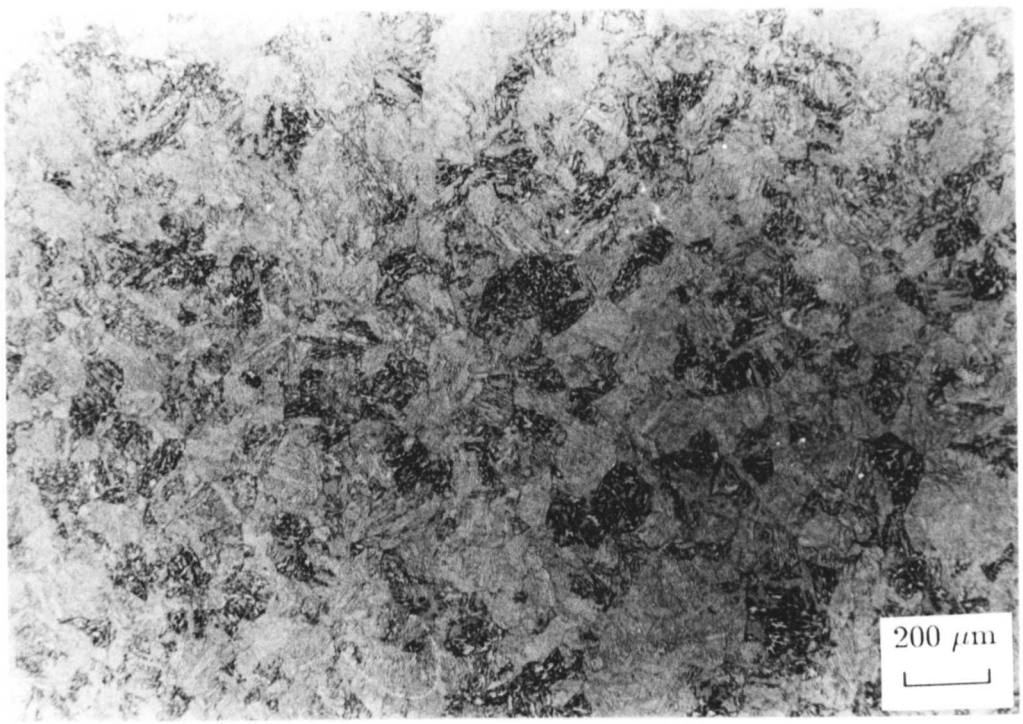

Figure 5.22: Optical microstructure from the fully bainitic specimen tempered for 2072 hours at 565°C.

Figure 5.23: Carbon extraction replica from the fully bainitic specimen tempered for 10 minutes at 565°C showing that cementite has begun to precipitate, in particular in between and parallel to the plates of upper bainite.

Figure 5.24: Transmission electron micrograph from a thin foil specimen from the fully bainitic specimen tempered for 10 minutes at 565°C showing a plate of tempered martensite containing cementite in three distinct orientations.

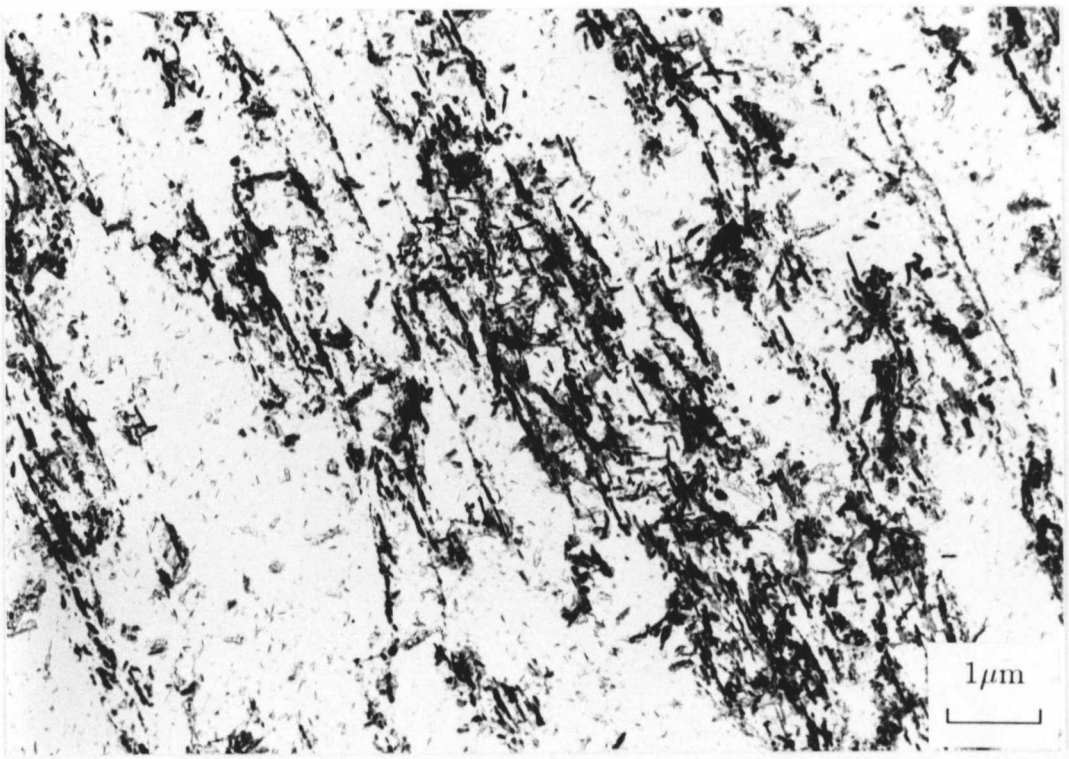

Figure 5.25: Carbon extraction replica from the fully bainitic specimen tempered for 64 hours at 565°C.

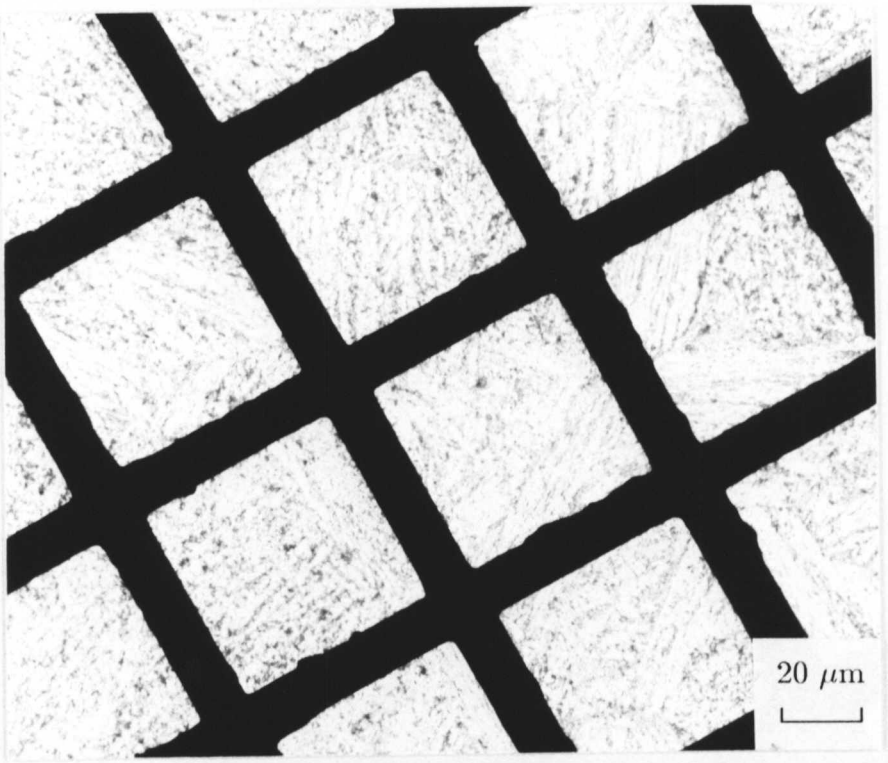

Figure 5.26: Low magnification transmission electron micrograph showing carbide particles delineating lath boundaries in the bainitic and martensitic regions after tempering at 565°C for 128 hours. The grid bars across the image are the copper grid on which the replica is supported.

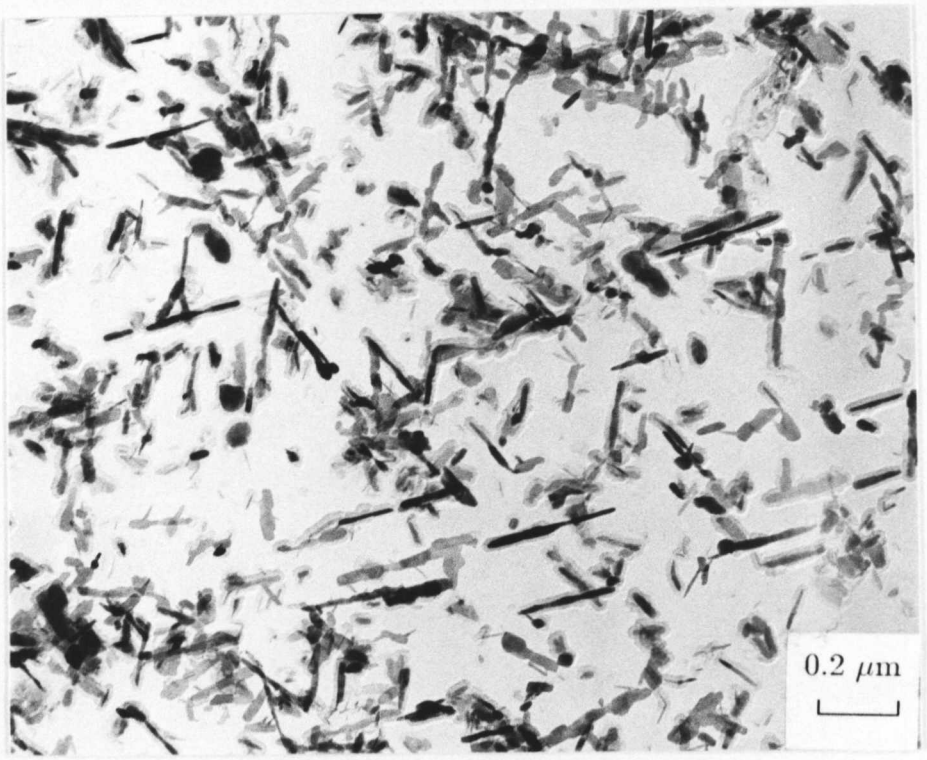

Figure 5.27: Cementite precipitation in the martensitic regions of a specimen tempered for 128 hours at 565°C in a Widmanstätten array.

a)

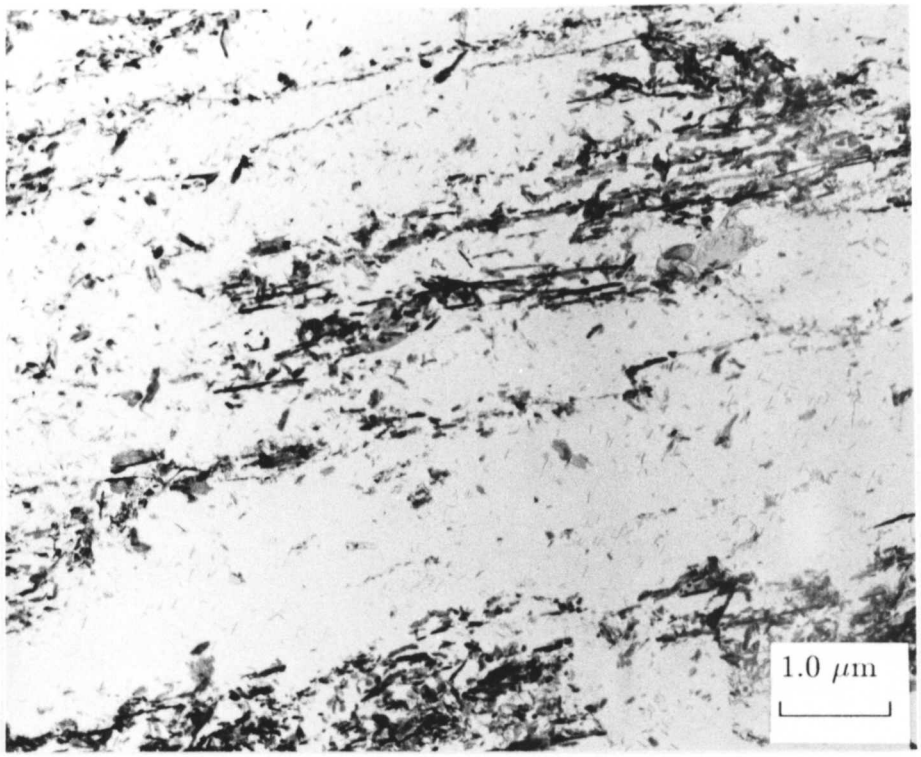

b)

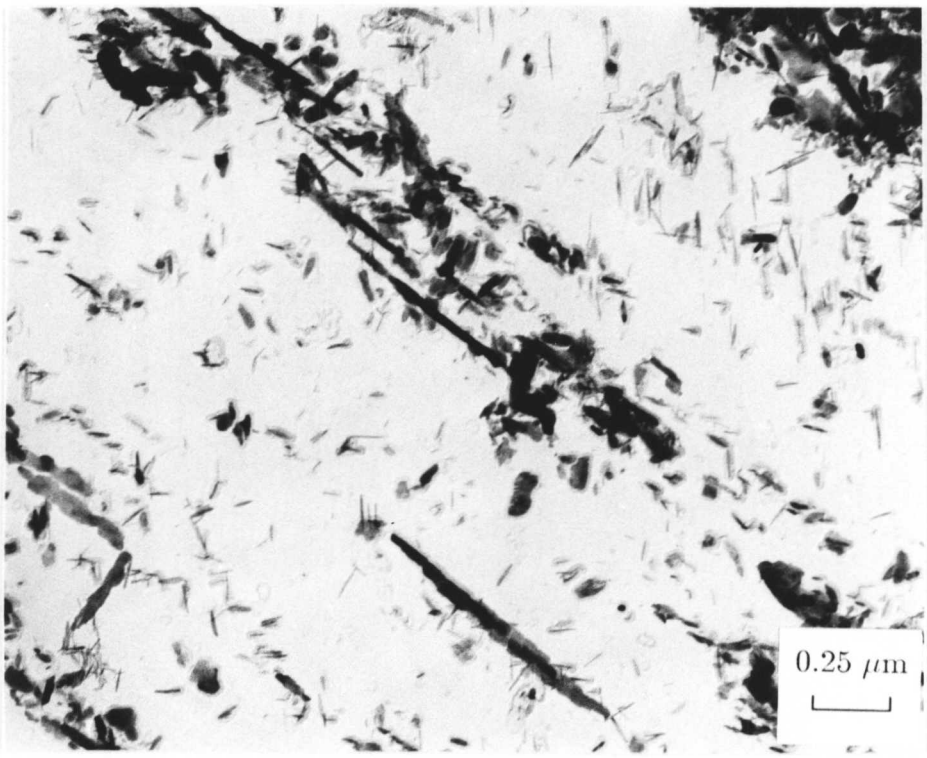

Figure 5.28: a) Low and b) high magnification carbon extraction replicas from the specimen tempered at 565°C for 128 hours showing cementite precipitation on the boundaries of the bainitic regions which contain extensive precipitation of M_2C needles in a Widmanstätten array.

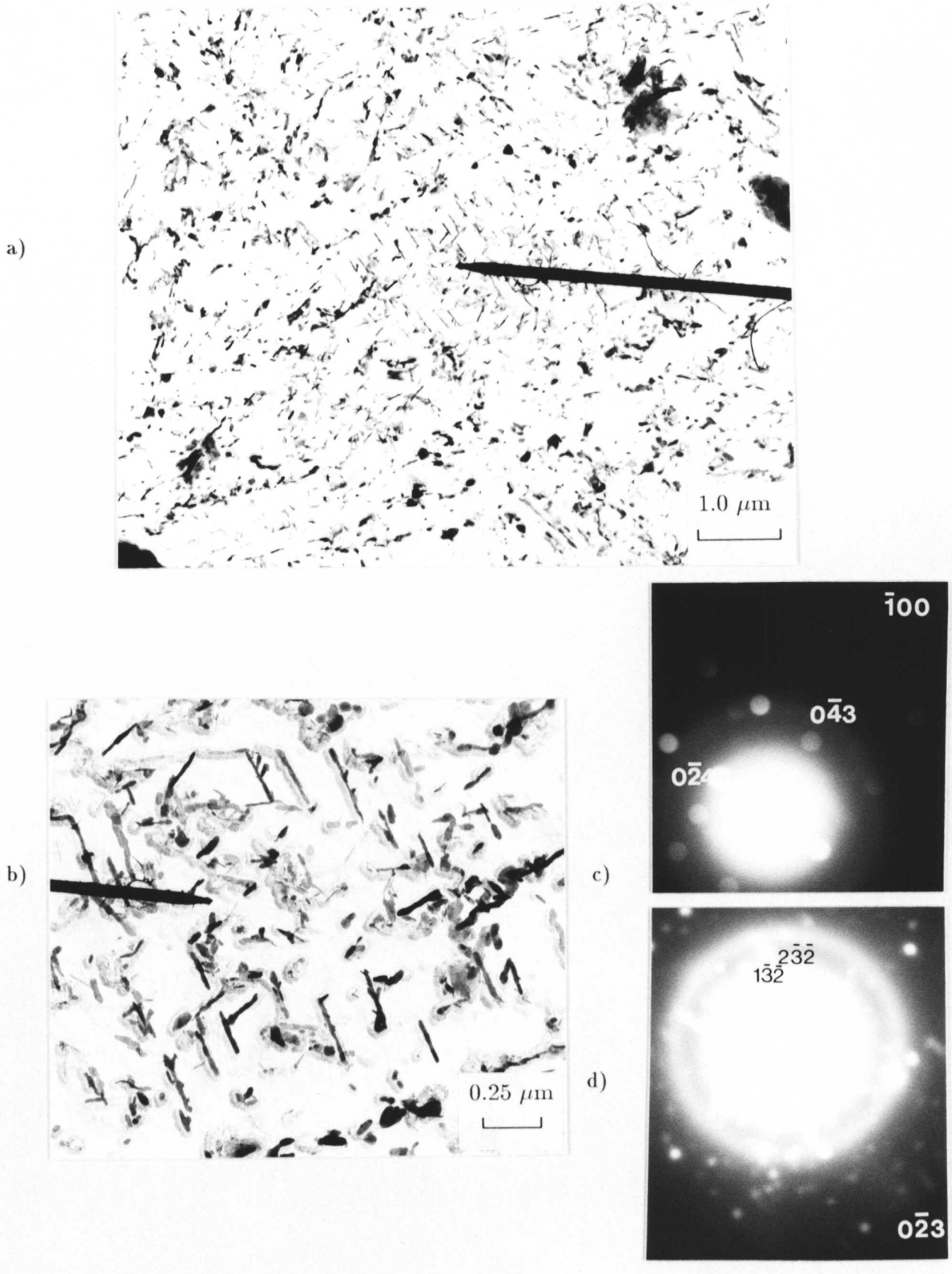

Figure 5.29: Low a) and high b) magnification transmission electron micrographs illustrating dense cementite precipitation in Widmanstätten arrays in martensitic regions of specimens tempered for 178 hours at 565°C. Convergent beam c) and selected area d) electron diffraction patterns from cementite particles in this region.

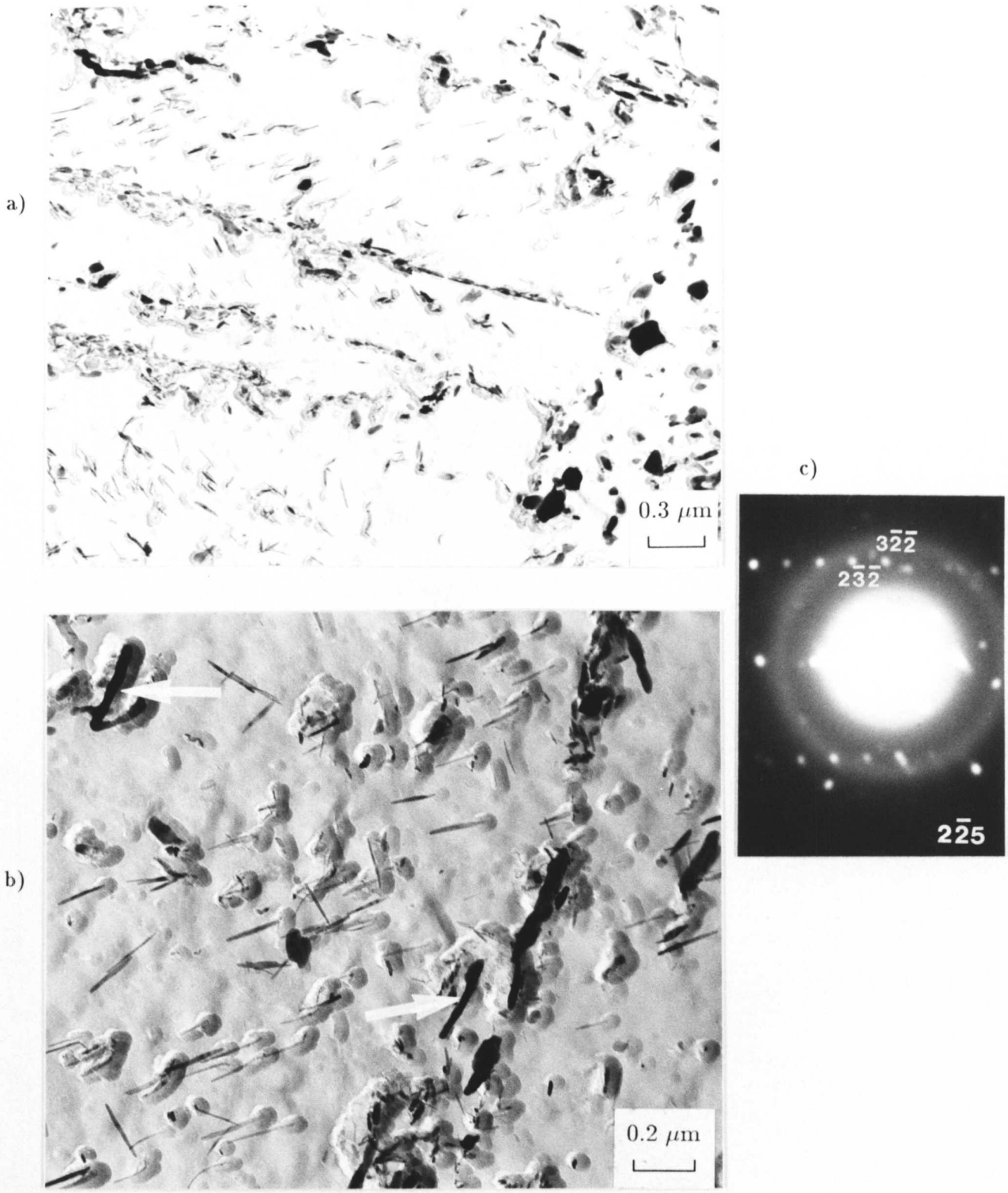

Figure 5.30: Low a) and high b) magnification transmission electron micrographs illustrating extensive M_2C precipitation between bainitic sheaves for specimens tempered for 178 hours at 565°C. The two carbides marked with arrows in b) contain virtually no Mo. A selected area electron diffraction pattern c) confirms that these particles are cementite.

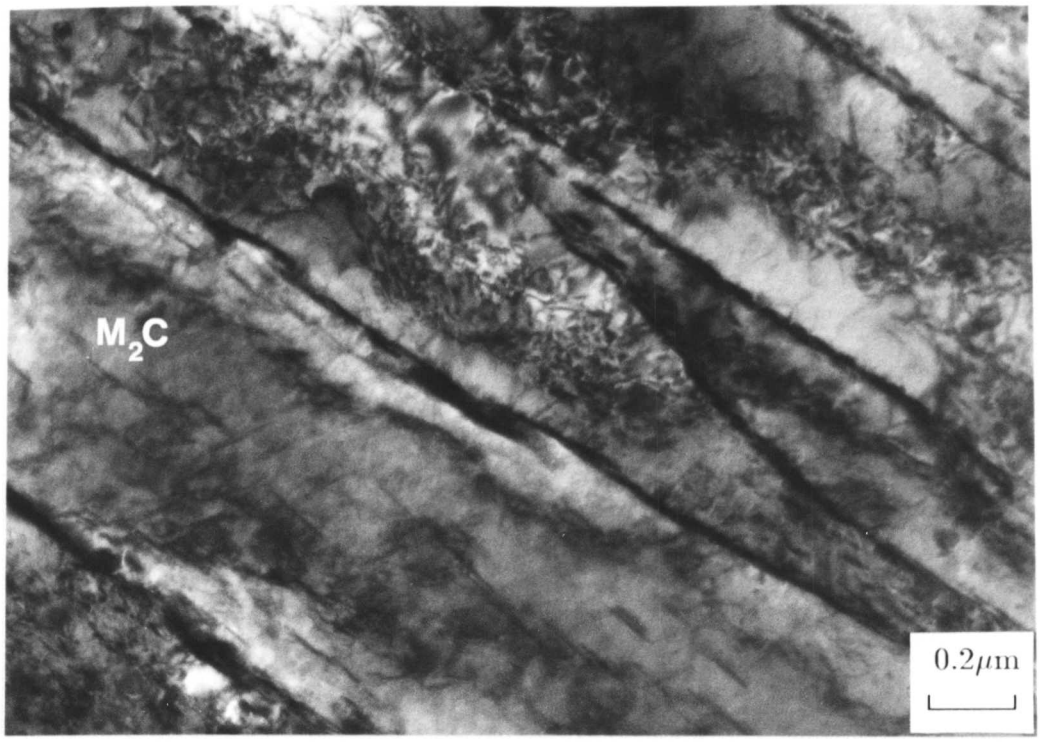

Figure 5.31: Transmission electron micrograph from a thin foil from a specimen tempered for 178 hours at 565°C showing the upper bainitic sheaves dominant in the microstructure. A few cementite particles and a larger M_7C_3 particle can be seen on the lath boundaries; there is also extensive Mo_2C precipitation within the sheaves.

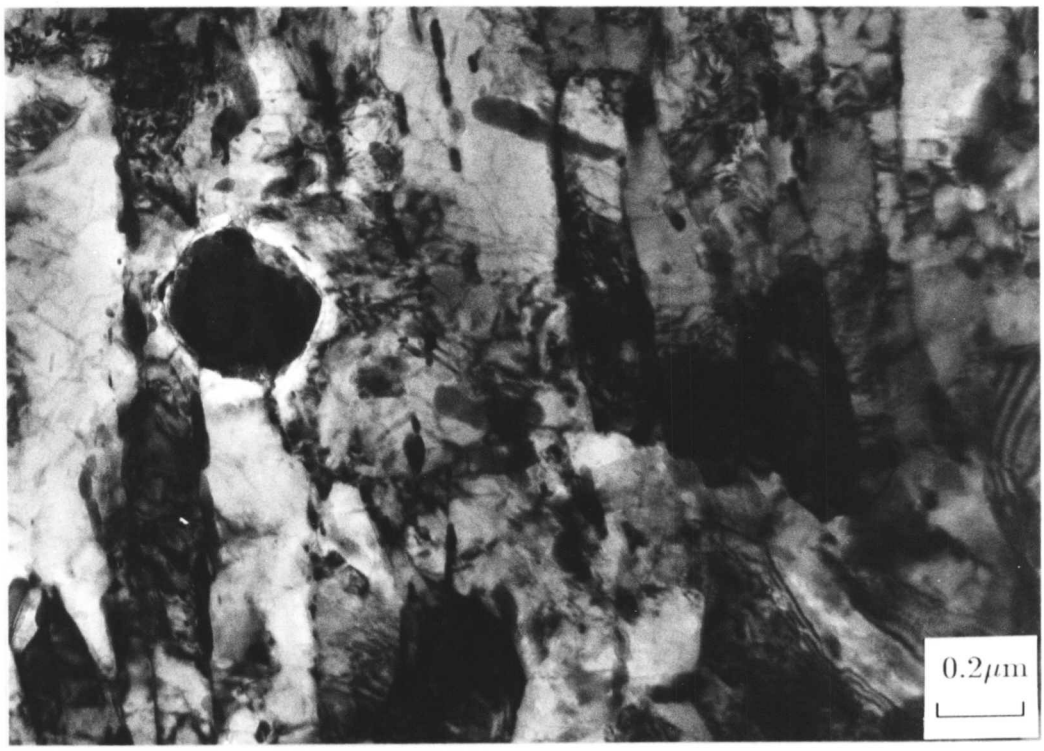

Figure 5.32: A similar upper bainitic region; a large MnS inclusion can be seen within the microstructure, and there is extensive cementite precipitation on the plate boundaries and Mo_2C within the sheaves.

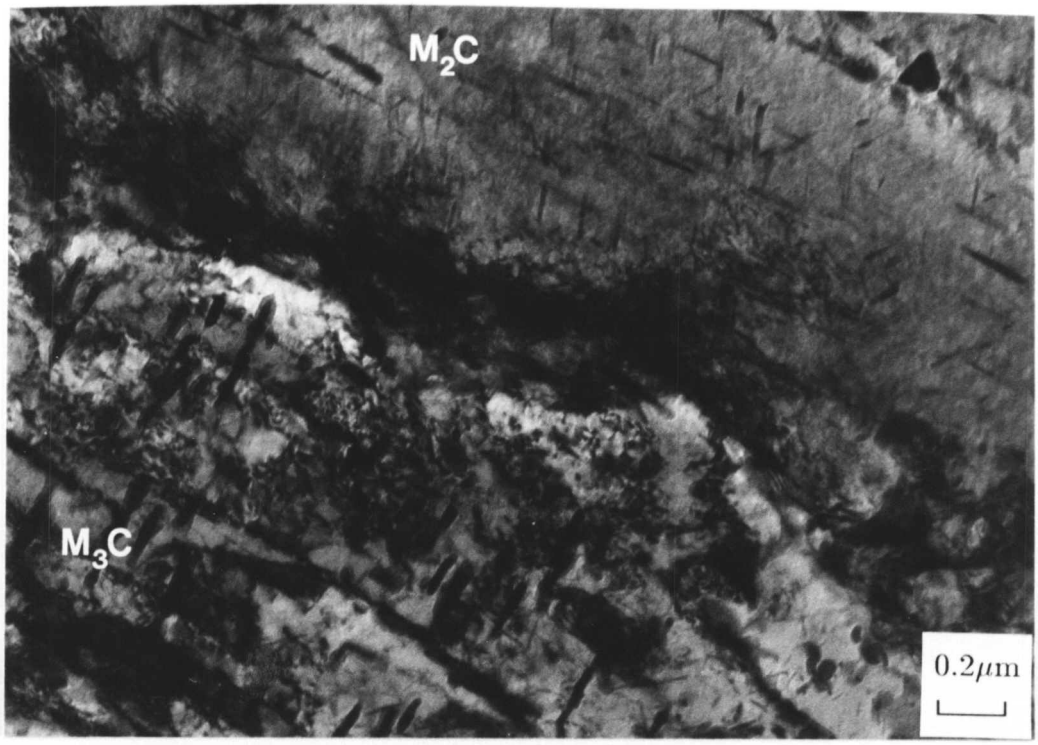

Figure 5.33: A thin foil from the specimen tempered for 178 hours at 565°C illustrating the differences between the different regions of the microstructure. There is dense cementite precipitation in the martensitic region and much finer Mo_2C precipitation in the bainitic region.

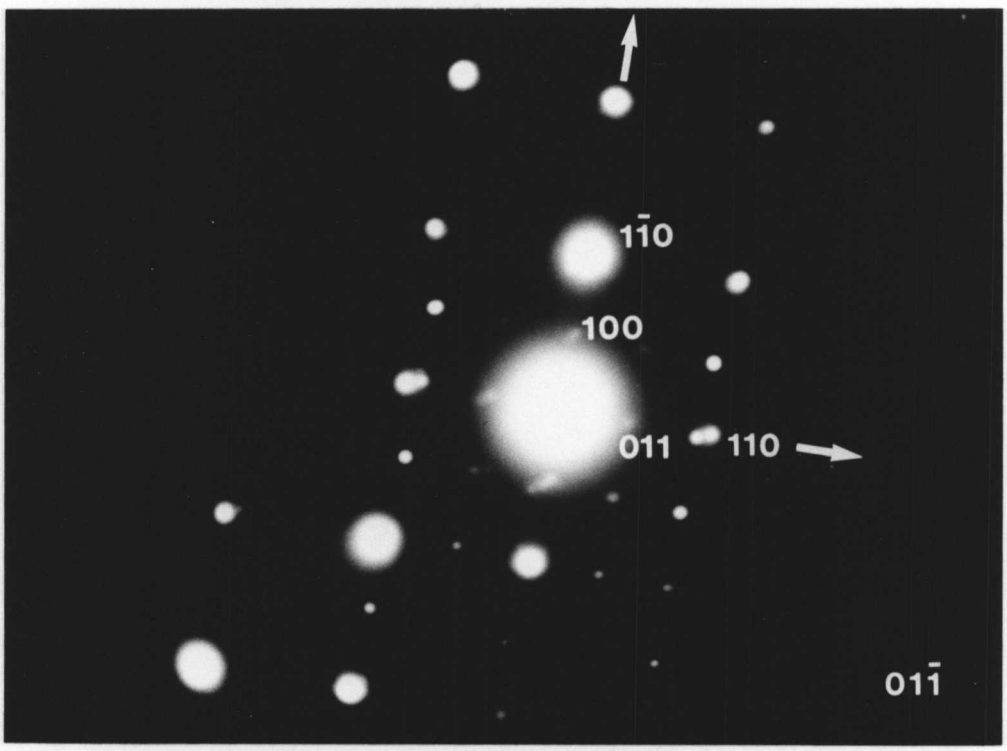

Figure 5.34: A selected area electron diffraction pattern from the martensitic region exhibiting the well known Bagaryatski (1950) orientation relationship.

a)

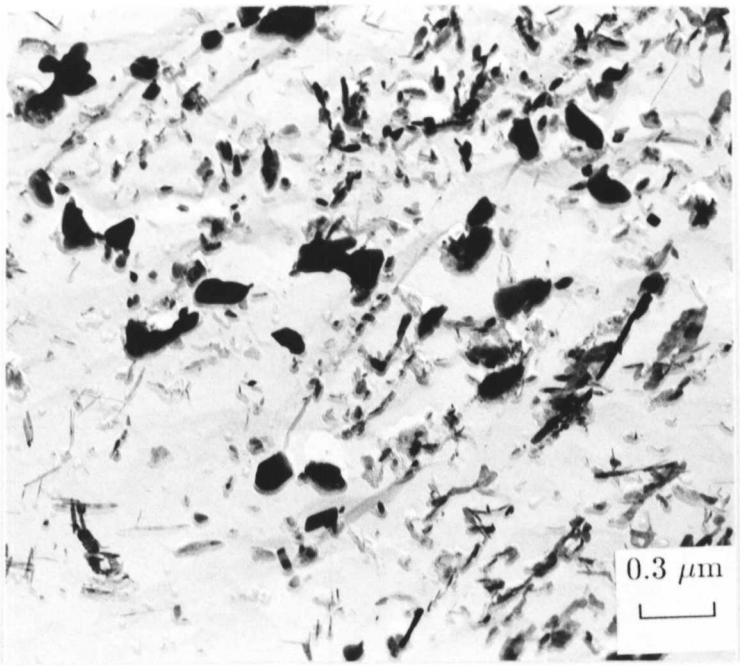

b)

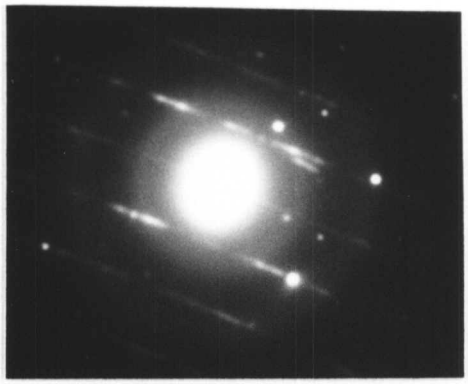

Figure 5.35: a) Carbon extraction replica from a specimen tempered for 238.5 hours at 565°C illustrating that the microstructure consists predominantly of M_7C_3 and M_2C. b) A selected area electron diffraction from M_7C_3 showing characteristic streaks due to the presence of stacking faults within the lattice.

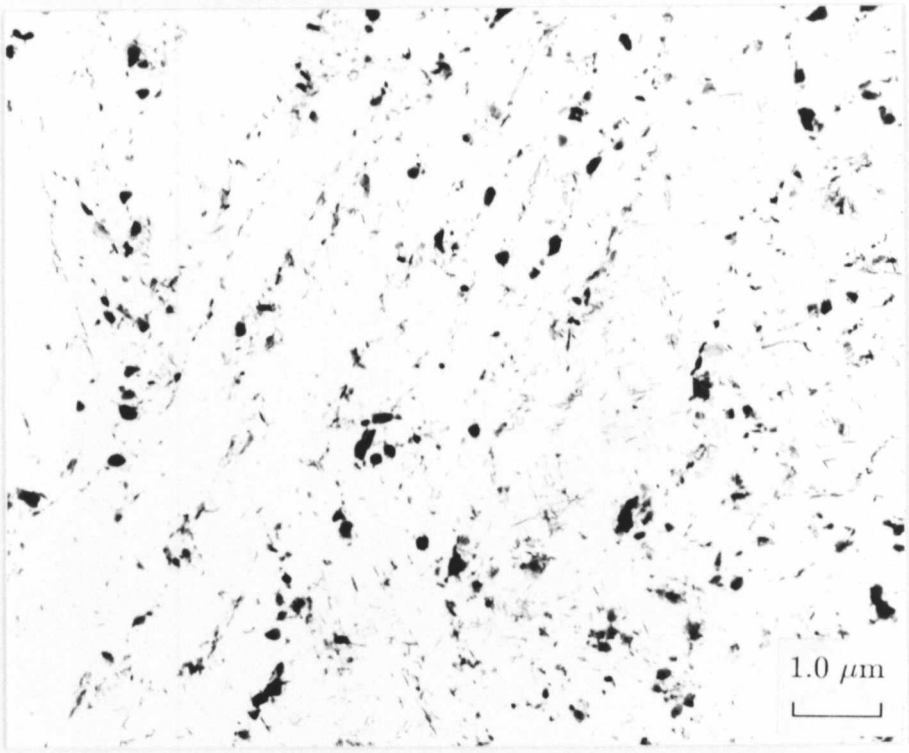

Figure 5.36: Carbon extraction replica from specimen tempered for 512 hours at 565°C, showing increasing precipitation of M_7C_3 at the expense of cementite.

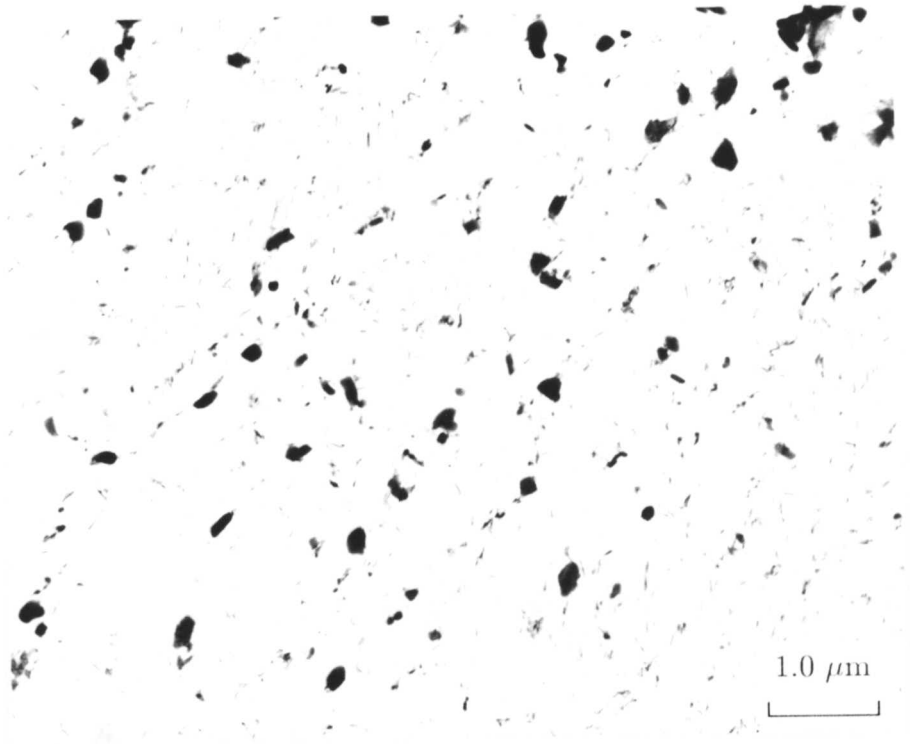

Figure 5.37: Carbon extraction replica from specimen tempered for 1048 hours at 565°C showing that the microstructure consists predominantly of large M_7C_3 and fine M_2C particles.

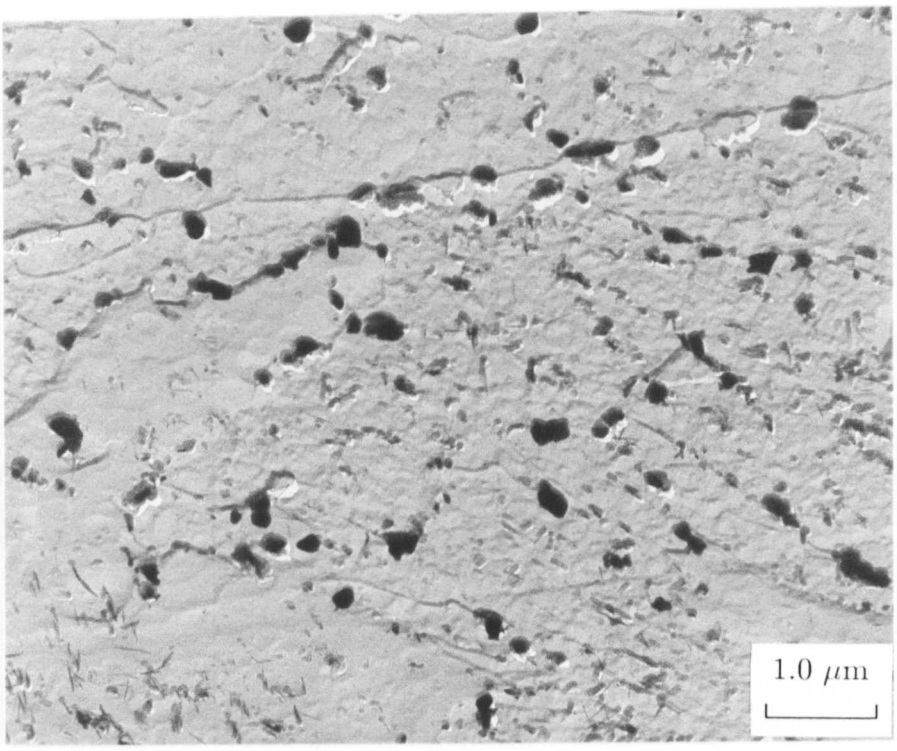

Figure 5.38: Carbon extraction replica from specimen tempered for 2072 hours at 565°C showing that the microstructure consists predominantly of large M_7C_3 and fine M_2C particles.

a)

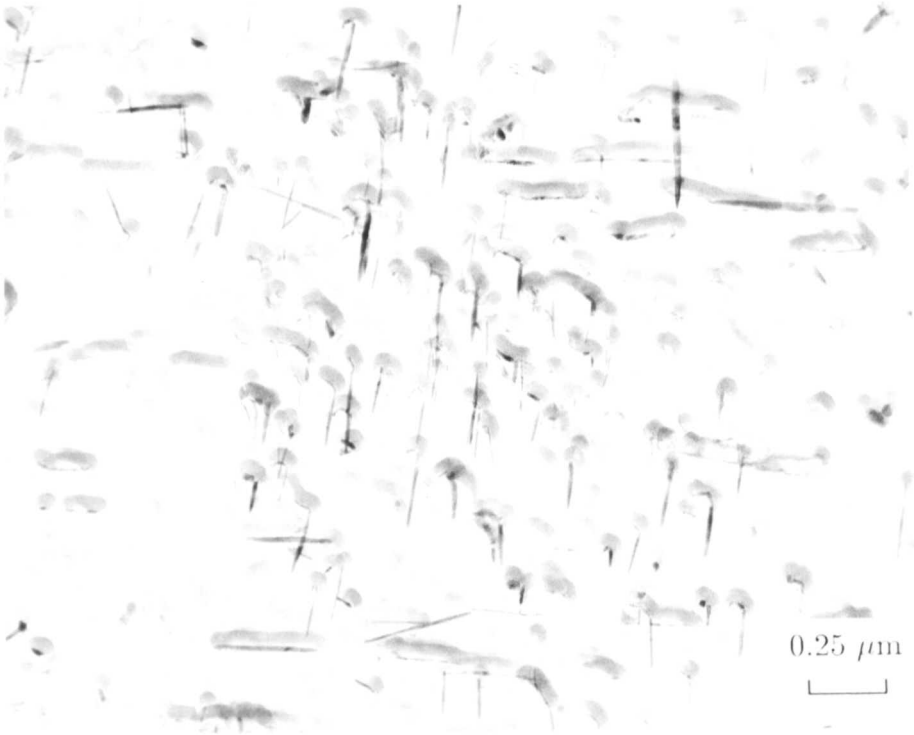

b)

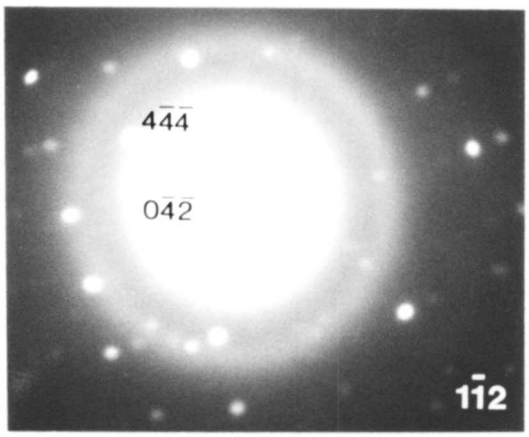

c)

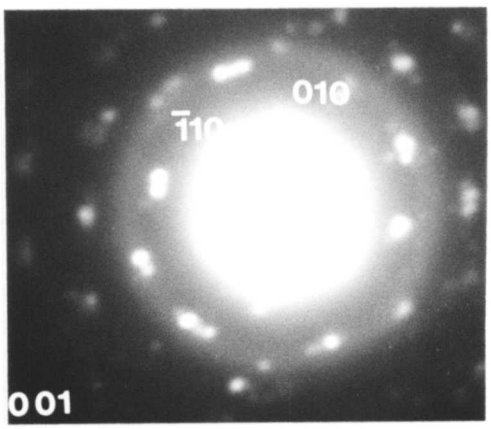

Figure 5.39: a) Carbon extraction replica from specimen tempered for 2072 hours at 565°C showing aligned M_2C particles with small, squarer M_6C carbides in between. Selected area electron diffraction patterns from M_6C carbides b) and a cluster of M_2C c).

5.5.3 EDX measurements of the Cr content of cementite at 565°C

The composition of isolated cementite particles was measured using EDX. A photograph was taken of each individual particle analysed in order to correlate the particle size with composition. Graphs are presented in Figure 5.40a)–g) showing the measured Cr concentration in cementite plotted as a function of the reciprocal particle size for the specimens tempered up to 128 hours at 565°C. The calculated regression line has been plotted on each graph. The correlation coefficient for each plot, the average particle size and the average Cr concentration are presented in Table 5.5.

Table 5.5: Summary of experimental measurements of Cr concentration and particle size for specimens tempered up to 178 hours at 565°C.

Tempering time /Hours	Correlation coefficient	Average Cr conc. /wt.%	Average particle size /nm
$\frac{1}{6}$	0.57	6.70	52
1	0.65	15.04	56
4	0.82	14.96	68
7	0.43	17.85	58
32	0.27	18.06	56
64	0.36	26.91	65
128	-0.05	25.30	65
178 (Martensitic)	–	24.57	72
178 (Bainitic)	–	16.34	75

It can be seen from the graphs that there is a definite trend for the smaller particles to be richer in Cr, although there is some scatter about the regression line. The correlation coefficient is observed to steadily increase with tempering time initially and then to decrease. This is to be expected because initially all the particles are formed under paraequilibrium conditions and have the same concentration as the matrix, then as tempering proceeds the smaller particles will enrich at a faster rate than large particles. This will initially result in an increase in the correlation coefficient, however, at increasing tempering times other effects dominate over the size dependence of the enrichment rate. These include the precipitation of alloy carbides with the subsequent dissolution of cementite in the bainitic regions of the specimens and soft impingement of the cementite particles as they approach the equilibrium concentration. The very poor correlation coefficient and scatter in the measured Cr concentrations for the 128 hour

specimen correspond with the precipitation of the Cr rich M_7C_3.

The measured Cr content of the cementite in the specimen tempered for 178 hours is presented separately in Figure 5.41a)–c). It has already been noted that two separate populations of cementite were observed in the bainitic and martensitic regions of the microstructure. Figure 5.41c) clearly shows the dichotomy of the cementite compositions; the upper points (marked with triangles) are from martensitic regions of the microstructure free from alloy carbide precipitation whereas the lower points (marked with circles) are from cementite particles in bainitic regions in which extensive alloy carbide precipitation has occurred. The two distributions are shown separately in Figure 5.41a) and b). The average Cr level in the martensitic and the bainitic regions are included in Table 5.5.

It has been shown that the Cr content of a cementite particle is dependent on its size. It is therefore important when finding the average Cr content after a given tempering time of a distribution of cementite particles to take an unbiased sample of particle sizes. To this end histograms have been plotted in Figure 5.42a)–f) showing the number of carbides analysed of different sizes for the specimens tempered for 10 minutes, 1, 4, 7, 32, and 64 hours at 565°C. Although the size distributions are not all identical, it is important to note that there is no significant bias for any of the tempering times towards smaller or larger particles.

5.5.4 Enrichment of M_7C_3 with tempering time

The carbide M_7C_3 was found to precipitate after tempering at 565°C for approximately 128 hours and then to coexist with cementite for some time before the cementite dissolves. The composition of the M_7C_3 was monitored along with the cementite by EDX. The average composition (measured from at least 10 particles per specimen and not taking into account carbon content) of the M_7C_3 is presented in Table 5.6. It was found that there was a gradual increase in the Cr concentration with tempering time from 58 to 65.5 wt.%. The Mn concentration was found to correspondingly decrease with tempering time. The Mo data as a function of tempering time were scattered. Some of the scatter can be attributed to the inherent difficulty in measuring the Mo content accurately with EDX because of the failure to account for absorption errors. It seems that the absolute level also depends on the particles surrounding the M_7C_3 particles. A similar effect to that already described for cementite particles in the vicinity of M_2C particles was observed; a few M_7C_3 carbides within clusters of M_2C needles contained very little molybdenum. No significant dependence of the composition on the particle size was observed for the M_7C_3 carbides for each tempering time.

Thermodynamic calculations were performed using MTDATA to investigate the equilibrium chromium levels of both M_7C_3 and $M_{23}C_6$ in equilibrium separately with ferrite. It was

a)

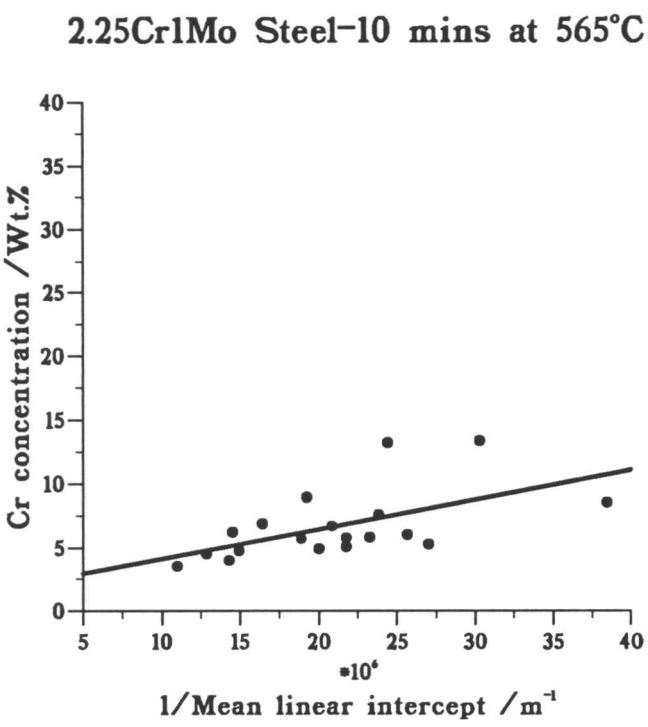

b)

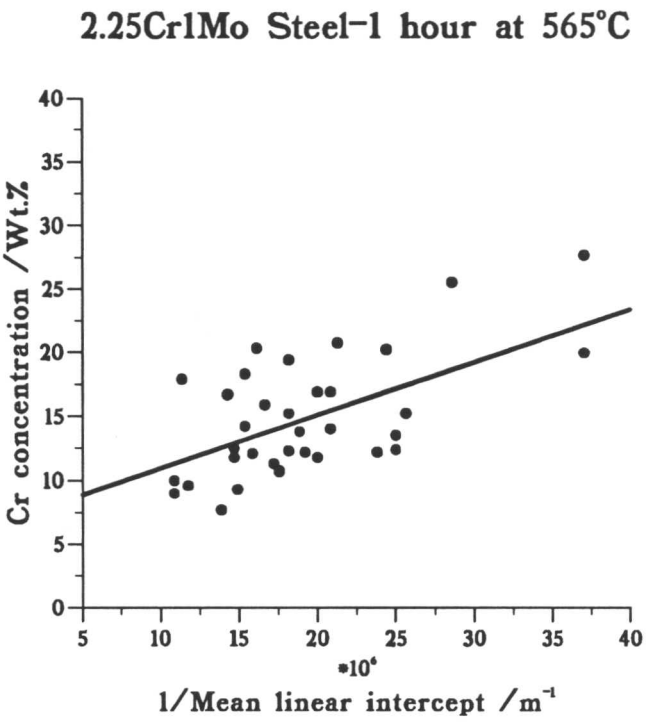

c)

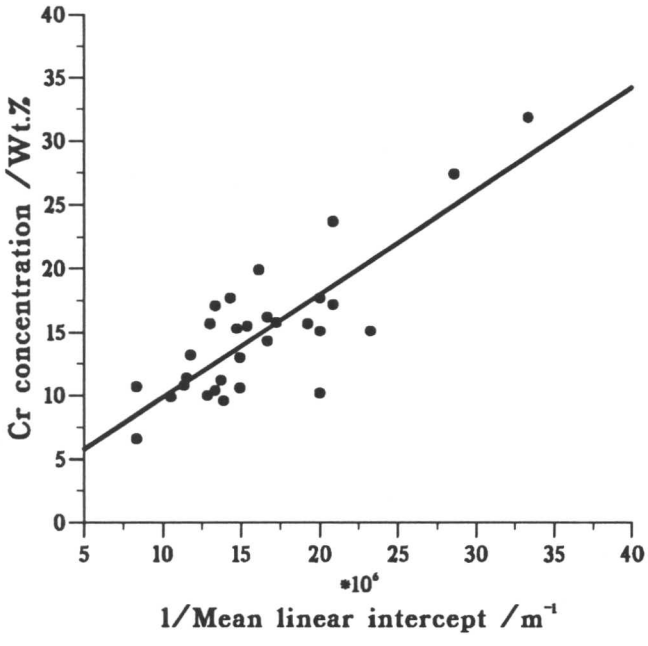

d)

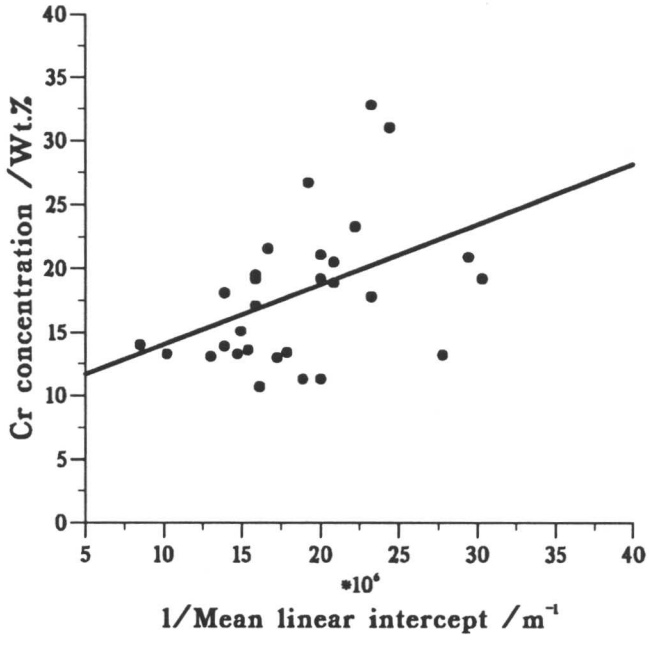

Figure 5.40: a)–g) Chromium concentration in cementite plotted as a function of reciprocal particle size for various tempering times at 565°C for fully bainitic microstructures.

e)

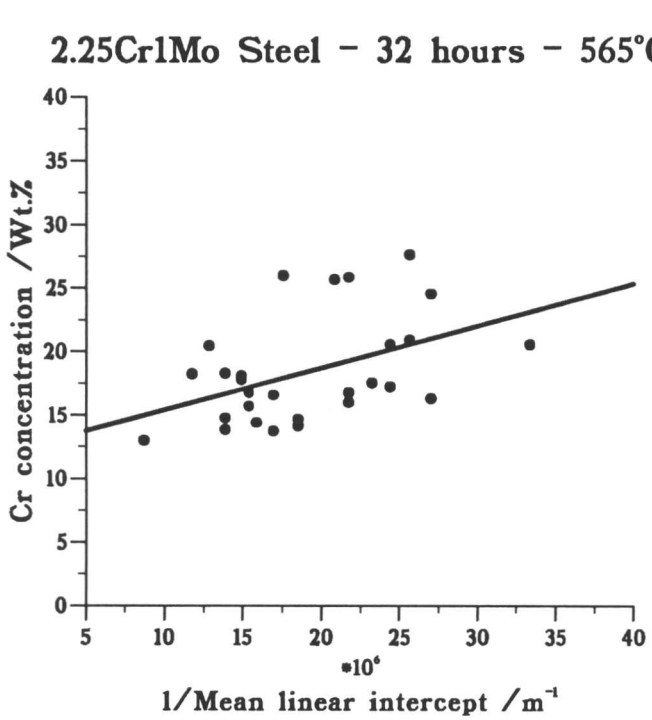
2.25Cr1Mo Steel - 32 hours - 565°C
Cr concentration /Wt.%
0
5
10
15
20
25
30
35
40
5
10
15
20
25
30
35
40
*10⁶
1/Mean linear intercept /m⁻¹

f)

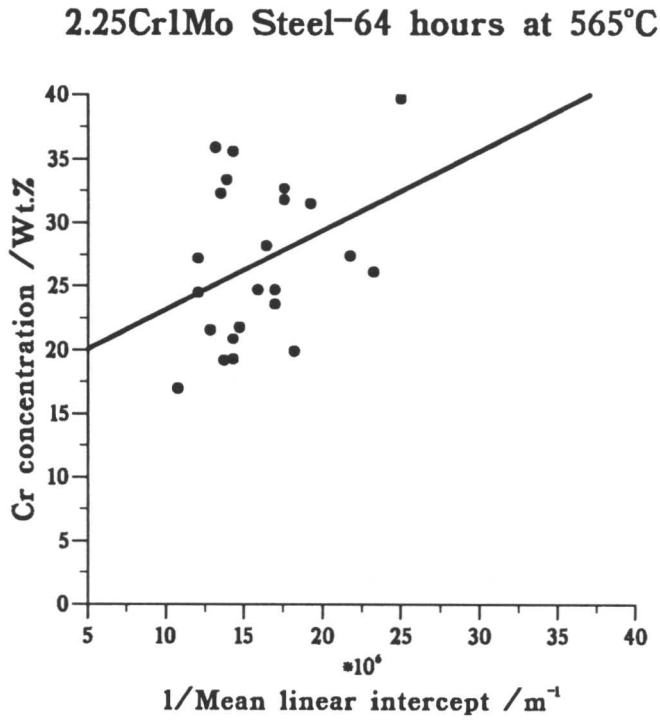
2.25Cr1Mo Steel-64 hours at 565°C
Cr concentration /Wt.%
0
5
10
15
20
25
30
35
40
5
10
15
20
25
30
35
40
*10⁶
1/Mean linear intercept /m⁻¹

g)

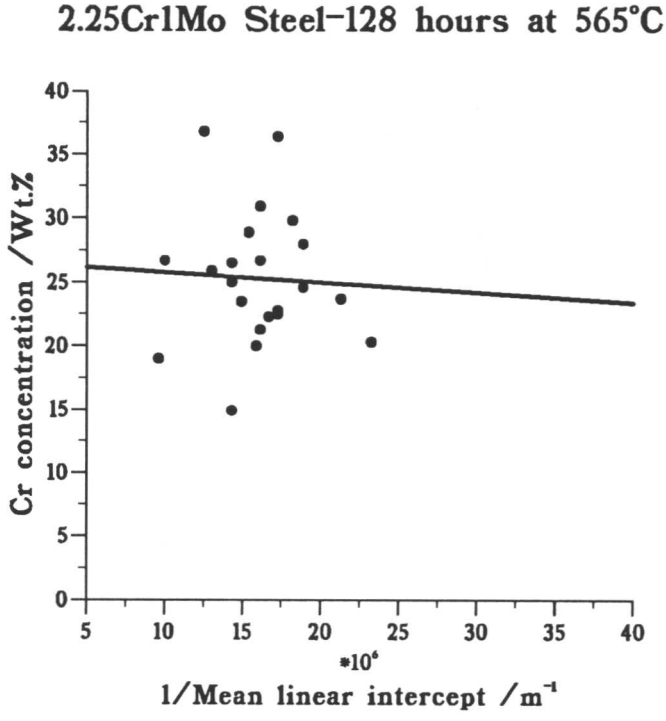
2.25Cr1Mo Steel-128 hours at 565°C
Cr concentration /Wt.%
0
5
10
15
20
25
30
35
40
5
10
15
20
25
30
35
40
*10⁶
1/Mean linear intercept /m⁻¹

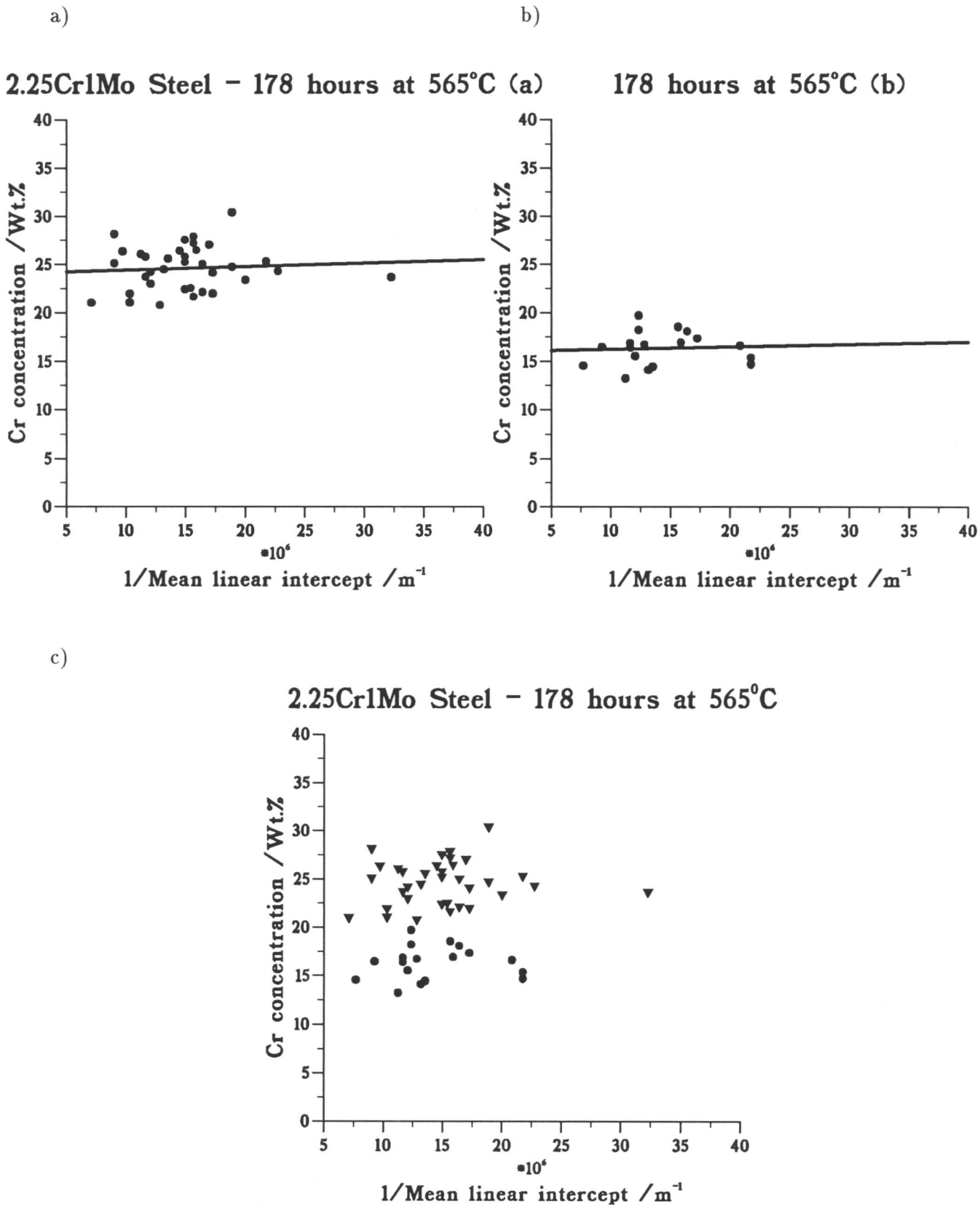

Figure 5.41: a)–c) Chromium concentration in cementite plotted as a function of reciprocal particle size for specimen tempered for 178 hours at 565°C for fully bainitic microstructures.

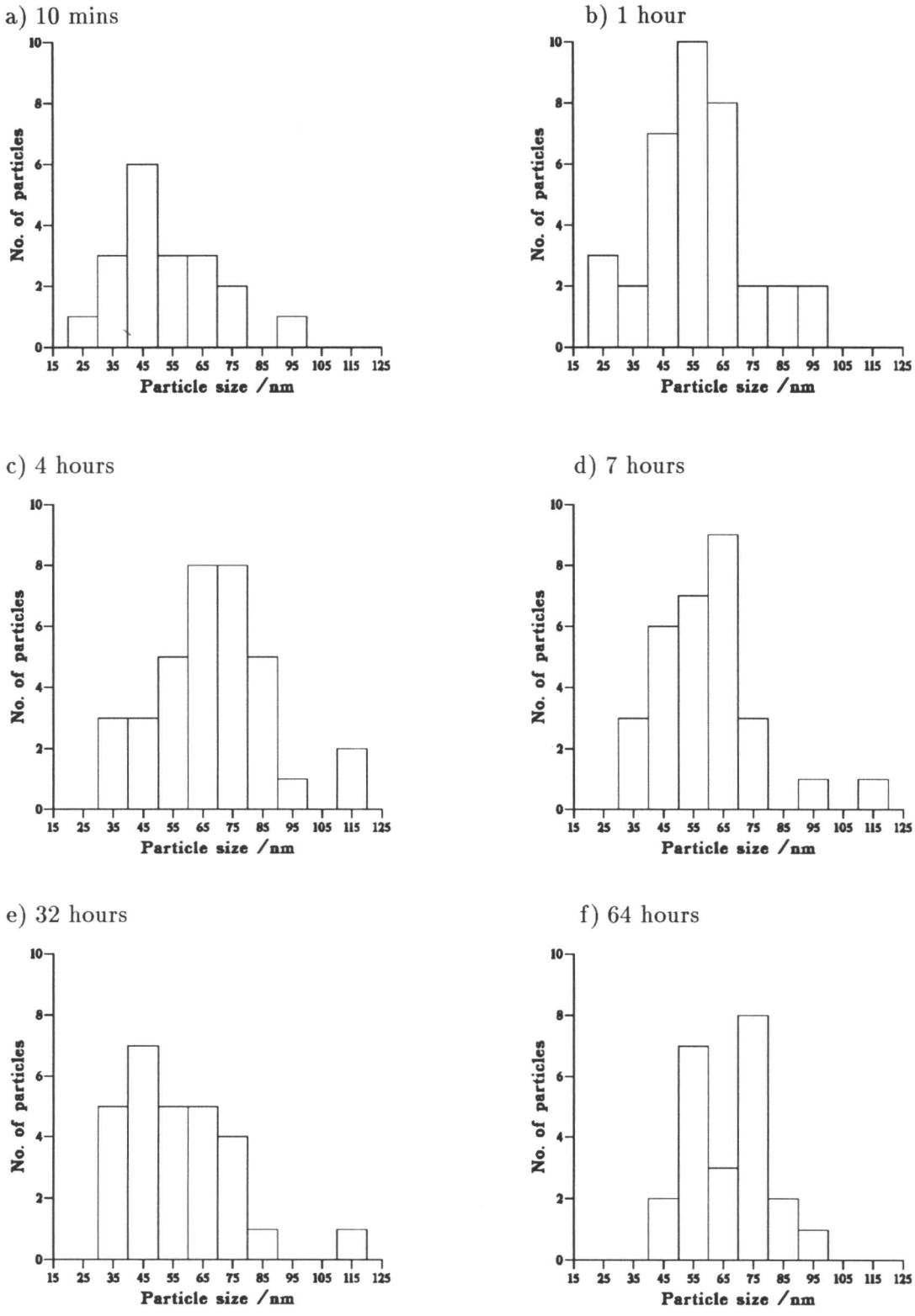

Figure 5.42: Histograms showing the distribution of particles sizes measured after a) 10 mins, b) 1 hour, c) 4 hours, d) 7 hours, e) 32 hours, f) 64 hours tempering at 565°C for the fully bainitic specimens.

Table 5.6: Composition of M_7C_3 with tempering time at 565°C measured by EDX.

Time /Hours	Cr /wt.%	Mn /wt.%	Mo /wt.%	Fe /wt.%
128	58	8	11	23
178	59	6	9	26
238.5	61	4.5	9	25.5
512	62	6.5	3	28.5
1048	63.5	5	7	24.5
2072	65.5	5	5	24.5

not possible to allow M_7C_3 and M_2C, and $M_{23}C_6$ and M_2C to coexist with ferrite. The calculations therefore give an idea of the chromium level only in each carbide because much of the molybdenum would be tied up in M_2C in the real situation. The calculated equilibrium chromium levels in M_7C_3 and $M_{23}C_6$ as a function of temperature are presented in Table 5.7. The predicted equilibrium level of $\simeq$59 wt.% Cr in M_7C_3 at 565°C is in reasonable agreement with the measured concentrations using EDX. The slightly lower value predicted compared with the observed value can be explained by the fact that some of the Mo predicted to be in the M_7C_3 would actually be in M_2C, leading to an increase in the predicted Cr level in the M_7C_3.

Table 5.7: Calculated equilibrium Cr levels in M_7C_3 and $M_{23}C_6$ as a function of temperature using MTDATA scaled to remove the stoichiometric carbon concentration to enable direct comparison with EDX measurements.

Temperature /°C	M_7C_3 Cr level /wt.%	$M_{23}C_6$ Cr level /wt.%
750	52.2	30.4
700	54.5	34.5
650	56.5	39.2
600	58.0	44.4
565	58.7	48.2
550	58.8	49.8

5.5.5 Enrichment of Mo_2C with tempering time

It has been observed (Pilling and Ridley, 1982) that the carbides M_2C and M_6C become richer in molybdenum as a function of tempering time in a $2\frac{1}{4}$Cr1Mo steel. These tempering heat treatments were carried out at 700°C. In this study, the M_2C carbide needles formed at

565°C are very fine and therefore attempts at measuring their composition by EDX are subject to considerable error, especially with respect to the concentration of molybdenum. M_6C was found to precipitate after 1048 hours tempering and contained $\simeq$ 60 wt.% molybdenum. This is in good agreement with the equilibrium composition calculated using MTDATA at 565°C, which suggests that there would be no further enrichment on prolonged tempering. At the higher temperatures used by Pilling and Ridley (1982) the molybdenum–based alloy carbides will precipitate quickly and therefore may not quite be at their equilibrium composition, whereas at lower temperatures they do not precipitate until much later tempering times. In this case the carbides appear to precipitate very close to their equilibrium compositions.

5.5.6 Consideration of the precipitation of $M_{23}C_6$

It was important to exclude completely the possibility that the cementite observed in the bainitic regions coexisting with M_2C could in fact be some other carbide, such as $M_{23}C_6$, because conclusive proof with selected area electron diffraction was difficult. Therefore, a fully bainitic specimen was tempered at 750°C for 48 hours in order to accelerate the precipitation of $M_{23}C_6$. The microstructure after this heat treatment presented in Figure 5.43a) consisted of two different carbide dispersions. The larger carbides were identified as $M_{23}C_6$ by both EDX and selected area electron diffraction (Figure 5.43b), and the smaller carbides as M_7C_3. The average composition of the $M_{23}C_6$ was

$$31 \text{ wt.\% Cr}, 2 \text{ wt.\% Mn}, 9 \text{ wt.\% Mo, and } 58 \text{ wt.\% Fe},$$

and that of the M_7C_3 as

$$51 \text{ wt.\% Cr}, 2.5 \text{ wt.\% Mn}, 7 \text{ wt.\% Mo, and } 39.5 \text{ wt.\% Fe}.$$

These Cr levels are in excellent agreement with those predicted by MTDATA (see Table 5.7 above) for tempering at 750°C, and confirm that the amount of Cr each carbide can support increases as the tempering temperature decreases. The predicted Cr level in $M_{23}C_6$ at the lower temperature of 565°C of 48 wt.% can therefore be assumed to be accurate. This means that were $M_{23}C_6$ to be present in the specimens tempered at 565°C it should contain 48 wt.% Cr, ruling out any possibility that the cementite with reduced Mo content and lower Cr levels in the bainitic regions could be $M_{23}C_6$. $M_{23}C_6$ was not observed in the bainitic microstructure for tempering times up to 3000 hours at 565°C.

5.5.7 Microstructural evolution during tempering at 510°C

The microstructural changes in specimens tempered at 510°C were considerably slower than at 565°C. The optical microstructure after tempering for 256 hours is presented in Figure 5.44.

a)

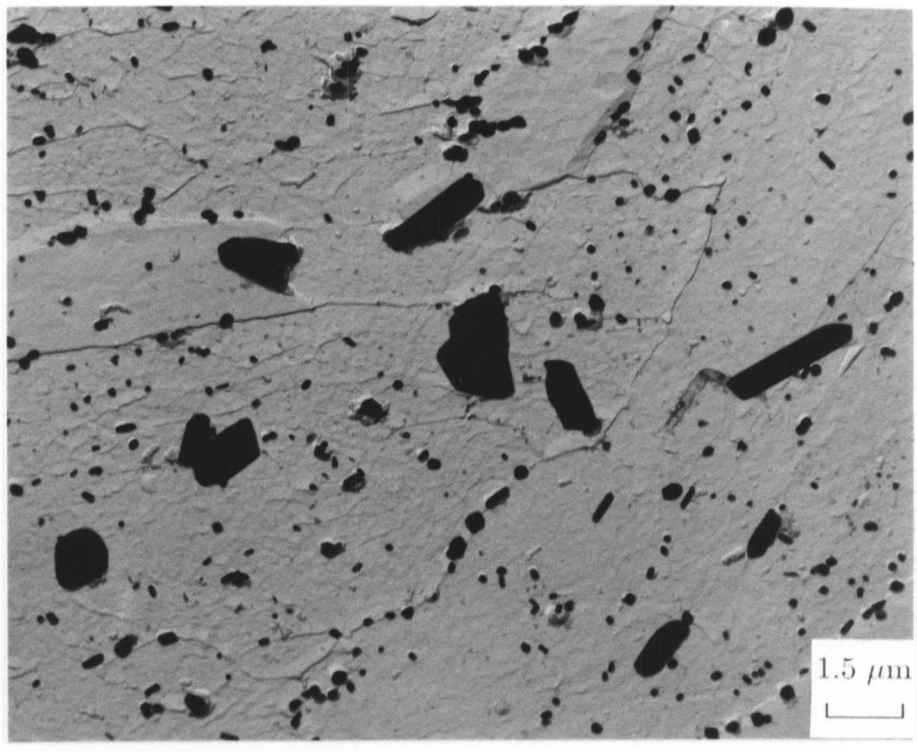

b)

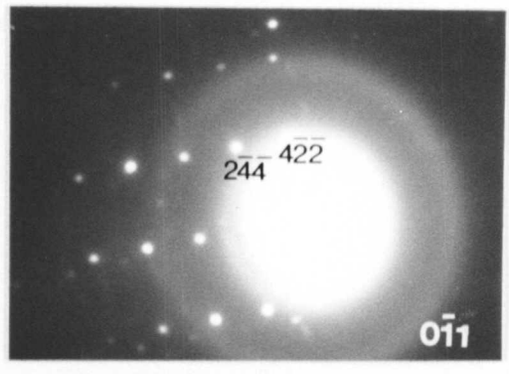

Figure 5.43: a) Carbon extraction replica from a fully bainitic specimen tempered for 48 hours at 750°C showing large particles of $M_{23}C_6$ and smaller particles of M_6C. b) Selected area electron diffraction pattern from an $M_{23}C_6$ carbide.

There are no observable differences compared with the starting microstructure. Figure 5.45 is a transmission electron micrograph from a replica taken from a specimen tempered for 1 hour; comparison with Figure 5.23 shows that the initial precipitation of cementite is much slower at the lower temperatures, as expected. Tempering for up to 256 hours allowed cementite to precipitate and enrich as in the specimens tempered at 565°C. The enrichment rate of the cementite was found to be a lot slower and no M_2C precipitation was found after 256 hours, compared with M_2C being found after 32 hours in the specimens tempered at 565°C.

5.5.8 EDX measurements of the Cr content of cementite at 510°C

The plots of Cr concentration against the reciprocal of particle size are presented in Figure 5.46a)–c) for the specimens tempered at 510°C. There is considerable scatter in the compositions measured after tempering for 1 hour, however, the slope of the regression line increases after tempering for 128 and 256 hours as the effect of the smaller particles enriching more quickly than the larger particles becomes more prominent. The results of these analyses are summarised in Table 5.8.

Table 5.8: Summary of experimental measurements of Cr concentration in cementite and particle size for specimens tempered up to 256 hours at 510°C.

Tempering time /Hours	Correlation coefficient	Average Cr conc. /wt.%	Average particle size /nm
1	-0.43	11.8	45
128	0.13	15.9	62
256	0.40	20.1	64

5.5.9 Microstructural evolution during tempering at 620°C

Microstructural changes at 620°C were rapid compared to those at 565°C. This is illustrated in Figure 5.47 which shows extensive cementite precipitation after tempering for only 1 hour taken from a carbon extraction replica. A MnS inclusion is also marked in the figure. The steel contains quite a number of MnS particles as a result of the manufacturing process, however, these are distributed evenly throughout the microstructure and therefore have no influence on the changes which occur. After 10 hours tempering there is extensive precipitation of M_7C_3 together with fine M_2C needles. After 25 hours the M_7C_3 is widespread, illustrated in Figure 5.48. M_7C_3 did not appear until after tempering for 128 hours at 565°C. It was clear that there were two different types of cementite, one richer in Cr and Mo, and one containing

less Cr and virtually no Mo, in the specimens tempered for only 25 hours at 620°C. This is illustrated in Figure 5.49. The two cementite particles marked with arrows at the boundary between two sheaves and in regions in which there is extensive M_2C precipitation both have the composition

$$15 \text{ wt.\% Cr}, 3 \text{ wt.\% Mn}, 0 \text{ wt.\% Mo, and } 82 \text{ wt.\% Fe,}$$

whereas the cementite particles in the martensitic regions have an average composition

$$23 \text{ wt.\% Cr}, 4.5 \text{ wt.\% Mn}, 5.0 \text{ wt.\% Mo, and } 67.5 \text{ wt.\% Fe.}$$

5.5.10 EDX measurements of the Cr content of cementite at 620°C

The plots of Cr concentration against the reciprocal of particle size are presented in Figure 5.50a)–c) for the specimens tempered at 510°C for 1, 10 and 25 hours respectively. These results exhibit considerably more scatter than do those at 510 and 565°C. The explanation of this is that microstructural changes are accelerated at the higher temperature with alloy carbide precipitation being present to some extent in all the specimens. The results are summarised in Table 5.9. The cementite has started to dissolve (corresponding to a drop in the experimentally measured cementite concentrations) after only 25 hours at 565°C.

Table 5.9: Summary of experimental measurements of Cr concentration and particle size for specimens tempered up to 25 hours at 620°C.

Tempering time /Hours	Correlation coefficient	Average Cr conc. /wt.%	Average particle size /nm
1	0.35	17.6	73
10	0.13	25.5	81
25	0.14	23.2	79

5.5.11 Coexistence of M_7C_3 with cementite

It has been noted that M_7C_3 precipitated whilst cementite was still present in the microstructure, and then the two coexisted for some time. The cementite in the immediate vicinity of M_7C_3 particles was found to have a lower Cr content than the average measured for an isolated cementite particle. It was thought that in the same way as the precipitation of M_2C appears to draw Mo from the cementite, precipitation of the Cr–rich M_7C_3 drew Cr away from any cementite particles nearby. This is illustrated in Figure 5.51 which shows a cementite

Figure 5.44: Optical micrograph for a fully bainitic specimen tempered at 510°C for 256 hours.

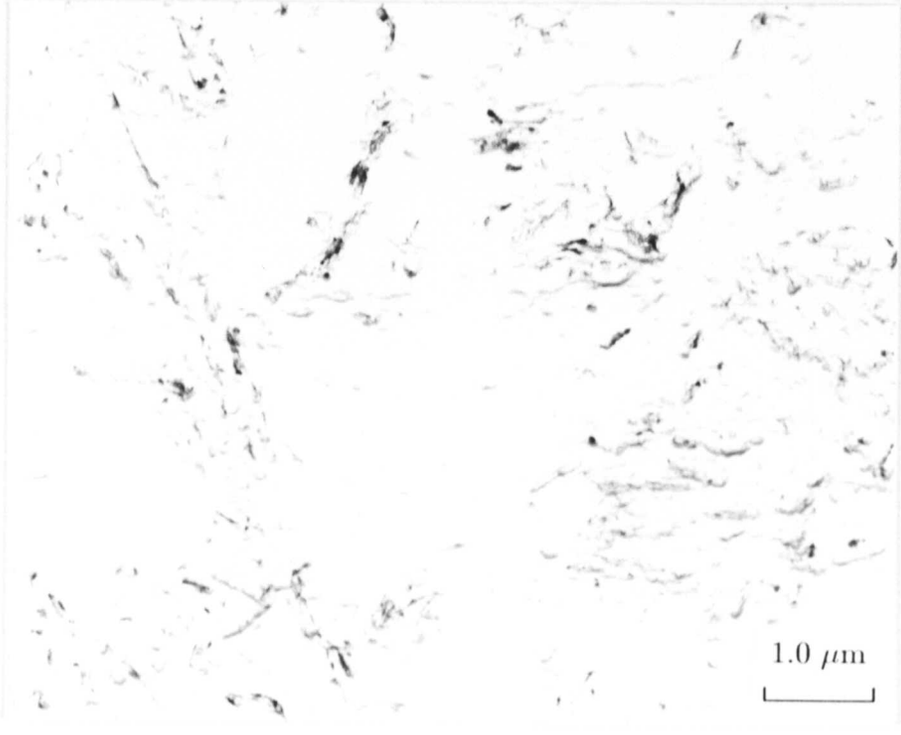

Figure 5.45: Carbon extraction replica taken from a bainitic specimen tempered at 510°C for 1 hour showing that cementite precipitation is very slow at this temperature.

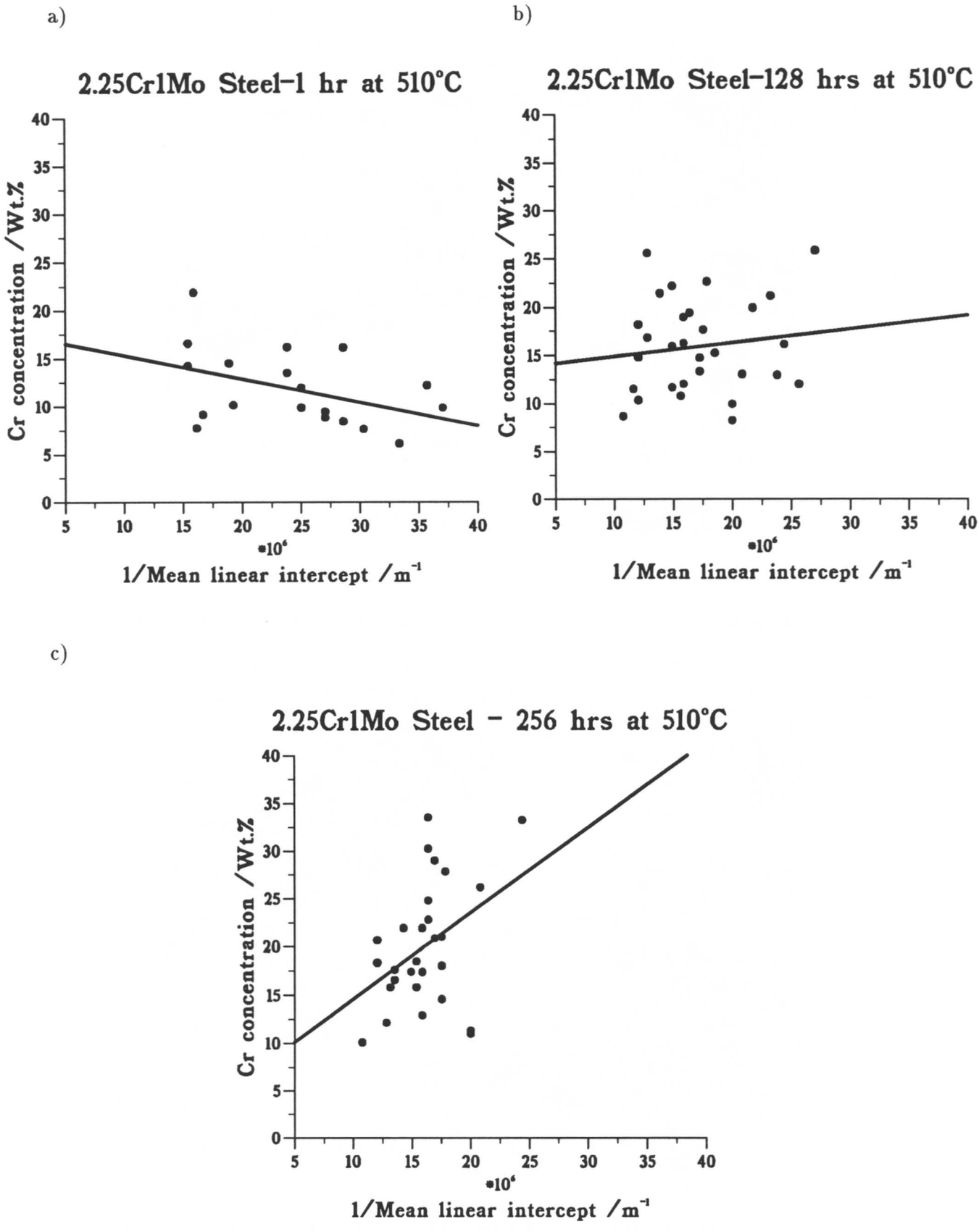

Figure 5.46: a)–c) Chromium concentration in cementite plotted as a function of reciprocal particle size for specimens tempered for various times at 510°C for fully bainitic microstructures.

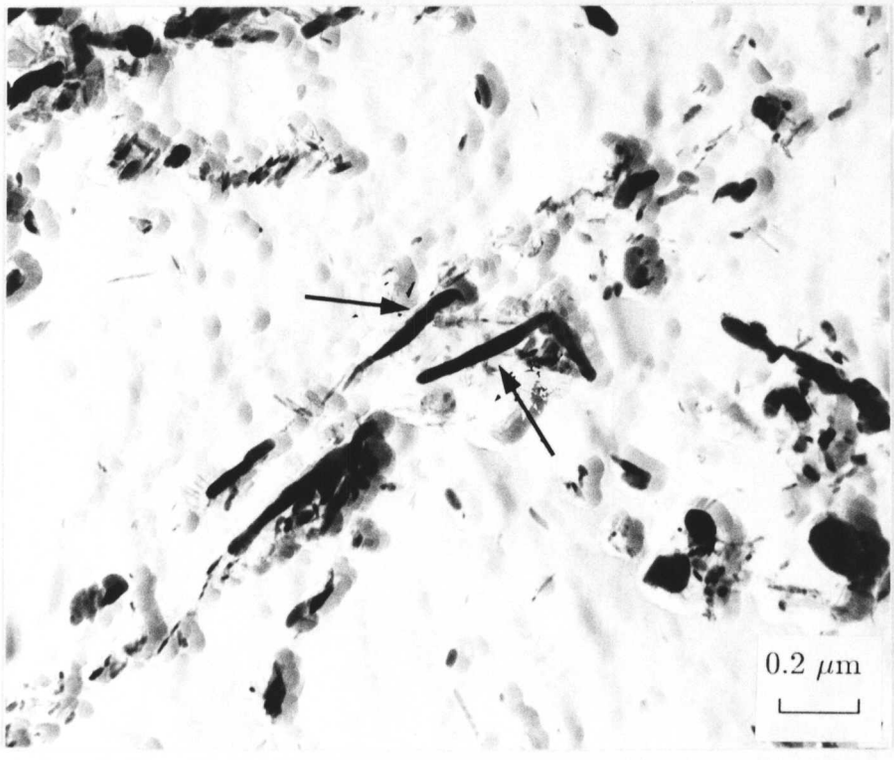

Figure 5.49: Carbon extraction replica from the fully bainitic specimen tempered for 25 hours at 620°C showing cementite particles with reduced Mo content in a region of extensive M_2C precipitation.

a)

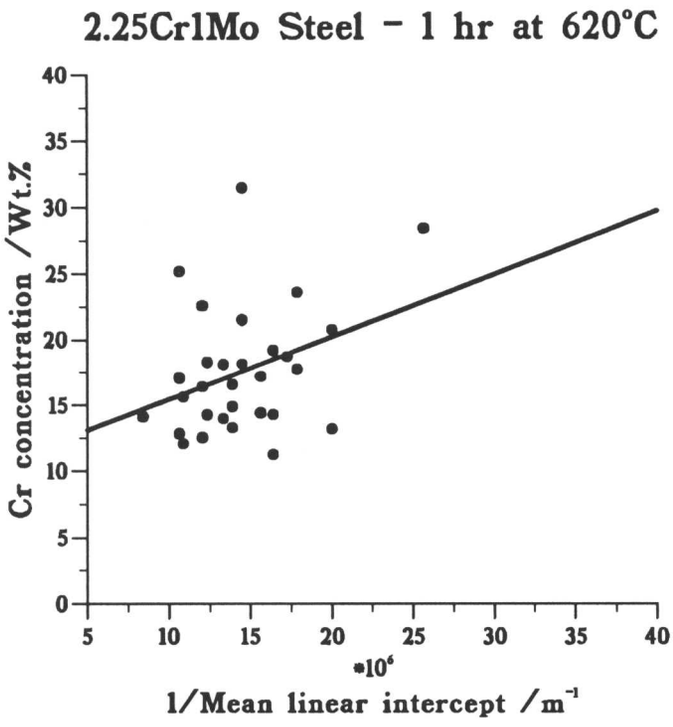

b)

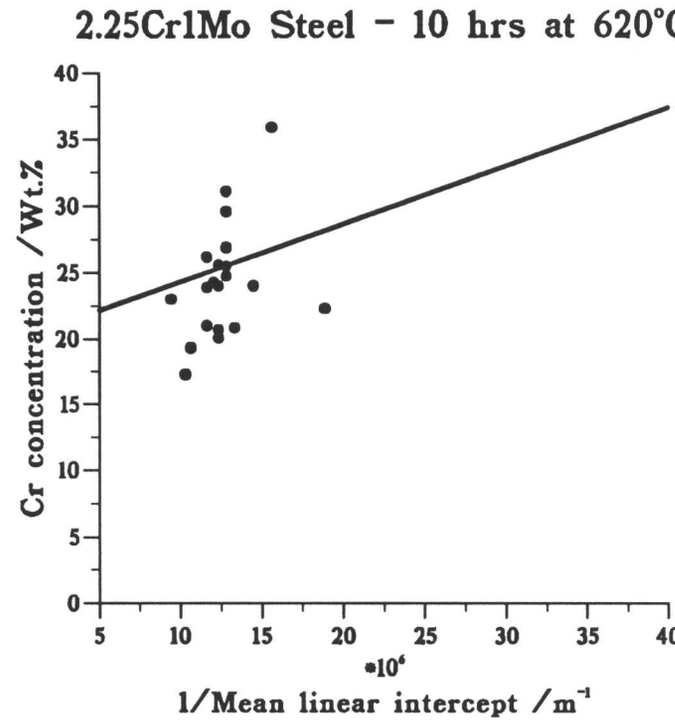

c)

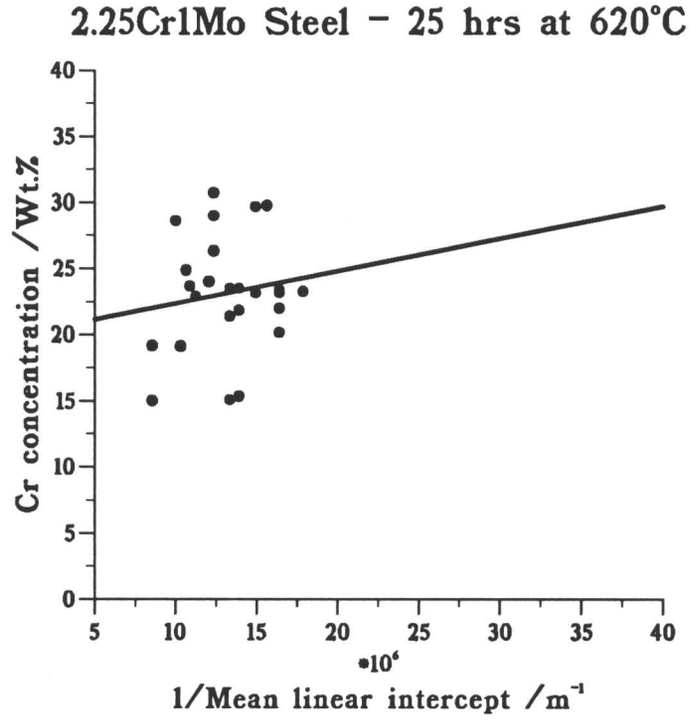

Figure 5.50: a)–c) Chromium concentration in cementite plotted as a function of reciprocal particle size for specimens tempered for various times at 620°C for fully bainitic microstructures.

particle next to an M_7C_3 particle in a fully bainitic specimen tempered for 10 hours at 620°C. The cementite has a composition

19 wt.% Cr, 4 wt.% Mn, 1 wt.% Mo, and 76 wt.% Fe,

compared with the Cr level in an isolated cementite particle of comparable size of

24 wt.% Cr, 4 wt.% Mn, 6 wt.% Mo, and 66 wt.% Fe.

The M_7C_3 particle contains 51 wt.% Cr. By considering the equilibrium Cr levels in cementite and ferrite and in M_7C_3 and ferrite using MTDATA it can be established whether there is a flux of Cr through the ferrite from cementite towards an M_7C_3 particle.

It was not possible to allow both cementite and M_7C_3 to exist at 565°C for the composition of the $2\frac{1}{4}$Cr1Mo steel used because MTDATA calculates the carbides present at equilibrium. When the three phases cementite, ferrite and M_7C_3 were allowed to coexist MTDATA correctly calculates the microstructure to consist of M_7C_3 and ferrite only. In order to investigate the possibility of a Cr flux from cementite to M_7C_3 when the two coexist as a consequence of kinetic factors, the bulk carbon concentration was increased until the cementite became thermodynamically stable again and coexists with the M_7C_3. This is a somewhat artificial procedure in that the calculated absolute equilibrium values in the three phases will not relate to the real situation, but it will allow the possibility of a Cr flux from cementite to M_7C_3 to be studied. Care was taken that as the bulk carbon concentration was increased to force the three phases to exist, the Fe/Cr ratio in the alloy overall was kept constant. Figure 5.52 shows the calculated equilibrium Cr level in cementite as a function of the bulk carbon concentration. It can be seen that for high carbon concentrations only cementite is the stable carbide, and for low carbon concentrations M_7C_3 is stable; for intermediate compositions M_7C_3 and cementite coexist. The lowest carbon concentration at which M_7C_3 and cementite were in equilibrium with ferrite, 0.75 wt.%, was chosen to perform further calculations because this point would be most closely related to the composition of the $2\frac{1}{4}$Cr1Mo steel. The equilibria between cementite and ferrite and between M_7C_3 and ferrite were then investigated separately at this overall concentration to find the Cr level in the ferrite at the interface between each of the particle types. The results of these calculations are presented in Figure 5.53. It can be seen that because the Cr level in the ferrite matrix surrounding a cementite particle is higher than that surrounding an M_7C_3 particle, a flux of Cr is stimulated from the cementite to the M_7C_3, hence explaining the drop in Cr level in a cementite particle in the vicinity of an M_7C_3 particle.

5.5.12 Coexistence of Mo_2C with cementite

A similar calculation was performed to that described in the previous section to study the coexistence of M_2C and cementite. Once again, in order to force MTDATA to allow M_2C and cementite to coexist in ferrite, the carbon concentration in the bulk alloy was increased, keeping the Fe/Cr ratio constant. Below 0.5 wt.% C only M_2C was stable, but further increasing the carbon concentration allowed M_2C and cementite to coexist. As the carbon concentration increased, the volume fraction of cementite was predicted to increase at the expense of the M_2C. The results of the calculation for an overall concentration of 0.5 wt.% C are presented in Figure 5.54. It can be seen that the increase in the matrix concentration of Cr and Mo around a cementite particle would result in a flux of both to the M_2C. This is consistent with the experimentally observed fact that once there is extensive M_2C precipitation within the bainitic plates, the cementite between the plates begins to 'lose' both chromium and molybdenum.

5.5.13 Calculation of the diffusion constants from experimental results

The enrichment kinetics of cementite particles were studied for various times at three different temperatures in order that the diffusion coefficient and the activation energy could be calculated for the diffusion of chromium in ferrite. The dependence of the diffusion coefficient of chromium in ferrite, D_α, is given by the analytical equation (3.28)

$$t_c = \frac{\pi {x_\theta}^2 (\bar{c} - c^\theta)^2}{16 D_\alpha (c^{\alpha\theta} - \bar{c})^2} \ .$$

The most accurate way of performing this calculation is to use all the experimental data gathered in the TEM and evaluate the quantity

$$\frac{\pi {x_\theta}^2 (\bar{c} - c^\theta)^2}{16 (c^{\alpha\theta} - \bar{c})^2} \tag{5.4}$$

for each individual particle analysed at each of the different tempering temperatures and times. Regression of the tempering time, t_c, against the expression 5.3 should then give a straight line passing through the origin with a gradient equal to the reciprocal of the diffusion coefficient. The tempering times and temperatures used in this analysis only included those specimens in which enrichment of the cementite was taking place rather than the dissolution due to the precipitation of Cr–based alloy carbides. This therefore included tempering times up to 64 hours at 565°C, all the specimens tempered at 510°C and excluded the 25 hour specimen tempered at 620°C.

The value of $c^{\alpha\theta}$, the equilibrium concentration of Cr in the ferrite, varies with temperature. The values used for the calculations of the diffusion coefficient were calculated using MTDATA

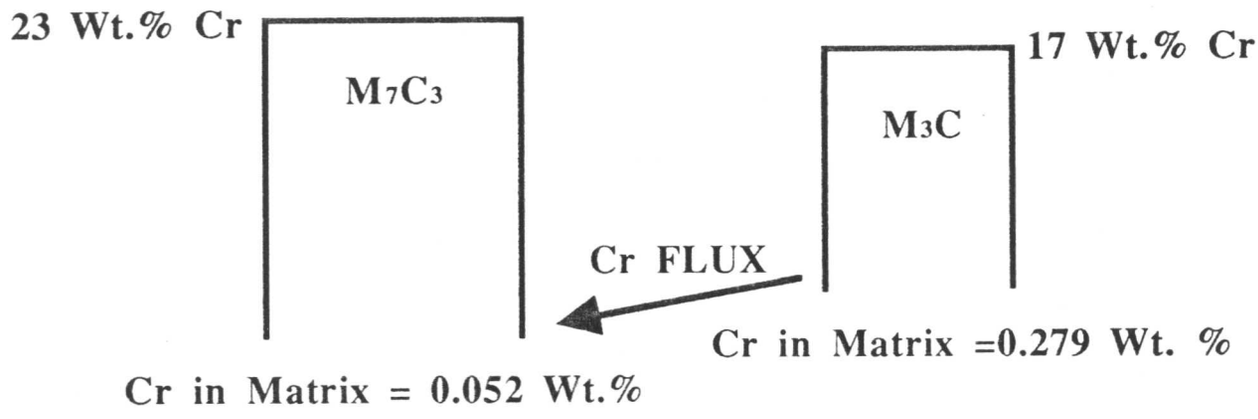

Figure 5.53: Schematic illustation of a cementite particle next to an M_7C_3 particle showing calculated equilibrium concentrations in the particles and the matrix using MTDATA.

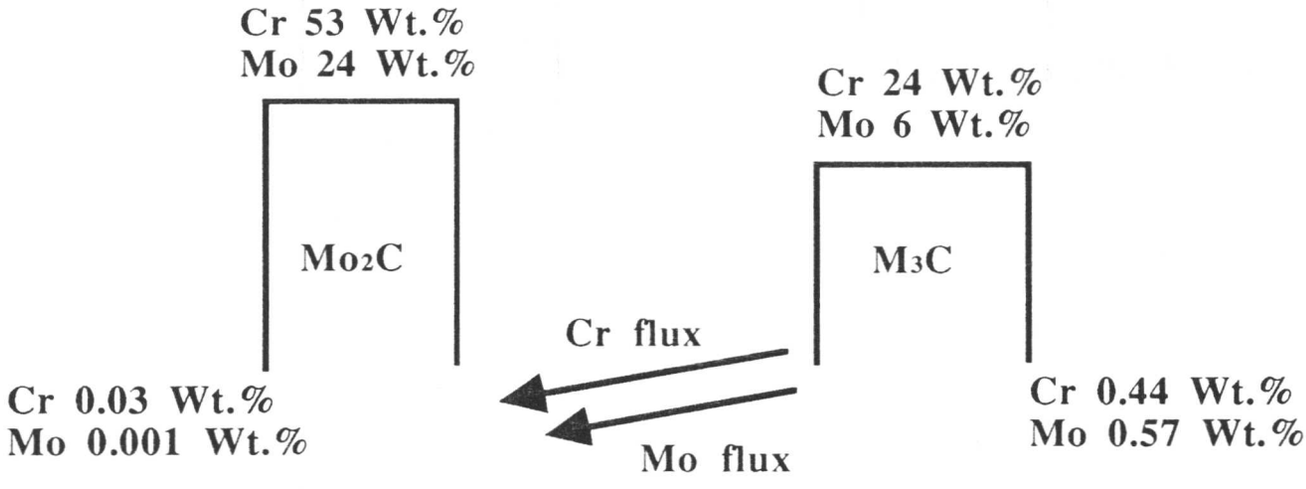

Figure 5.54: Schematic illustation of a cementite particle next to an M_2C particle showing calculated equilibrium concentrations in the particles and the matrix using MTDATA.

allowing only the phases cementite and ferrite to exist. These data have been presented in Table 5.2. The predicted chromium level in the cementite is higher than that observed in the particles experimentally (because of the precipitation of Cr–based alloy carbides discussed above) and therefore the predicted of $c^{\alpha\theta}$ should be slightly higher than that used in the calculations. The effect of this difference will be very small because it will not change the value of the regression constant, and hence the value of D_α, at any one temperature because it would simply be changing the absolute value of the constant in the denominator of expression 5.3. The volume fraction of cementite is small compared to the ferrite and therefore any changes in the overall concentration in the matrix due to changes in the cementite composition will also be small.

The equilibrium values also take into account the carbon content of the cementite, which the EDX data do not. The EDX measurements were therefore scaled to allow for 6.67 wt.% of C to be contained in the cementite (the stoichiometric carbon content for M_3C).

A computer program was written to calculate the regression coefficient, and therefore the diffusion constant, at each of the three tempering temperatures. The results of the calculations are presented in Table 5.10.

Table 5.10: Calculated diffusion coefficient as a function of temperature for the fully bainitic specimens.

Temp /°C	D_α /m^2s^{-1}
510	$3.5\pm0.2 \times 10^{-19}$
565	$2.5\pm0.1 \times 10^{-18}$
620	$2.7\pm0.3 \times 10^{-17}$

The calculated value of the diffusion coefficients at the three temperatures were then used to calculate the activation energy for the diffusion of Cr in ferrite using the Arhenius relationship

$$D = D_0 \exp\left(-\frac{Q}{RT}\right), \tag{5.5}$$

where Q is the activation energy, R is the universal gas constant, T is the temperature in Kelvin and D_0 is the pre–exponential factor. Taking the natural logarithm of equation 5.5 results in the expression,

$$\ln D = -\frac{Q}{R}\frac{1}{T} + \ln D_0 \tag{5.6}$$

from which it can be seen that plotting a graph of the logarithm of D_α against reciprocal temperature yields a slope equal to $-\frac{Q}{R}$. Such a graph is plotted in Figure 5.55; a regression line is plotted through the experimental points. The correlation coefficient for these three data

points was found to be 0.99. The value for the activation energy of diffusion, Q, was found to be 230,000±10,000 J mol^{-1}, and the pre–exponential factor was found to be $7.0\pm0.3\times10^{-4}m^2s^{-1}$. The values given by Fridberg *et al.* (1969) for the inter–diffusion of Cr in ferrite are an activation energy of 240,000 J mol^{-1}, and a pre–exponential factor of $1.5\times10^{-4}m^2s^{-1}$.

5.6 Results and discussion from mixed microstructures

5.6.1 Precipitation within the allotriomorphic ferrite

A carbon extraction replica from the isothermally transformed mixed microstructure before tempering showed that although there was no precipitation in the bainitic regions of the microstructure, extensive precipitation had occurred in the ferrite. Fibrous carbides were found to exist in the allotriomorphic ferrite, both at grain boundaries with other ferrite grains (Figure 5.56 and Figure 5.57) and at the ferritic/bainitic grain boundaries (Figure 5.58). The fibres were approximately 30 nm thick and up to 2 μm long. Selected area electron diffraction (Figure 5.58c) from a cluster of such fibres (Figure 5.58a) showed that a unique spot diffraction pattern could be obtained from the cluster suggesting all the fibres had the same orientation. A dark field electron micrograph from one such spot is presented in Figure 5.58b), again illustrating that parallel fibres can be illuminated from a single diffraction spot. The selected area electron diffraction pattern is attributable to hexagonal M_2C. EDX analyses were possible on clusters of fibres and they were found to have a chemical composition of 50 wt.% Mo, 40 wt.% Cr with small amounts of Fe and Mn, consistent with the electron diffraction results. A second morphology of M_2C clusters was also observed in the ferrite. These particles, illustrated in Figure 5.59, were much smaller than the fibres (length$\simeq$60 nm, $\simeq$20 nm thick), precipitating in a Widmanstätten array usually parallel to the prior austenite grain boundaries. The M_2C fibres and small particles present in the as–transformed microstructure persisted throughout tempering, also being observed in the specimens tempered for 180 hours at 565°C. This interphase precipitation of M_2C has been discussed in Chapter 2. Larger precipitates, identified by EDX as both M_2C and M_6C, were also found on ferrite–ferrite grain boundaries. Precipitation of this type is illustrated at a triple point in Figure 5.60. The M_6C precipitates become larger during tempering at the expense of some of the smaller M_2C particles.

5.6.2 Precipitation within the bainitic regions

The characteristics of precipitation in the bainitic regions of the mixed microstructures are broadly the same as in the fully bainitic specimens. However, cementite precipitation in the bainitic regions of the mixed microstructure specimens is very dense compared with the

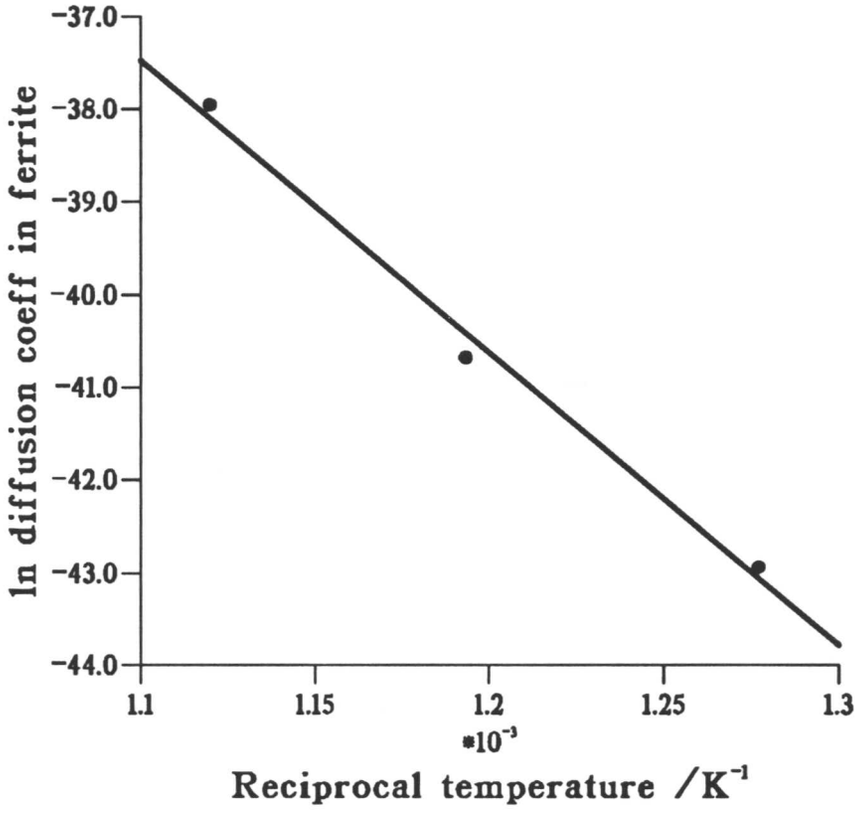

Figure 5.55: Plot of the logarithm of the calculated diffusion coefficient in ferrite as a function of temperature showing the regression line through the points

fully bainitic specimens. This is to be expected because of the increased carbon concentration in the bainitic regions due to the rejection of carbon into the austenite as the allotriomorphic ferrite forms. The carbon extraction replica taken from a specimen tempered for 47 hours at 565°C presented in Figure 5.61 illustrates this point. The contrast between the dense cementite precipitation in the bainitic regions and the empty ferritic regions is illustrated in Figure 5.62. Large M_6C particles are also visible on the ferrite grain boundaries. Figure 5.63 shows a replica from a specimen tempered for 180 hours. Widmanstätten type cementite is clearly visible within a martensite lath.

It has been shown that the bainitic and martensitic regions contain extensive cementite precipitation, whereas the ferritic regions contain M_2C (which is replaced by M_6C on prolonged tempering). This difference must be related to the mechanism of transformation. The ferrite forms reconstructively and therefore the atomic mobility inherent in this process could also permit the simultaneous precipitation of alloy carbides. The growth of bainite and martensite is displacive, precluding the formation of alloy carbides during transformation.

5.6.3 EDX measurements of the Cr content of cementite in mixed microstructures

The plots of Cr concentration against the reciprocal of particle size are presented in Figure 5.64a)–e) for the mixed microstructure specimens tempered at 565°C for 1, 47, 80, 128 and 180 hours respectively. The calculated regression lines are plotted on the first four plots, however the results for the 180 hour specimen were beginning to show a division of the cementite particles into those associated with bainitic and martensitic regions, and therefore it was not thought appropriate to find a single regression line for two different distributions. The results of these analyses are summarised in Table 5.11.

Table 5.11: Summary of experimental measurements of Cr concentration in cementite and particle size for mixed microstructure specimens tempered at 565°C.

Tempering time /Hours	Correlation coefficient	Average Cr conc. /wt.%	Average particle size /nm
1	0.74	9.1	76
47	0.44	15.9	68
80	0.55	20.2	59
128	0.41	21.9	71
180	–	26.2	63

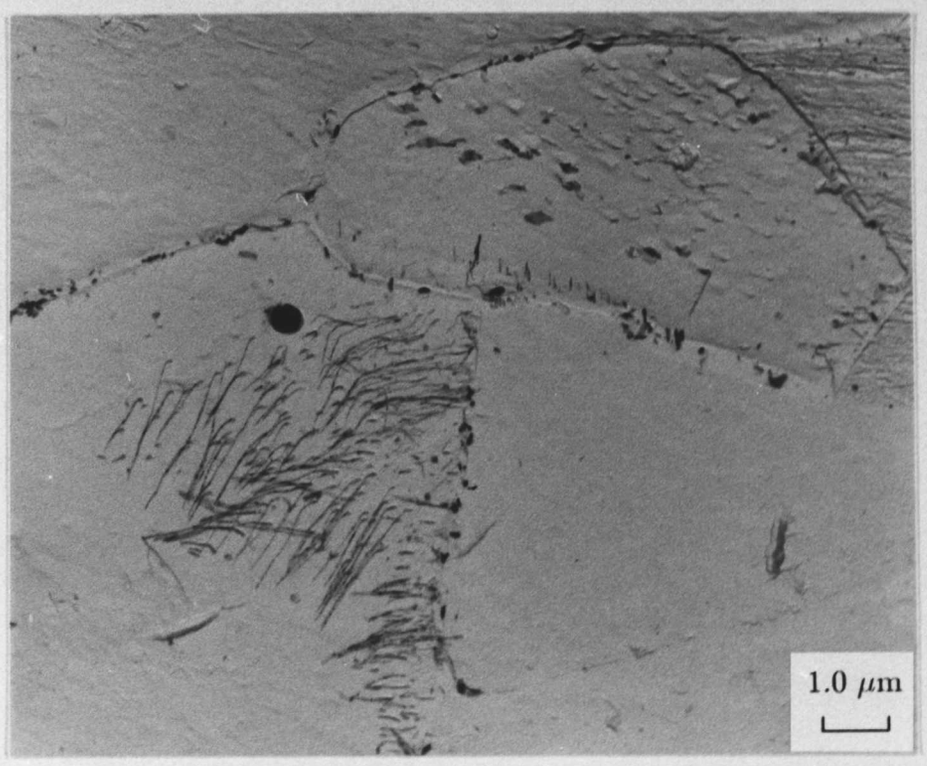

Figure 5.56: Carbon extraction replica from the as–transformed mixed microstructure showing fibrous M_2C carbides at ferritic/ferritic grain boundaries.

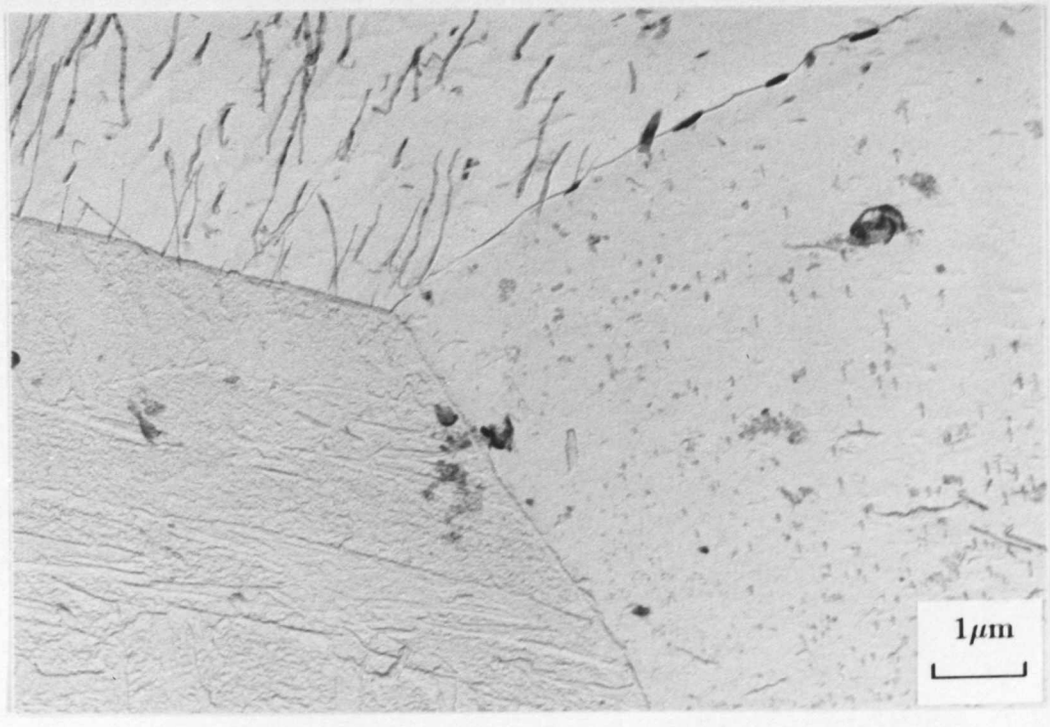

Figure 5.57: Carbon extraction replica from the as–transformed mixed microstructure showing fibrous M_2C carbides at ferritic/bainitic grain boundaries.

a)

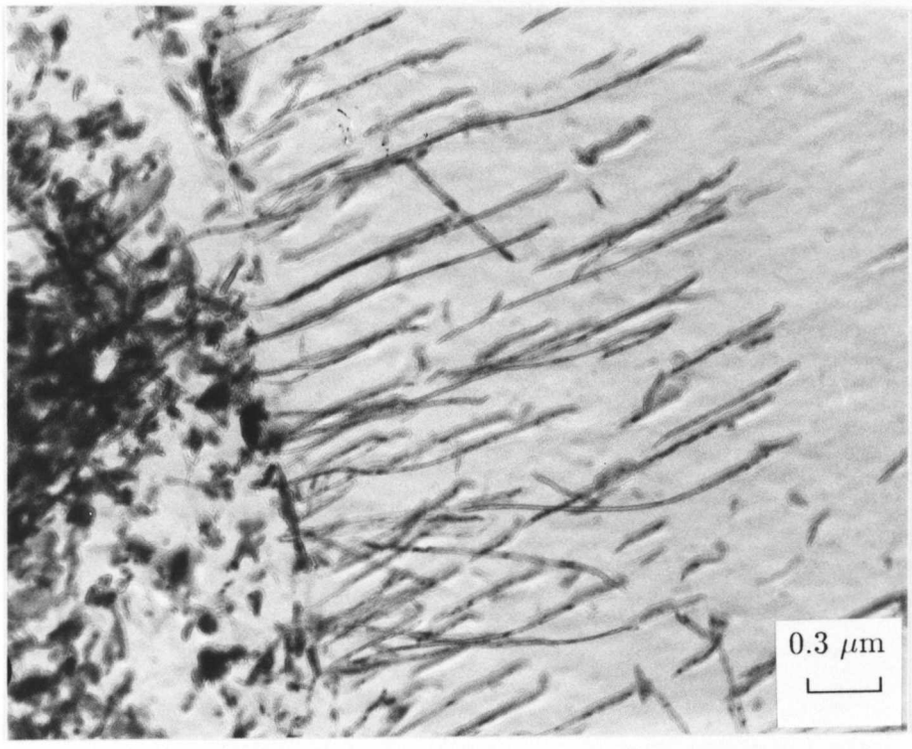

b)

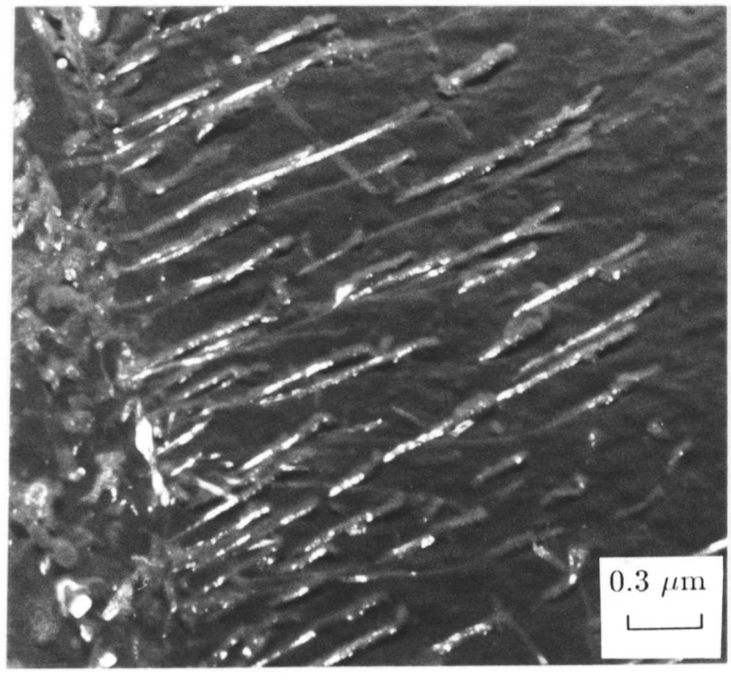

c)

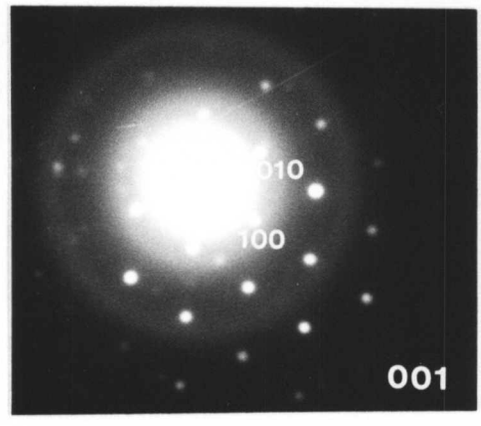

Figure 5.58: Carbon extraction replica from the mixed microstructure after tempering for 180 hours at 565°C. a) Bright field and b) dark field images of fibrous M_2C particles showing that all the fibres have the same orientation. c) Selected area electron diffraction pattern from a cluster of the fibres showing that a single spot pattern is obtained.

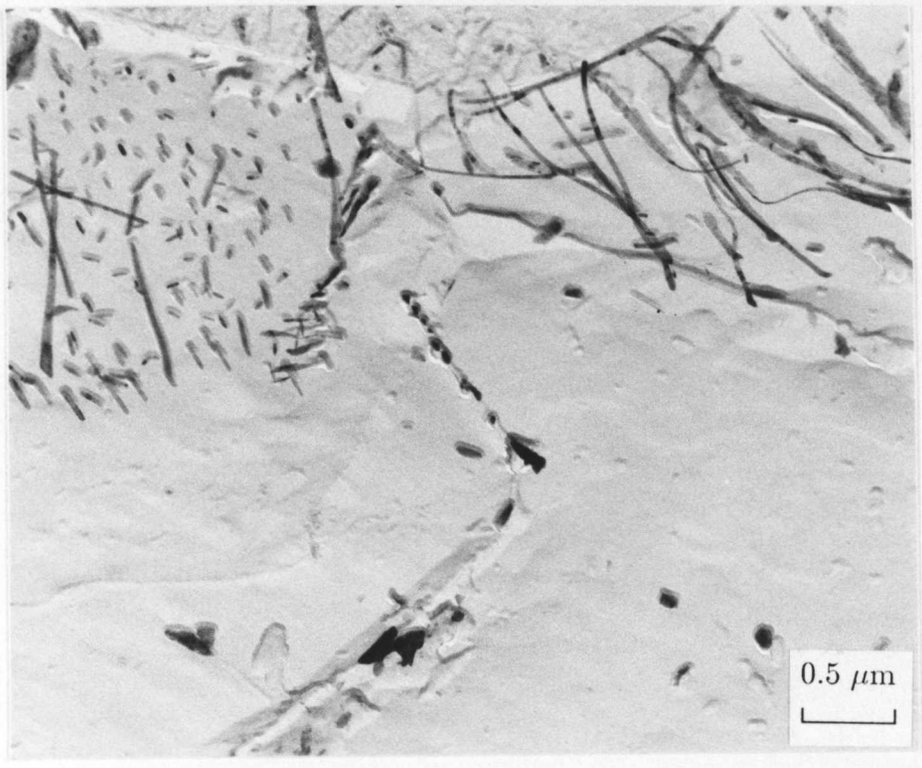

Figure 5.59: Carbon extraction replica from the as–transformed mixed microstructure showing a second morphology of M_2C clusters precipitating in a Widmanstätten array.

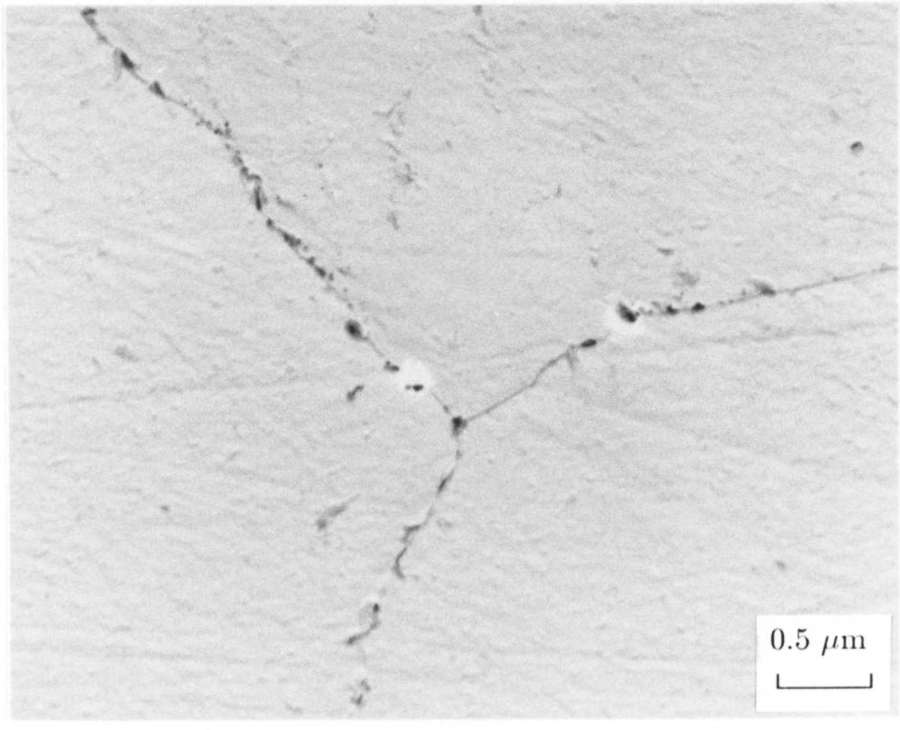

Figure 5.60: Carbon extraction replica from the as–transformed mixed microstructure illustrating precipitation of M_6C at a triple point between ferrite grains.

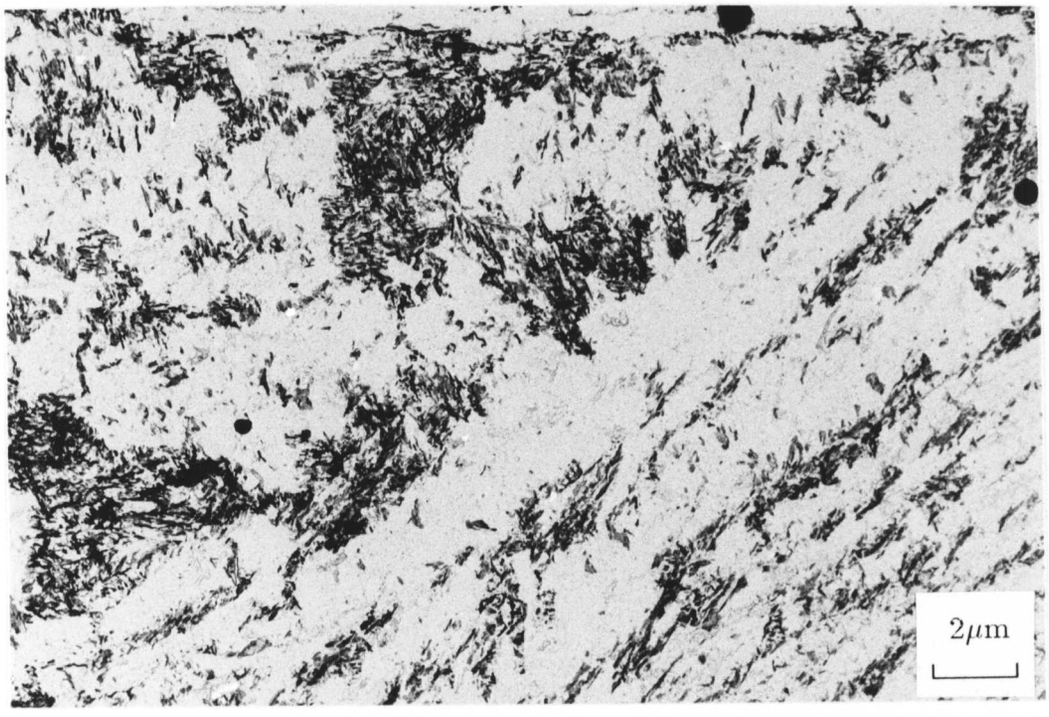

Figure 5.61: Carbon extraction replica from a mixed microstructure specimen tempered for 47 hours at 565°C showing dense cementite precipitation.

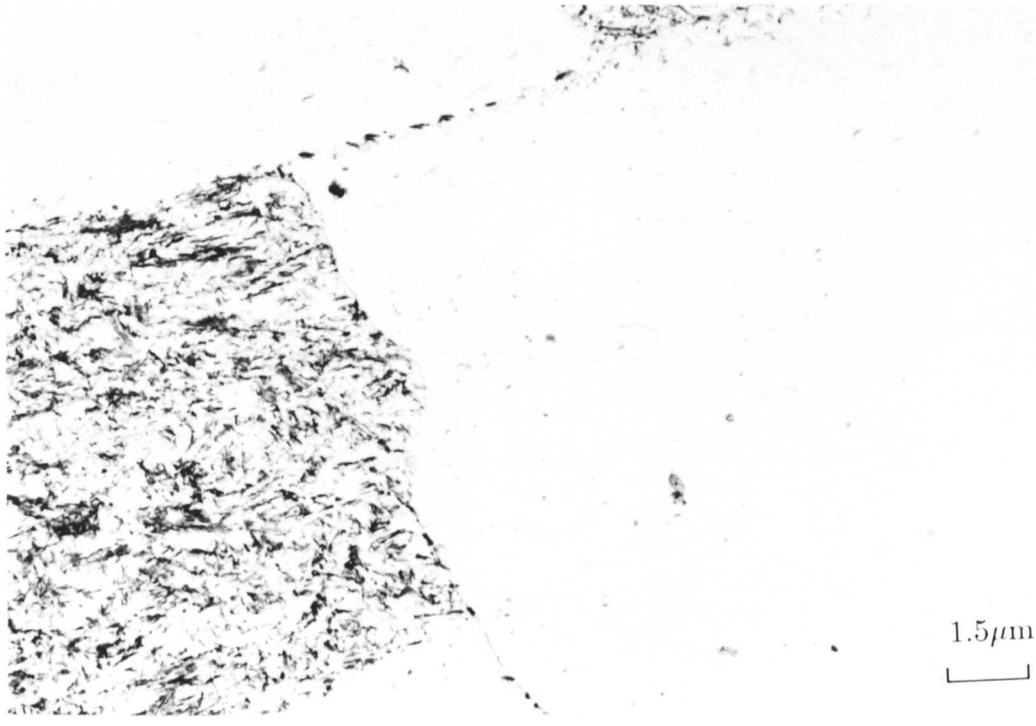

Figure 5.62: Carbon extraction replica from a mixed microstructure specimen tempered for 47 hours at 565°C showing the contrast between the dense cementite precipitation in the bainitic regions and the empty allotriomorphic ferrite regions.

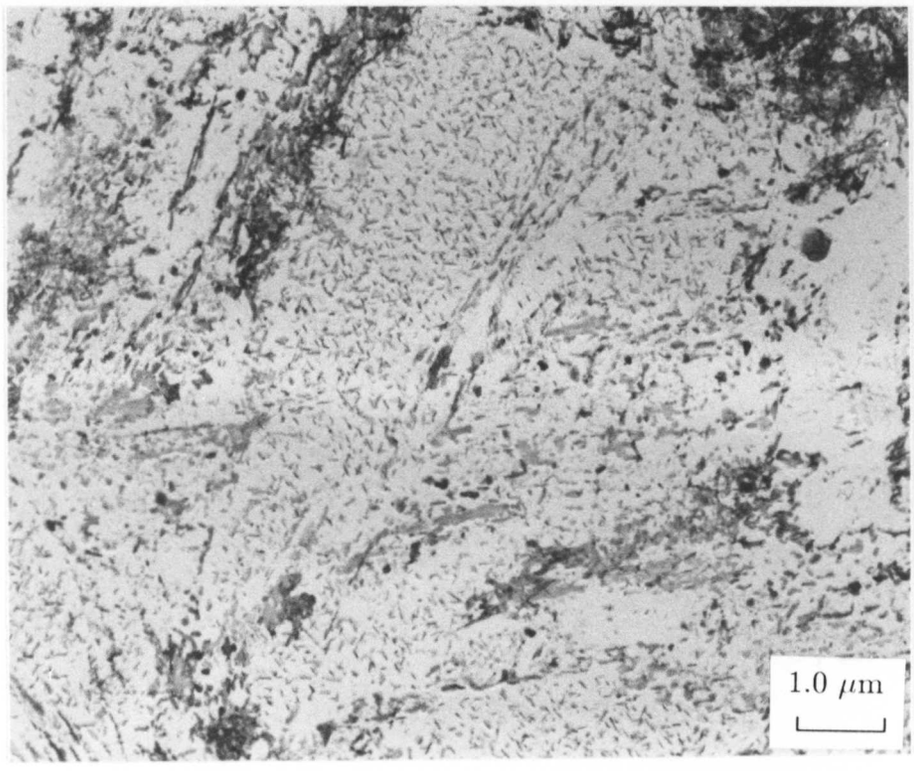

Figure 5.63: Carbon extraction replica from a mixed microstructure specimen tempered for 180 hours at 565°C showing Widmanstätten type precipitation of cementite within a martensite lath.

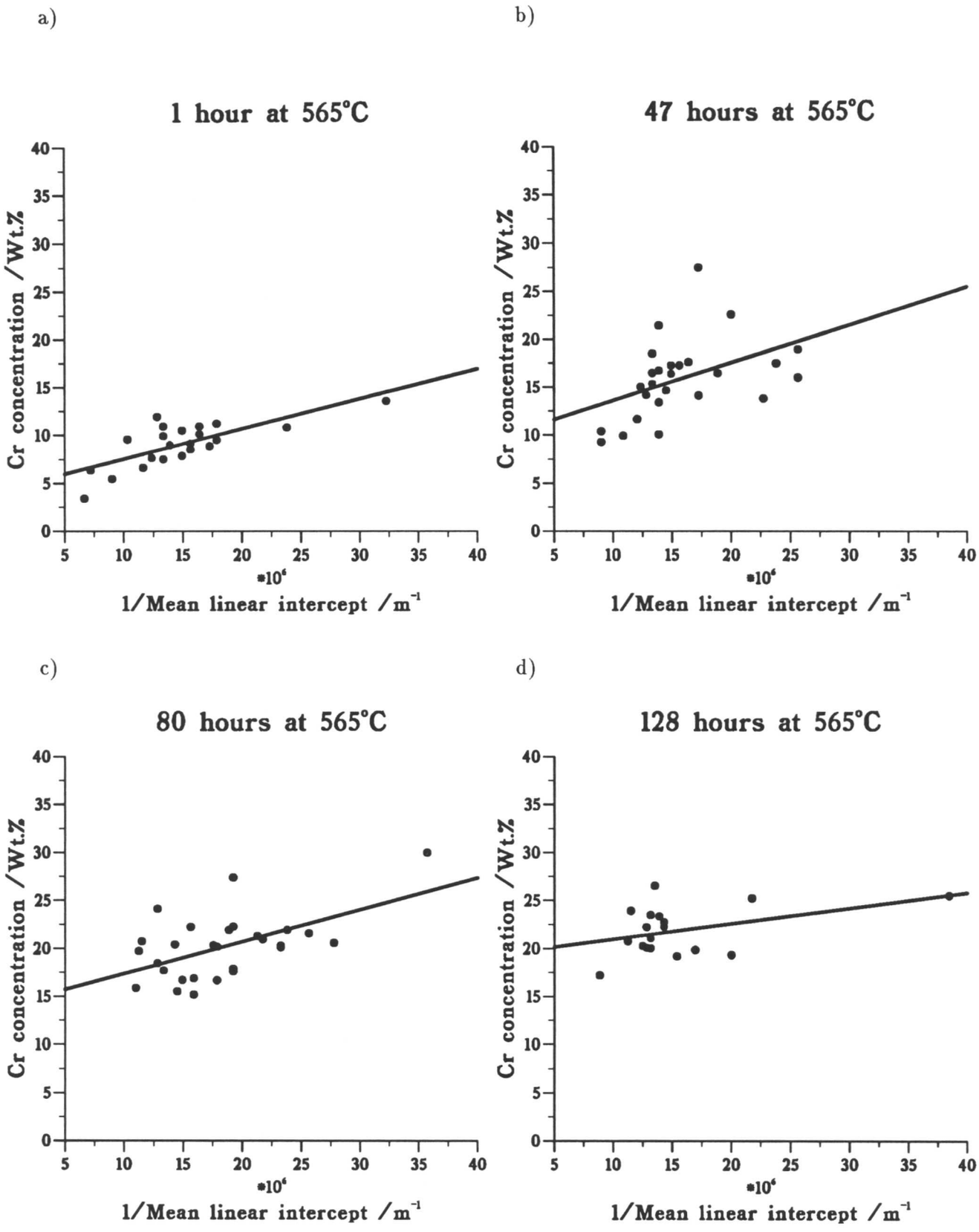

Figure 5.64: a)–e) Chromium concentration in cementite plotted as a function of reciprocal particle size for various tempering times at 565°C for mixed microstructure specimens.

e)

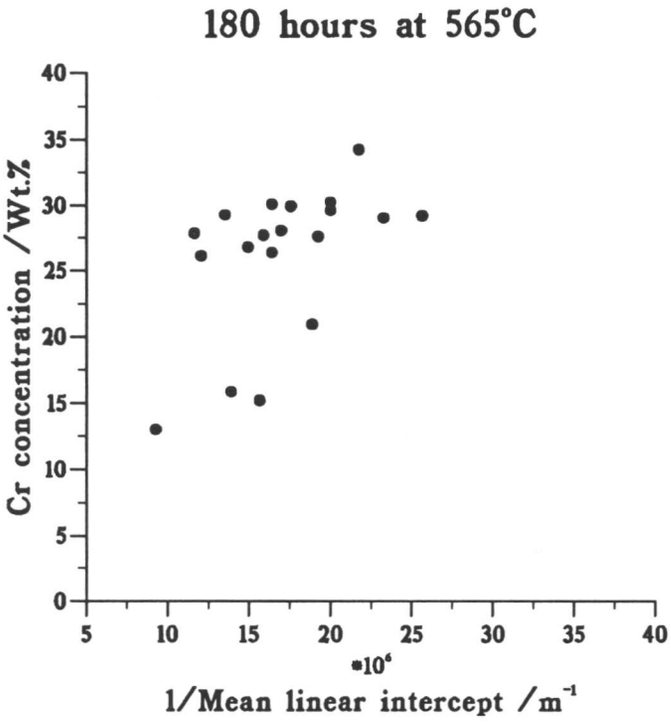
180 hours at 565°C
Cr concentration /Wt.%
40
35
30
25
20
15
10
5
0
5
10
15
20
25
30
35
40
*10⁴
1/Mean linear intercept /m⁻¹

5.7 Comparison of experimental results and theoretical predictions

The experimental measurements of Cr concentration in cementite in the fully bainitic and mixed microstructure specimens are summarised in Figure 5.65. It can be seen that the cementite in the fully bainitic specimens enriches more quickly than in the specimens containing only 50% bainite. This is to be expected because the formation of allotriomorphic ferrite in the mixed microstructure specimens causes an increase in the carbon concentration of the bainitic regions. The carbon concentration in the two different regions can be determined from a simple mass balance equation:-

$$\overline{x} = V_\alpha x_\alpha + (1 - V_\alpha)x_\gamma \ , \tag{5.7}$$

where $\overline{x}$ is the average carbon concentration in the alloy, V_α is the volume fraction of allotriomorphic ferrite, and x_α and x_γ are the carbon concentrations in the ferrite and the austenite respectively. $\overline{x}$ is 0.15wt.%, V_α is 0.5 in the specimens used, x_α (determined from the program used to calculate the TTT curve in section 5.3.1) =0.0228 wt.% and hence x_γ is calculated to be 0.277 wt.%. This is by definition the carbon concentration in the bainite which forms from the carbon–enriched austenite. There is therefore approximately twice as much carbon available for carbide precipitation initially in the mixed microstructure specimens than in the fully bainitic specimens.

The symmetric and asymmetric finite difference methods discussed in Chapter 3 can be used to predict the enrichment rate of cementite in the fully bainitic and mixed microstructures respectively. Both calculations were carried out at 565°C, and for average particle sizes of 60 nm in the bainitic and 70 nm in the mixed microstructures. These are consistent with the particle sizes measured experimentally. The two curves are shown in Figure 5.66, plotted as a function of time. Experimentally it is observed that the bainite in the mixed microstructure specimens, which has formed from enriched austenite, contains cementite which enriches more slowly than that in the fully bainitic specimens. This is consistent with the predictions of the model.

Figure 5.67 and Figure 5.68 show the predicted curves for the bainitic and mixed microstructures respectively, for short times only, plotted against the experimental results. The deviation of the experimental points tempered for more than 64 hours in the fully bainitic specimens corresponds to the precipitation of M_7C_3 and the subsequent dissolution of the cementite particles. It can be seen that the model is consistently underpredicting the value of chromium in cementite after a given time compared with the experimental results. The most probable explanation for this is that the value of the diffusion coefficient of chromium in cementite is a little high. A lower value would cause the predicted enrichment rate to be higher, increasing the

predicted concentration for a given tempering time. The relatively small size of the particles ($\simeq$60 nm) increases the sensitivity of the model to the values of the diffusion constants used. This point is discussed further in Chapters 3 and 8. However, it is important to note that the experimental results clearly show a linear dependence of enrichment rate on the square root of tempering time, as predicted by the model.

The experimental results have highlighted the dependence of enrichment on particle size, smaller particles enriching more quickly than larger ones. Figure 5.69 shows the results of a calculation using the finite difference model of the enrichment rate at 565°C for three different particle sizes, 50 nm, 75 nm and 100 nm. The model predicts a difference of $\simeq$20 wt.% Cr between the 50 and 100 nm particles after tempering for 100 hours. This is consistent with the measured variation of composition with size, and illustrates the importance of making the two measurements simultaneously.

5.8 Conclusions

Detailed experimental studies of cementite composition changes in fully bainitic and mixed ferritic/bainitic microstructures have been made. The enrichment rate has found to be slower in the bainitic regions of the mixed microstructures than in the fully bainitic specimens. A strong dependence of enrichment on particle size has been observed, the smaller particles enriching more quickly than the larger ones. Both of these observations are consistent with the predictions of the computer model. Differences in precipitation behaviour between bainitic, martensitic and ferritic regions of the microstructure have been established. This has important consequences for remanent life assessment in that a simple measurement of cementite composition is not sufficient; the size and position in the microstructure must be simultaneously determined.

The calculated value for the activation energy of chromium diffusion in ferrite, and hence the diffusion coefficient, show good agreement with previously measured values. The need for a measurement of the diffusivity of chromium in cementite has been highlighted. The usefulness of equilibrium thermodynamic calculations in predicting the microstructural changes which occur has also been demonstrated.

No significant dependence of the composition of the chromium–rich alloy carbide, M_7C_3, on size or tempering time has been found. Indications are that once alloy carbides have precipitated any further enrichment is too small to be useful in estimating the average temperature experienced by the microstructure. This is discussed further in Chapter 7.

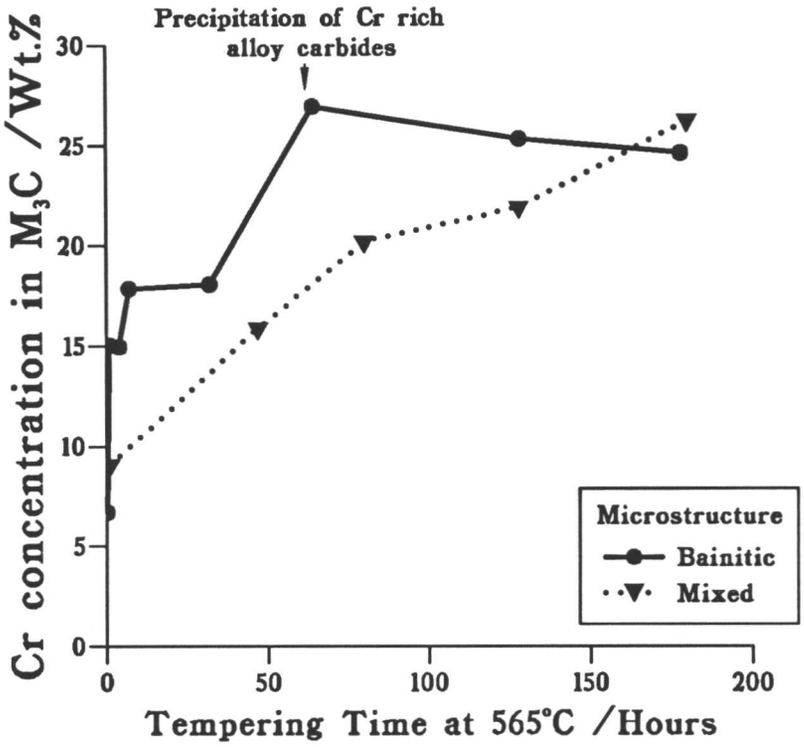

Figure 5.65: Comparison of the average chromium content in cementite in fully bainitic and mixed microstructure specimens as a function of tempering time at 565°C.

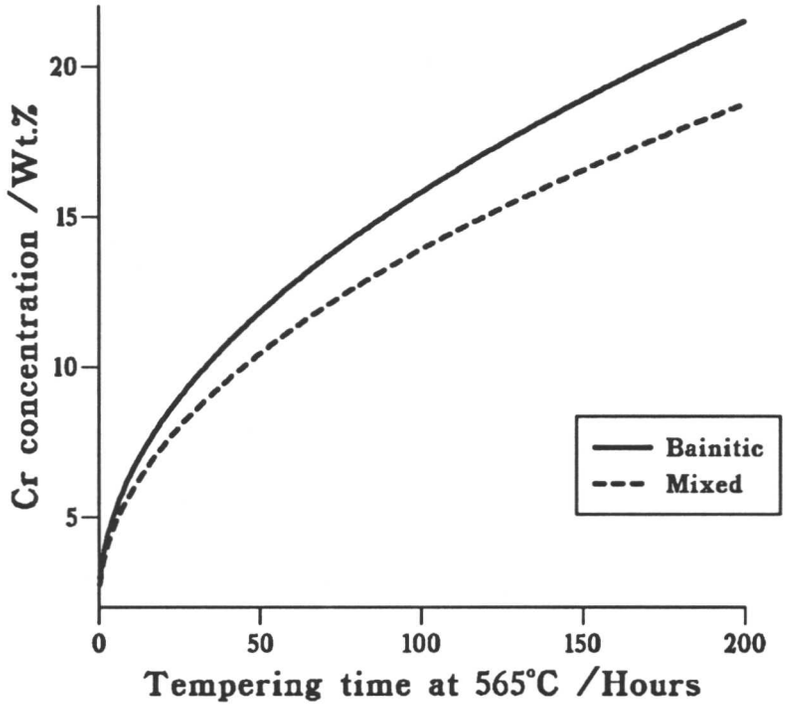

Figure 5.66: Predicted rate of enrichment in cementite in the bainitic and mixed microstructure specimens using the asymmetric finite difference model described in Chapter 3.

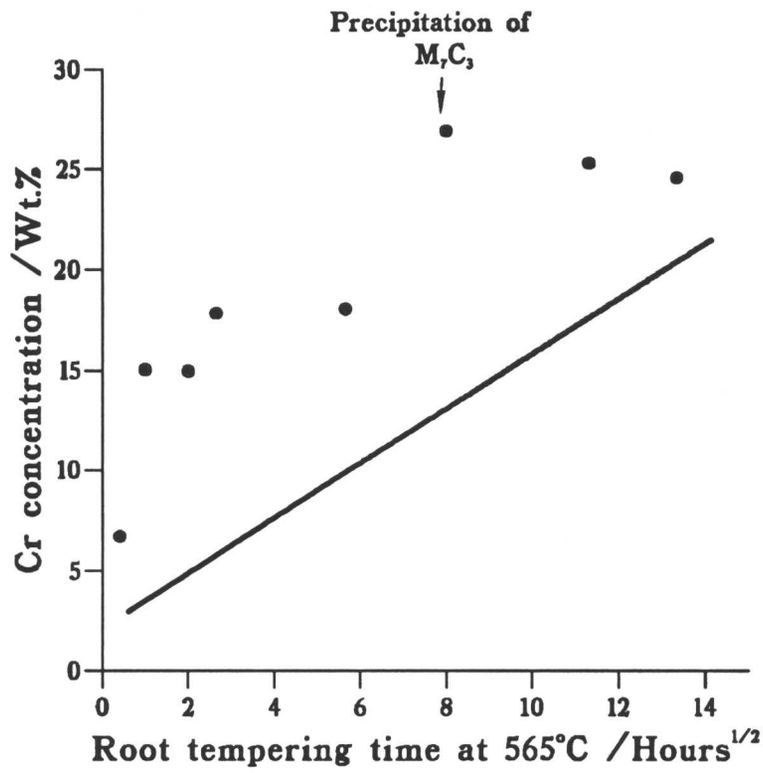

Figure 5.67: Comparison of the experimentally measured Cr concentration in cementite in the bainitic specimens with the predicted rate of enrichment using the asymmetric model described in Chapter 3.

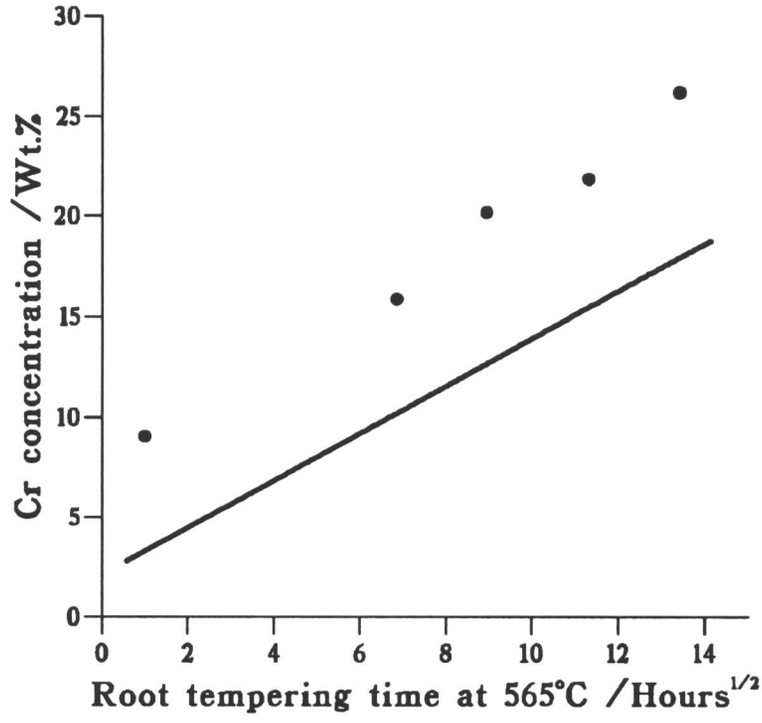

Figure 5.68: Comparison of the experimentally measured Cr concentration in cementite in the bainitic regions of the mixed microstructure specimens with the predicted rate of enrichment using the asymmetric model described in Chapter 3.

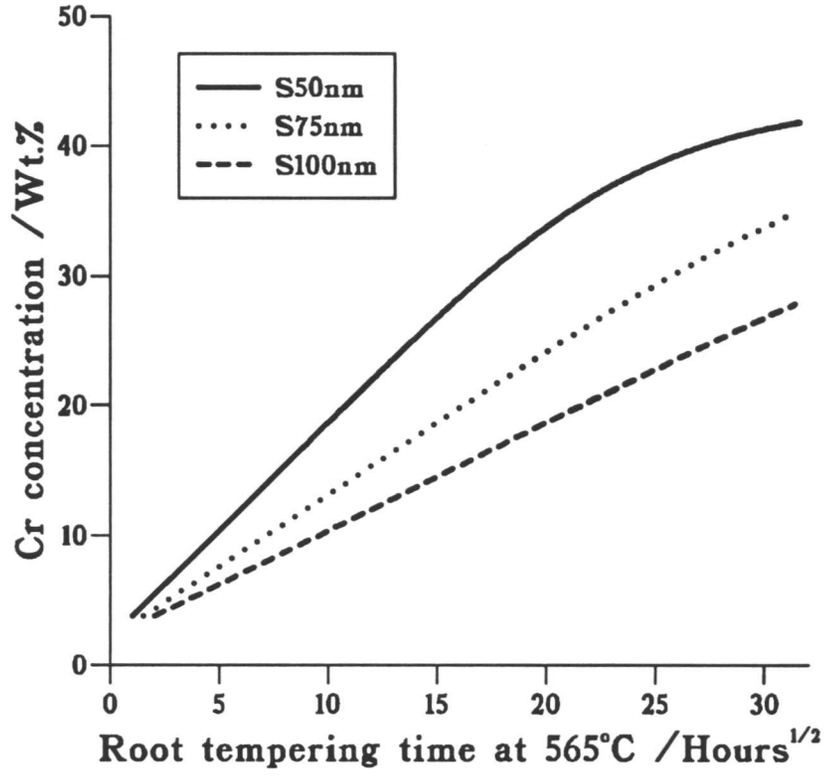

Figure 5.69: Illustration of the dependence of the enrichment of cementite on the particle size calculated at 565°C using the finite difference model.

CHAPTER 6

$\frac{1}{2}$Cr$\frac{1}{2}$Mo$\frac{1}{4}$V STEEL

Measurements of composition changes in cementite over long periods of time in a pearlitic $\frac{1}{2}$Cr$\frac{1}{2}$Mo$\frac{1}{4}$V steel have been carried out at a variety of tempering temperatures. The original measurements were made by Du (1986), although only empirical expressions describing the results were found. In this chapter additional measurements made by myself on the original specimens to determine the variation of cementite concentration with particle size are discussed. Having obtained the particle size data, the composition changes are modelled theoretically. Very good agreement is found between theory and experiment.

The material described in this chapter has been published in Materials Science and Engineering A, **155**, 1992, p. 197–205.

CHAPTER 6

$\frac{1}{2}Cr\frac{1}{2}Mo\frac{1}{4}V$ STEEL

6.1 Introduction

In bainitic microstructures in which cementite grows without partitioning of the substitutional alloying elements, the initial composition of bainitic cementite can be readily estimated. This work, however, focusses on the ferritic/pearlitic microstructures in a $\frac{1}{2}Cr\frac{1}{2}Mo\frac{1}{4}V$ steel. Investigations by Carruthers and Collins (1980) on this material have shown that changes in the substitutional solute concentration of cementite may be a viable technique for the estimation of an effective service temperature. $\frac{1}{2}Cr\frac{1}{2}Mo\frac{1}{4}V$ steel is probably the most widely used low alloy steel in power plant.

The pearlite reaction is fundamentally different from that of bainite in that it is a reconstructive transformation in which growth occurs at an incoherent interface with the parent austenite. Diffusion of all the elements is therefore an integral part of the reaction, and the partitioning of substitutional elements has been reported (Al–Salman *et al.*, 1979; Chance and Ridley, 1981) for all transformation conditions. Paraequilibrium growth of pearlite does not occur, nor does the cementite have an equilibrium composition. Therefore, there is an uncertainty about the starting chemistry of pearlitic cementite. In addition, the cementite is rather coarse compared with that associated with bainite. In fact, each pearlite colony is a bicrystal of cementite and ferrite, the so–called cementite lamellae being interconnected in three dimensions (Hillert, 1962). Consequently it is of considerable interest, both from an industrial and an academic point of view, to investigate any changes in carbide characteristics with tempering heat treatments.

6.2 Materials and heat treatment

The material used in these experiments was a standard $\frac{1}{2}Cr\frac{1}{2}Mo\frac{1}{4}V$ steel supplied by National Power designated as cast M1. The chemical composition is given in Table 6.1. The samples were normalized from an austenitising temperature of 950°C and then tempered at 690°C for one hour in order to simulate the commercial stress–relief heat treatment for this steel. Specimens were then machined to 10×20 mm and tempered at a variety of temperatures between 640 and 525°C in a specially designed furnace (Carruthers and Collins, 1980) for varying times. Within the furnace, the samples were screwed into a nimonic 80a bar to ensure an even temperature distribution. The temperature error at any specimen position was

±2°C. There was no significant oxidation or decarburisation of the threaded test pieces during tempering. Tempering was discontinuous because the specimens were removed at various time intervals to prepare samples for examination in the transmission electron microscope, and then put back for further heat treatment. It was confirmed in a separate experiment that the cementite compositions of samples tempered continuously and discontinuously were, as expected, the same within experimental error.

Table 6.1: Chemical composition of the $\frac{1}{2}Cr\frac{1}{2}Mo\frac{1}{4}V$ steel in wt.%

Cast	C	Si	Mn	P	S	Cr	Mo	V	Ni	Cu
M1	0.14	0.23	0.61	0.007	0.023	0.36	0.66	0.26	0.21	0.13

6.3 Experimental results

6.3.1 Microstructure and carbide morphologies

The microstructures after the normalisation heat treatment at 950°C were mixtures of ferrite, pearlite and bainite. The development of the microstructure as tempering proceeds is illustrated in Figure 6.1; the transmission electron micrographs were taken from carbon extraction replicas and are therefore specific to the carbide distribution. After the stress–relief heat treatment at 690°C for one hour the main ferritic and pearlitic regions were still clearly defined, however, it can be seen from Figure 6.1b) that the pearlitic cementite had already begun to spheroidise. Further coarsening occurs during prolonged tempering. Figures 6.1c) and d) illustrate this in specimens tempered at 640° for 483 and 2996 hours respectively. Cementite particles located at the ferrite grain boundaries were generally found to be coarser than those within the grains. The coarsening process ultimately dissolved most of the intragranular cementite particles, leaving relatively few large particles on the boundaries. It is found that eventually very much larger alloy carbides, $M_{23}C_6$ and M_6C, precipitate at the expense of the cementite which dissolves completely. The transformation to alloy carbides was found to be much faster at the higher tempering temperatures. $M_{23}C_6$ is found after 5,850 hours at 640°C and M_6C after 9,353 hours, whereas after 9,381 hours at 565°C only $M_{23}C_6$ is found, and cementite remains the stable carbide after 12,887 hours tempering at 525°C.

In addition to the chromium–rich M_3C, $M_{23}C_6$ and M_7C_3 carbides, a fine dispersion of molybdenum and vanadium based carbides, M_2C and MC respectively, also precipitated during the stress–relief heat treatment and persisted throughout the tempering process.

6.3.2 Composition of the carbides

The representative energy dispersive X–ray spectra of the various carbides are presented in Figure 6.2. M_3C is characterised by a low vanadium and molybdenum concentration, whereas $M_{23}C_6$ has a much higher chromium and molybdenum content. M_6C contains a slightly smaller chromium content than $M_{23}C_6$, but can be identified by its high molybdenum and silicon contents. Figure 6.2d) illustrates the charcteristic spectra from MC, a vanadium based carbide which can dissolve some molybdenum, and Figure 6.2e) that from M_2C, which is molybdenum–rich, although it contains a significant amount of vanadium, and traces of chromium, manganese and iron.

The experimentally determined composition bands spanning the ranges of temperatures studied of the alloying elements in the carbides in atomic % , allowing for the stoichiometric carbon content in each alloy carbide (for example, 25 at.% of carbon in cementite) are summarised in Table 6.2.

Table 6.2: Chemical composition ranges of the carbides M_3C, $M_{23}C_6$ and M_6C in at. %

Carbide	V	Cr	Mn	Mo	C
M_3C	0.7–1.1	2.0–7.6	2.0–10.0	0.6–1.0	25.0
$M_{23}C_6$	0.3–0.6	9.0–15.0	6.0–8.0	3.0–5.0	20.7
M_6C	2.0–3.0	5.5–8.0	6.0–8.0	16.0–20.0	14.3

The chromium content of the cementite was found to increase steadily with time at the tempering temperature, the rate of enrichment being higher at the higher tempering temperatures. Manganese was found to diffuse into the cementite faster than the chromium, and saturated at a higher concentration. At the lower tempering temperatures saturation was not observed within the time periods studied. The saturation levels of chromium and manganese were also found to increase with decreasing tempering temperature. In the $M_{23}C_6$ the chromium content also appeared to increase slightly with tempering time, whereas the manganese content decreased. However, much longer service times are needed before the enrichment kinetics of $M_{23}C_6$ can be established with confidence. The vanadium content of the $M_{23}C_6$ was much lower than that in the other carbides. M_6C was found to have an almost constant composition at all stages of tempering.

The dissolution of cementite and precipitation of $M_{23}C_6$ occurred after the cementite had reached saturation. The literature suggests that the alloy carbide sequence usually involves first a transformation to M_7C_3 prior to $M_{23}C_6$, but this sequence was not observed experimentally.

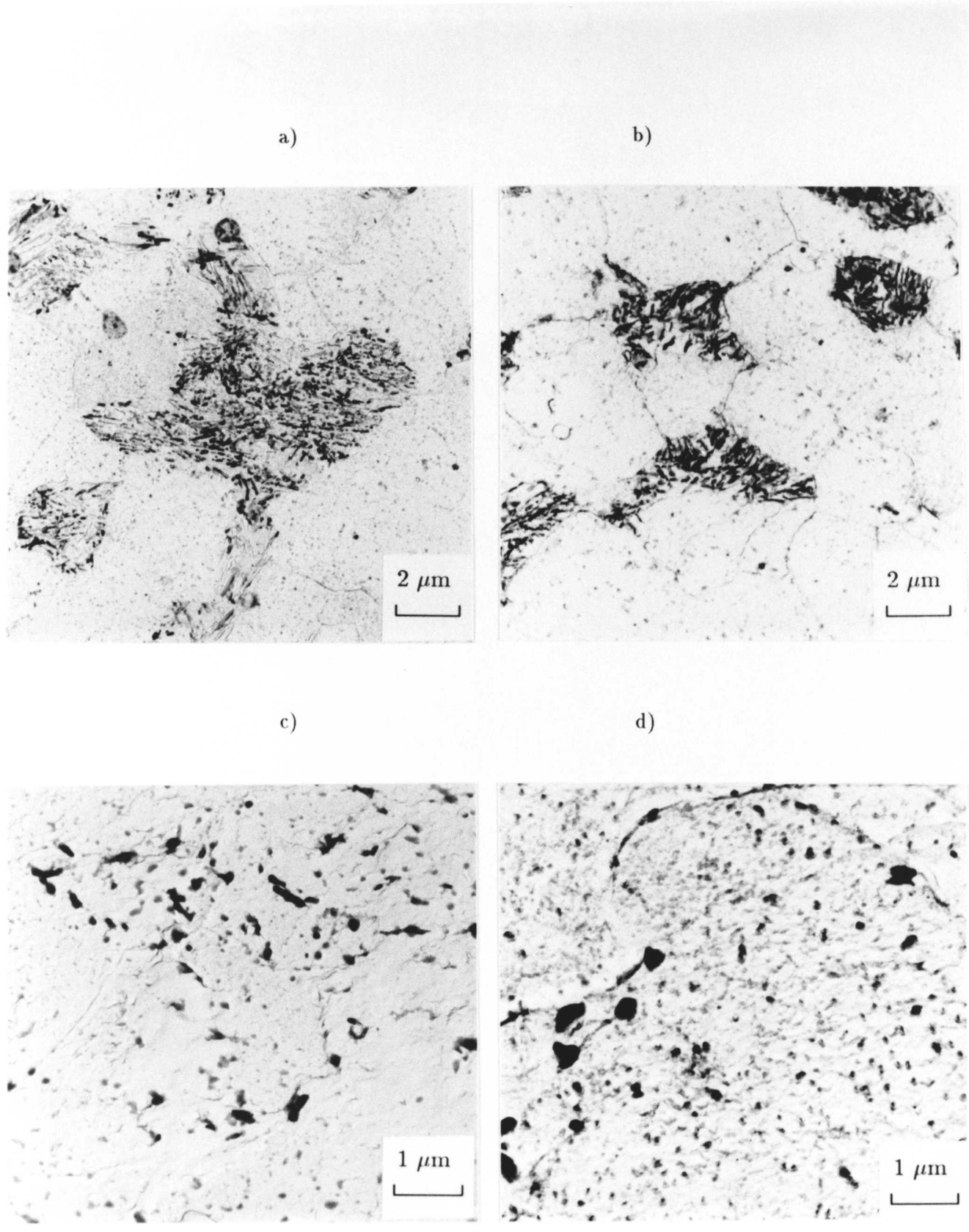

Figure 6.1: The development of the carbide distribution during long term tempering at 640°C; a) after normalizing at 950°C, b) as a), but additionally tempered at 690°C for 1 hour, c) further tempered at 640°C for 483 hours and d) tempered at 640°C for 1996 hours.

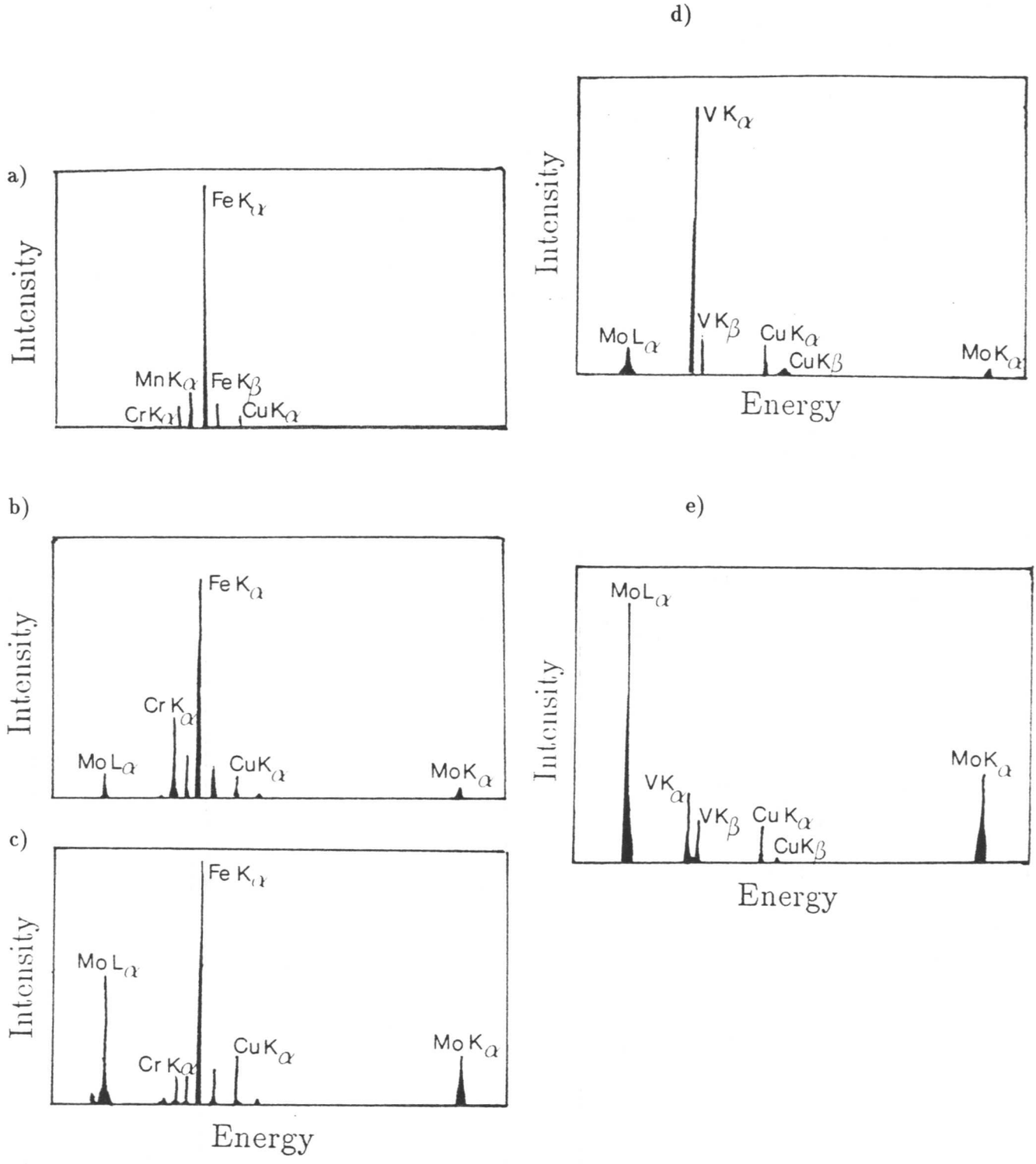

Figure 6.2: Characteristic energy dispersive X–ray spectra for the various alloy carbides found to precipitate during the tempering heat treatments: a) M_3C, b) $M_{23}C_6$, c) M_6C, d) MC and e) M_2C.

A possible explanation for this is that the chromium content of the steel, and its ratio to molybdenum was too low for M_7C_3 to form. It is also probable that the small molybdenum–based carbides in the matrix limited the molybdenum content of the larger $M_{23}C_6$ and M_6C carbides, and stabilized the $M_{23}C_6$ to longer times.

6.4 Modelling of the diffusion process

6.4.1 Thermodynamic calculations

Thermodynamic calculations were performed to calculate the equilibrium carbides expected in M1 steel as a function of temperature, and to study the metastable equilibrium between ferrite and cementite. The calculations allowed for the elements Fe, Cr, Mn, Mo, C, V, Si, Ni, Sn, Cu, P and S and the phases $M_3C, M_7C_3, M_6C, M_{23}C_6, M_2C$, VC, austenite and ferrite.

The equilibrium carbides at all temperatures were found to be $M_{23}C_6$, M_6C and VC which is in good agreement with the carbides observed after long ageing times in all the specimens (Mo_2C is assumed to have all transformed to M_6C under equilibrium conditions). Calculations were then performed by suppressing all carbides except cementite, thereby allowing the equilibria between the metastable cementite and the ferrite matrix to be studied. The calculated chromium levels in the ferrite and cementite are presented in Table 6.3. These data are also plotted in Figure 6.3. It can be seen that the maximum permitted concentration of chromium in cementite increases with decreasing temperature, as observed experimentally.

Table 6.3: Equilibrium concentration (at.%) of chromium in ferrite and cementite calculated using MTDATA as a function of temperature in steel M1.

Phase	690°C	640°C	630°C	620°C	610°C	590°C	575°C	565°C	525°C
Ferrite	0.25	0.23	0.22	0.22	0.21	0.20	0.19	0.18	0.16
Cementite	5.53	6.35	6.53	6.72	6.91	7.31	7.63	7.85	8.77

The equilibria between ferrite/$M_{23}C_6$ and ferrite/M_6C can also be calculated. The calculated equilibrium chromium concentration in $M_{23}C_6$ varies between 7–9 at.% from 690–525°C respectively, and that in M_6C from 2–4 at.% over the same temperature range. These equilibrium calculations also predict that the level of molybdenum at equilibrium is 10 at.% in $M_{23}C_6$ and 45 at.% in M_6C.

6.4.2 Finite difference modelling

Calculations were performed using the model described in Chapter 3 to predict the enrichment rate of cementite for comparison with the experimental results. The initial compostitions

in the cementite and ferrite are obtained by assuming that there is no partitioning of the substitutional solute elements during transformation. The particle size used in the model was 175nm; this represented the mean value obtained from particle size measurements over many specimens. The effect of the chosen particle size on the enrichment rate is illustrated in Figure 6.4 for particles of 150, 175 and 200nm at 590°C. Obviously there is no effect on the saturation level of chromium which is determined by equilibrium thermodynamics, but the enrichment rate is slightly faster for a smaller particle.

In order to simulate the industrial heat treatment, calculations were carried out in which the composition changes in cementite resulting from a stress–relief heat treatment at 690°C for one hour were evaluated prior to the modelling of long term tempering at the lower service temperatures. As an initial approximation it is assumed that there is no redistribution of substitutional solute elements during the formation of pearlite. The starting concentrations were therefore set to be the bulk chromium composition of the alloy in both the ferrite and cementite. The interface concentrations used were the equilibrium concentrations of chromium in the cementite and ferrite respectively, calculated using MTDATA as described in the previous section. The measured chromium concentrations are compared with the theoretical predictions in Figure 6.5a)–h), for specimens tempered at 640, 630, 620, 610, 590, 575, 565, and 525°C. It should be noted that the saturation level in cementite predicted by MTDATA is slightly different from that measured experimentally. This is thought to be due to the presence of the fine M_2C in the steel, precipitated during the stress–relief heat treatment, which reduces the molybdenum content in the cementite and raises the chromium content above that predicted if only cementite and ferrite are allowed to exist. The experimentally determined chromium contents of $M_{23}C_6$ and M_6C are also plotted to illustrate the time at which the cementite transforms to alloy carbides at the various tempering temperatures. The absolute chromium levels in the alloy carbides are higher than those predicted by thermodynamic calculations. The high molybdenum concentrations predicted in $M_{23}C_6$ and M_6C are not observed experimentally, resulting in larger chromium concentrations being measured in the alloy carbides than their predicted values. Again this can be attributed to the fact that molybdnum is tied up in fine M_2C precipitates, reducing the amount of molybdenum available for inclusion in $M_{23}C_6$ and M_6C. The effect of the M_2C precipitation altering the absolute chromium levels predicted in carbides is very small in the case of cementite, where the predicted level is 2–3 at.% and the measured level is approximately 1 at.%.

It has already been mentioned in the introduction that the chemical composition of cementite in pearlitic steels is found to be somewhere in between equilibrium and paraequilibrium

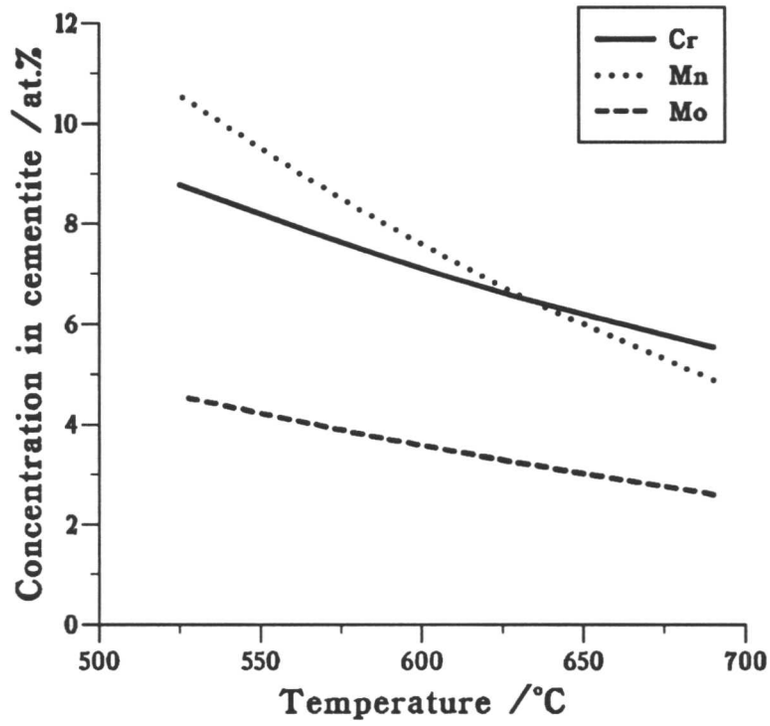

Figure 6.3: Equilibrium substitutional alloying content of cementite as a function of temperature calculated using MTDATA.

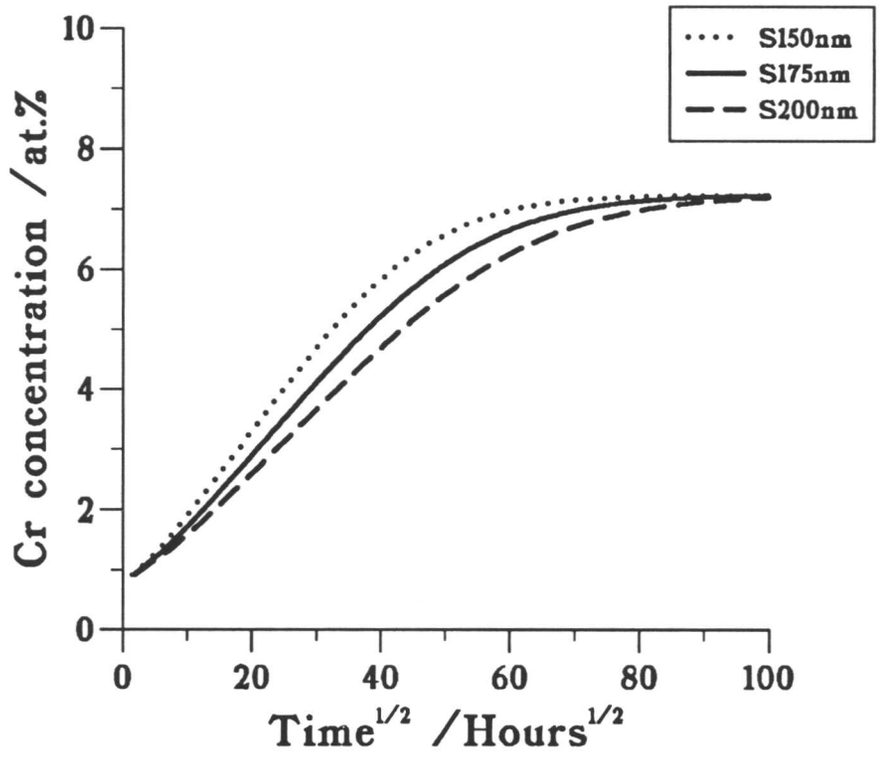

Figure 6.4: The effect of particle size on the enrichment kinetics of cementite.

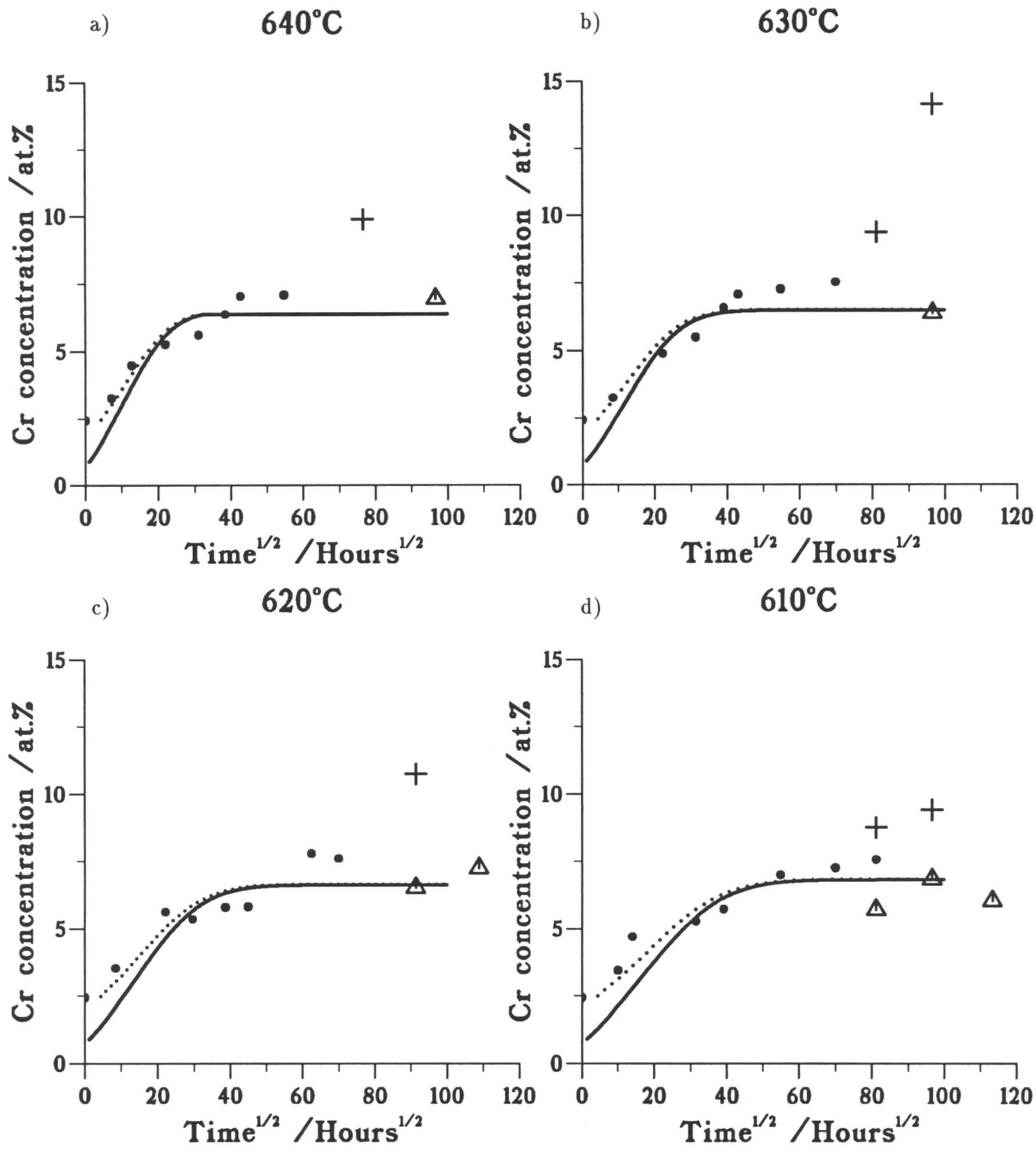

Figure 6.5: a)–h) A comparison of experimental measurements of chromium concentration in cementite, •, with the finite difference model (solid line). The dotted line represents the predictions of the model in the case where partitioning of some chromium is allowed for. The chromium concentration of the alloy carbides occurring at long service times is plotted for comparison: + $M_{23}C_6$, △ M_6C.

e)

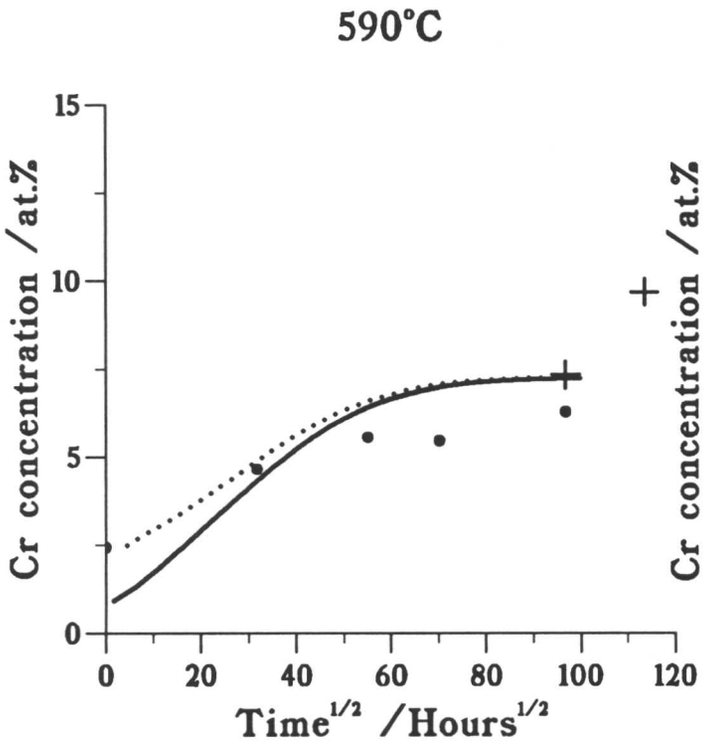
590°C
Cr concentration /at.%
Time$^{1/2}$ /Hours$^{1/2}$
0
5
10
15
0
20
40
60
80
100
120

f)

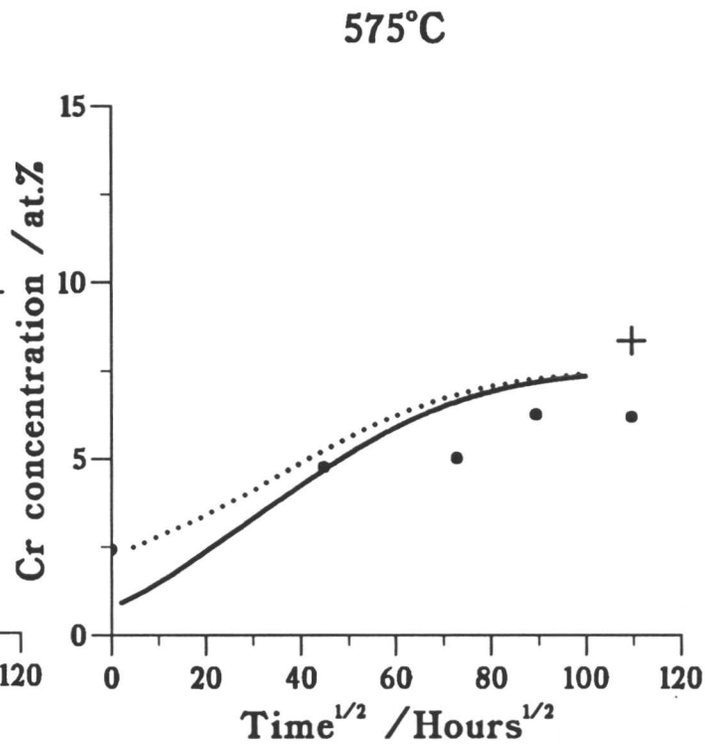
575°C
Cr concentration /at.%
Time$^{1/2}$ /Hours$^{1/2}$
0
5
10
15
0
20
40
60
80
100
120

g)

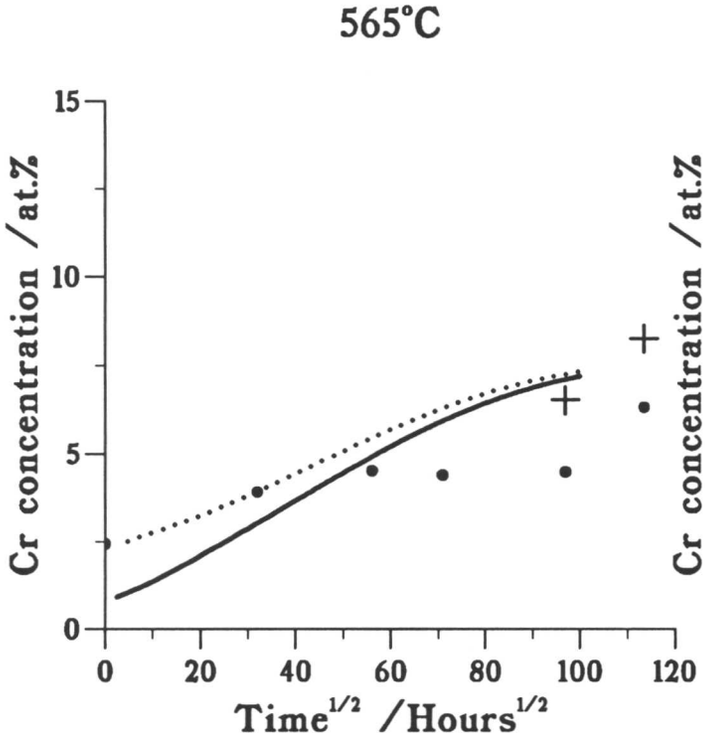
565°C
Cr concentration /at.%
Time$^{1/2}$ /Hours$^{1/2}$
0
5
10
15
0
20
40
60
80
100
120

h)

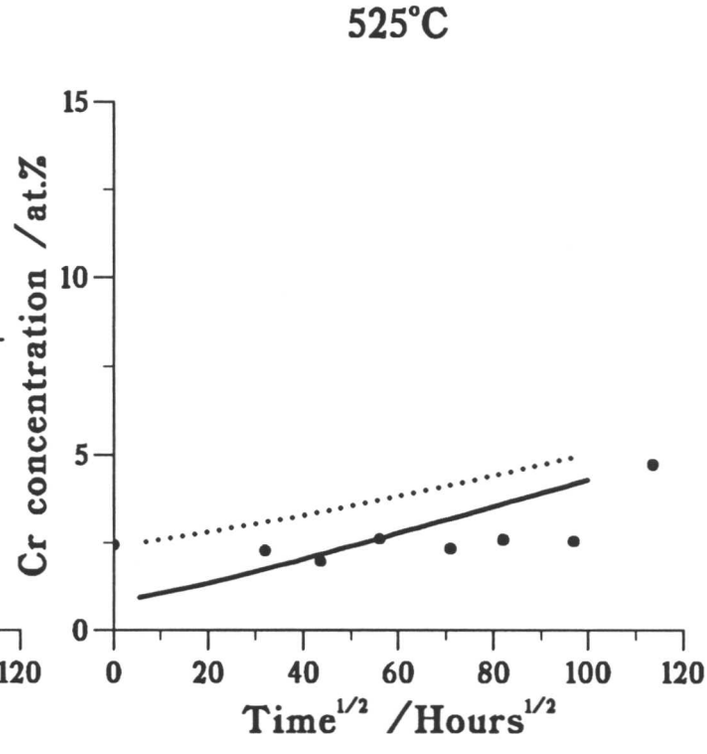
525°C
Cr concentration /at.%
Time$^{1/2}$ /Hours$^{1/2}$
0
5
10
15
0
20
40
60
80
100
120

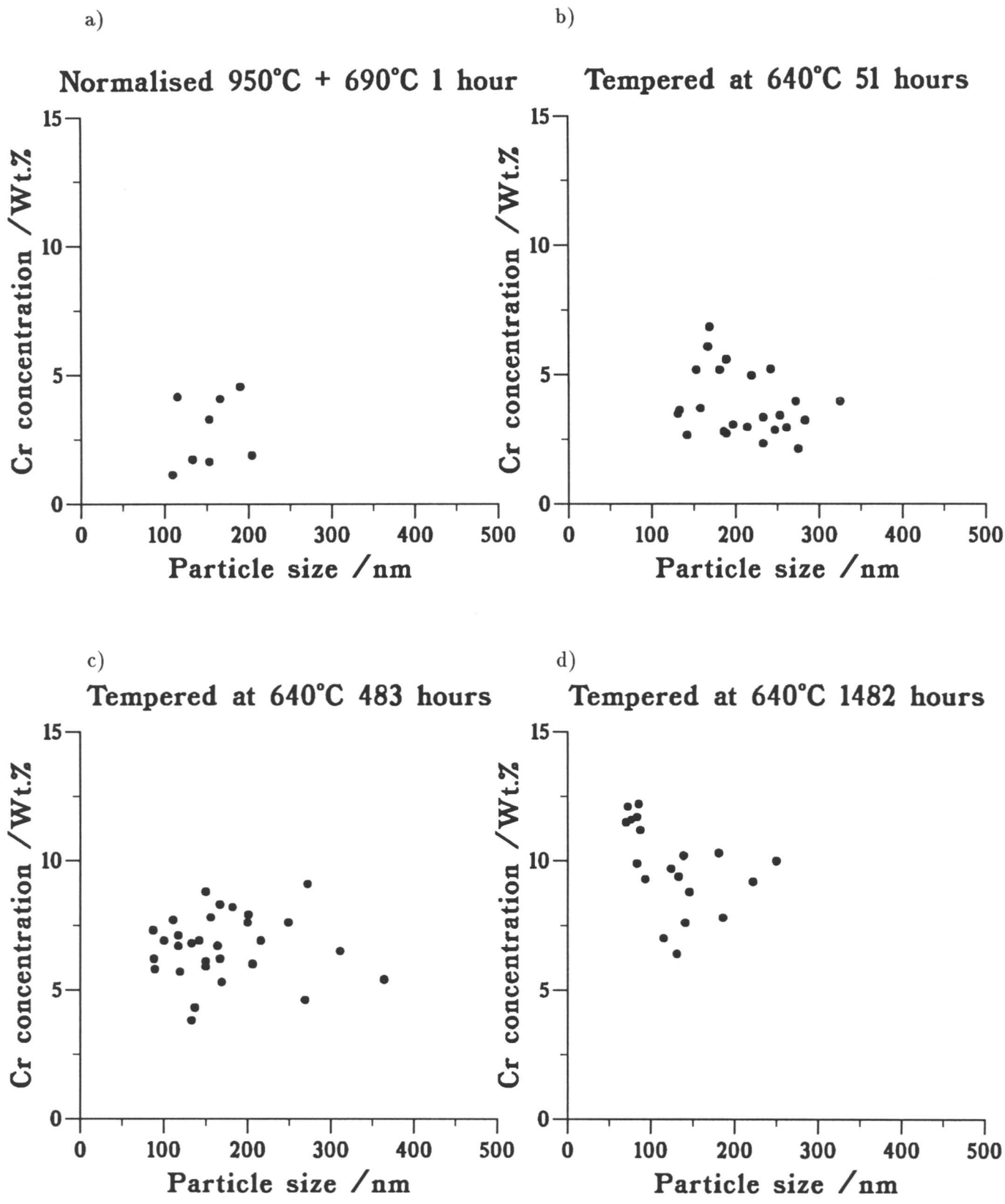

Figure 6.6: a)–f) Chromium concentration in cementite plotted against particle size for specimens tempered for varying times at 640°C.

e)

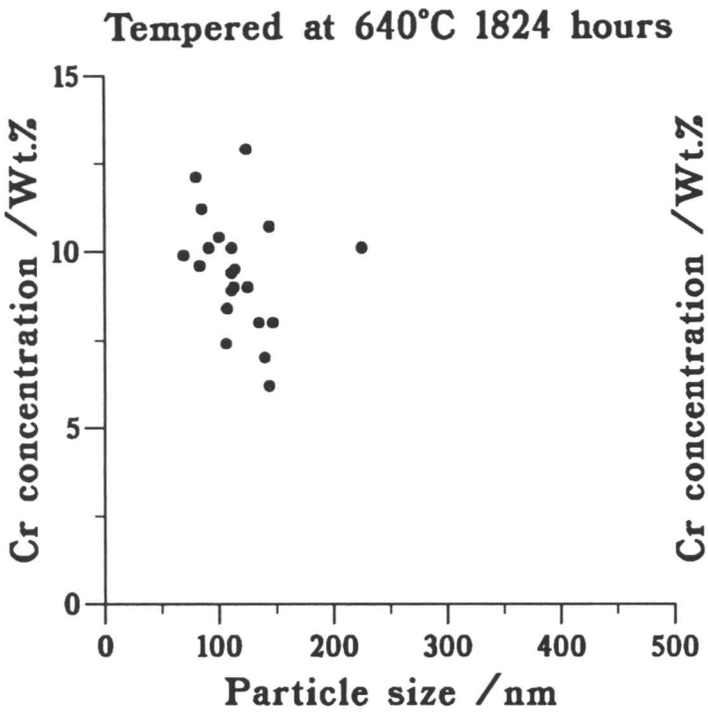
Tempered at 640°C 1824 hours
Cr concentration /Wt.%
15
10
5
0
0
100
200
300
400
500
Particle size /nm

f)

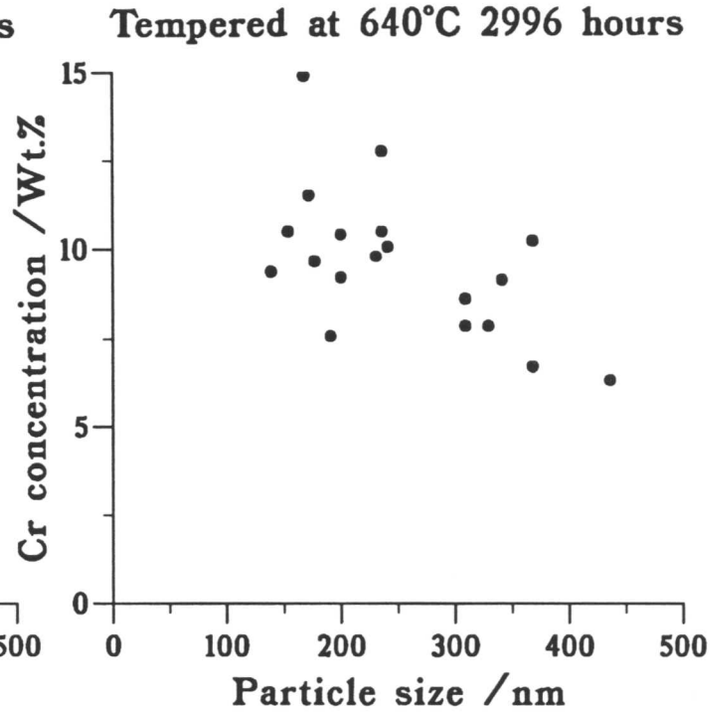
Tempered at 640°C 2996 hours
Cr concentration /Wt.%
15
10
5
0
0
100
200
300
400
500
Particle size /nm

after transformation, and there is as yet no theory to predict the starting composition of the cementite. This is in contrast to bainitic cementite in which it can be assumed that there is negligible partioning of substitutional solute elements during transformation. It can be seen in Figure 6.5 that there is an error in the predicted starting composition of the pearlitic cementite after the stress–relief heat treatment because any partitioning occurring on transformation is not taken into account. To allow for this problem with the inital stage of modelling, the simulation of the stress–relief heat treatment was allowed to run until the composition of the cementite had reached that measured experimentally. This corresponded to a period of tempering at 690°C for 18 hours rather than the one hour experienced in the practical situation. This is an artificial procedure because it considers partitioning to occur during the stress–relief heat treatment rather than on transformation, but it simply allows the use of the correct starting composition of the pearlitic cementite. The improvement in the agreement between the predicted and measured values is shown by the dotted line superimposed on the graphs in Figure 6.5. This problem will be overcome when a theoretical basis for the precipitation of pearlitic cementite during transformation can be established.

6.4.3 Particle size

The size and concentration of a series of particles were examined in specimens tempered at 640°C. Plots of chromium concentration against particle size are presented in Figure 6.6a)–f). The situation is complicated by the fact that the initial cementite lamellae appear to spheroidise and coarsen during tempering.

The physical explanation of the size effect is that the total amount of solute that any particle can hold scales with particle size. A smaller particle will therefore reach its equilibrium concentration at an earlier stage in the tempering process. Therefore, size effects are unlikely to be easily detected during the early stages of tempering when most of the particles are below their saturation concentration and capable of accumulating solute. It is expected therefore that the size effect becomes more prominent during the later stages of ageing. A second point to note is that at any given ageing time, the average concentration of the solute in the particle, c^θ, varies inversely with particle size, x^θ. Thus c^θ will only be sensitive to x^θ when the latter is small. This is illustrated in Figure 6.4, where variations in x^θ within the expected range for the present study do not cause very large changes in c^θ when compared with experimental error. Nevertheless it is evident from the data presented in Figure 6.6 that the dependence of c^θ on x^θ begins to emerge with statistical significance only at the longest tempering time studied. Longer times could not be studied because of the onset of alloy carbide formation.

6.5 Conclusions

In a $\frac{1}{2}Cr\frac{1}{2}Mo\frac{1}{4}V$ steel after normalisation at 950°C followed by a stress–relief heat treatment at 690°C for an hour, the cementite composition varies on further tempering at temperatures in the range 640–525°C. The chromium and manganese content of the cementite increase with tempering time at the expense of the ferrite content. After the equilibrium composition of the cementite has been reached, transformation to the alloy carbides $M_{23}C_6$ and M_6C occurs. The diffusion of the substitutional solute elements to cementite has been modelled and very good agreement has been found with the experimentally determined compositions. Further theoretical work is necessary to model the formation of cementite from austenite so that the starting composition of pearlitic carbides can be predicted. The dependence of composition on particle size was found not to be significant due to the relatively large size of the pearlitic cementite, and the fact that the calculated equilibrium concentration of chromium in cementite in this steel was relatively low, approximately 8 at.%. This is contrast to the particle size dependence of alloy element concentration discussed in the previous chapter for bainitic cementite. Comparison of the experimentally determined chromium concentration in cementite, after a particular operating time, with the predictions of the numerical model of the diffusion process can therefore be used to estimate the service temperature of $\frac{1}{2}Cr\frac{1}{2}Mo\frac{1}{4}V$ steel power plant components.

CHAPTER 7

12Cr1Mo STEEL

Carbide precipitation studies in 12Cr1MoV steel are discussed in this chapter. As a result of the very high chromium concentration of 12Cr1MoV steel, the reaction kinetics are rapid compared to those in low alloy steels. It is found that the equilibrium alloy carbide precipitates during the commercial stress–relief heat treatment and does not change in composition during further tempering. This is an important result; indications are that once the cementite transforms to alloy carbides, any changes in their composition are not large enough for this method to be used as a quantitative estimation of remanent life. (Low alloy steels, however, contain cementite for a considerable fraction of their useful service life.)

The material described in this chapter has been published in Metallurgical Transactions A, **23A**, 1992, p. 1171–1179.

CHAPTER 7

12Cr1Mo STEEL

7.1 Introduction

The vast majority of creep–resisting steels used in power plant or in the petrochemical industry are based on low–carbon, low–alloy steels containing carbide forming elements such as chromium, molybdenum and vanadium as deliberate additions. In addition to creep resistance, prolonged service at elevated temperatures also requires good oxidation and hot–corrosion resistance, possibly in environments containing hydrogen and sulphur. In the United Kingdom, the steels are often used within the temperature range 480–565°C, the service stresses being of the order of 15–30 MPa over time periods of some thirty years. There is currently considerable research in progress to implement higher alloy steels with the aim of improving the creep strength so that the service temperature can be increased (Alberry and Gooch, 1983; Middleton, 1986). Alternatively, the higher strength can be exploited by reducing section size, which can be beneficial from the viewpoint of welding, thermal fatigue and the reduced cost of support structures. A lot of the effort to date has focussed on 12Cr1MoV steel. The purpose of this work was to examine the effect of representative heat–treatments on the chemistry and some other characteristics of the carbides to be found in 12Cr1MoV type steels.

7.2 Materials and heat treatment

The material used in this work was a 12Cr1MoV steel supplied by National Power Technology and Environment Centre, Leatherhead, from heat 60348. The steel was supplied in the form of a rod of diameter 4 cm×1 m long. Thinner rods of 3 mm diameter and bars 1×1×4 cm were machined from the original sample. Experimental results were compared with 'ex–service' material (i.e. steel which has been in service in a power station), courtesy of Laborelec, Belgium. The service history of this latter pipe was 68,646 hours at 592°C followed by 146,000 hours at 587°C, both at a pressure of 175 bar. The compositions of both steels, which are both within British Standard, BS3604, and the German standard X20 for 12Cr1MoV steels, are given in Table 7.1. In spite of this, it is worth noting that the chromium concentration of the ex–service steel is significantly higher.

Heat treatments were carried out in order to recreate the microstructures used in the commercial condition when the steels are first implemented for service. The material is metallurgically complex and requires careful control of the heat treatment to ensure that the starting

Table 7.1: Chemical compositions of the 12Cr1MoV steels in wt. %

	C	Si	Mn	P	S	Cr	Mo	V	Ni	Cu	Al	Co	Nb+Ta
12Cr1MoV	0.21	0.25	0.46	0.009	0.012	10.9	1.03	0.30	0.52	0.02	<0.005	0.02	0.06
Ex-service X20CrMoV12 1	0.18	0.22	0.58	0.01	0.007	12.4	1.07	0.28	0.64	0.13	0.01	0.03	<0.01

microstructure is 100% martensitic. The specimens were sealed in silica tubes containing a partial pressure of argon of 150 mm Hg. Austenitisation was carried out at 1060°C for 15 minutes. It has been shown by Barraclough and Gooch (1985) that the austenitising temperature for 12Cr1MoV steels is crucial in determining the microstructure and mechanical properties. Too low a temperature will cause heavily spheroidised microstructures with dramatically reduced creep resistance, and too high a temperature can result in the formation of δ ferrite and a large austenite grain size, which is undesirable. Yet the temperature must be high enough to ensure the complete dissolution of carbides. After austenitisation the specimens were air–cooled, and re–sealed in silica tubes and tempered for up to 2 hours at 700°C, in order to simulate the commercial stress–relief heat treatment, and then further tempered at 565°C to simulate service conditions.

7.3 Results

7.3.1 Microstructural changes

A typical optical micrograph is shown in Figure 7.1. It can be seen that the microstructure is 100% martensite and does not contain any δ ferrite. TEM micrographs of the as–quenched microstructure are presented in Figure 7.2. Figure 7.2a) shows martensite platelets containing some internal twins, confirmed by selected area electron diffraction. Figure 7.2b) demonstrates the fact that there are no carbides in the as–quenched microstructure, i.e. that no autotempering has occurred. Gooch (1982) reported that the microstructure obtained by cooling from 1100°C contained a fine dispersion of cementite particles. This difference is attributed to the relatively slower speed of the quench.

Figure 7.3a) and b) illustrate the carbides beginning to form at prior austenite grain and lath boundaries, and also intra–lath, in a specimen which has been tempered at 700°C for 15 minutes. The carbides were identified by selected area electron diffraction as both M_7C_3 and $M_{23}C_6$.

The carbide M_7C_3 was also found in specimens aged for up to 30 minutes at 700°C, but these had all dissolved at the end of the stress–relief heat treatment. Figure 7.4 shows that

M_7C_3 was mainly found within the martensite laths and distant from the clustered $M_{23}C_6$ precipitates. This is in agreement with Beech and Warrington (1966) who found that $M_{23}C_6$ and M_7C_3 were both present from an early stage of tempering, and that on spheroidisation the particles within the martensite laths disappeared. The diffraction pattern in Figure 7.4 illustrates the characteristic streaks of M_7C_3 resulting from its faulted structure compared with that of pure Cr_7C_3 (Westgren *et al*, 1928). No difference in morphology was found between M_7C_3 and $M_{23}C_6$, apart from a tendency for the former carbides to be much finer.

A typical carbon extraction replica from a sample which had been given the commercial stress–relief heat treatment, i.e. tempering at 700°C for 2 hours, is shown in Figure 7.5. The distribution of the carbides in relation to the martensite boundaries is clearly illustrated. The carbides at the end of the stress–relief heat treatment were found to consist chiefly of a dispersion of $M_{23}C_6$ particles concentrated on the austenite grain and lath boundaries.

A comparison between the distribution of coarse $M_{23}C_6$ carbides in the ex–service material and in a specimen isothermally heat treated at 700°C for 1173 hours is presented in Figure 7.6. The empirical Larson–Miller (Larson and Miller, 1952) parameter, defined as $T(20 + \log t)$, where T is the temperature in Kelvin and t is the time in hours, indicates that these two different heat treatment conditions are comparable. The carbide size and distribution is similar in the two materials, although for reasons which are not clear there appears to be a tendency for increased clustering of the carbides in the ex–service material.

Macrohardness measurements were made on all the specimens using a 30 kg load. These results are presented in Table 7.2. Each data point is the average of three measurements on each sample, with the total scatter being no more than 10 HV. The macrohardness data confirms that the microstructure of the ex–service material and the 12Cr1MoV steel are similar, and that little change in carbide precipitation occurs on tempering.

Table 7.2: Macrohardness measurements

Specimen	Macrohardness /HV
Pre–tempering	622
700 °C–15 mins	315
700 °C–30 mins	309
700 °C–60 mins	296
700 °C–120 mins	315
700 °C–1173 hours	293
Ex–service material	302

The appearance of additional phases, such as Laves phase, on tempering a 12Cr1MoV steel depends critically upon the base composition of the steel. In the steels used in this work no additional phases were found during tempering which is consistent with the work of Briggs and Parker (1965).

7.3.2 Thermodynamic calculations

Thermodynamic calculations were performed using MTDATA in order to calculate the equilibrium phases in the 12Cr1MoV steel. The carbide $M_{23}C_6$ was found to be the stable carbide, coexisting with ferrite, at all temperatures in the range of interest, 400–800°C. The equilibrium solution temperature of the carbides was found to be 950°C. Barraclough and Gooch (1985) found that 30 minutes at 950°C was not an adequate solution heat treatment, although 30 minutes at 1000°C was satisfactory. The temperature at which delta ferrite became stable on heating was calculated as 1220°C in the 12Cr1MoV steel, and as 1110°C in the ex–service material, which contained an additional 1.5 wt.% chromium. This difference is consistent with the work of Irvine *et al.* (1960) who found that an increase in chromium content of 1 wt.% led to an increase in δ–ferrite content of $\simeq$14%. This confirms that the commercial austenisation temperature range of 1020–1070°C is adequate to completely dissolve carbides and will not produce large amounts of δ–ferrite.

$M_{23}C_6$ was found to be the most stable carbide, then M_7C_3, followed by cementite. A precipitation sequence of $M_3C \rightarrow M_7C_3 \rightarrow M_{23}C_6$ is therefore possible.

The results of the thermodynamic calculations for 700°C (the stress–relief heat treatment) and for 565°C (the service temperature) are presented in Table 7.3. The alloying element content of the two carbides of interest, M_7C_3 and $M_{23}C_6$, is presented as a function of temperature in Figure 7.7a) and b).

Table 7.3: Chemical compositions of the carbides in both the 12Cr1MoV steels used in wt.%. The calculations were performed using MTDATA at 700°C and 565°C respectively.

	12Cr1MoV Steel					'Ex–service' 12Cr1MoV steel				
700°C	Fe	Cr	Mo	Mn	C	Fe	Cr	Mo	Mn	C
M_7C_3	5.2	82.2	3.1	0.6	8.9	4.6	83.2	2.7	0.7	8.8
$M_{23}C_6$	10.7	65.1	19.1	–	5.1	9.0	66.4	19.5	–	5.1
565°C	Fe	Cr	Mo	Mn	C	Fe	Cr	Mo	Mn	C
M_7C_3	1.6	84.4	4.5	0.7	8.8	1.4	85.1	4.0	0.7	8.8
$M_{23}C_6$	4.2	70.3	20.4	–	5.1	3.6	70.9	20.4	–	5.1